

Truncation Errors, Exact and Heuristic Stability Analysis of Two-Relaxation-Times Lattice Boltzmann Schemes for Anisotropic Advection-Diffusion Equation

Irina Ginzburg*

IRSTEA, Antony Regional Centre, HBAN, 1 rue Pierre-Gilles de Gennes CS 10030, 92761 Antony cedex, France.

Received 21 December 2010; Accepted (in revised version) 28 June 2011

Available online 23 December 2011

Abstract. This paper establishes relations between the stability and the high-order truncated corrections for modeling of the mass conservation equation with the two-relaxation-times (TRT) collision operator. First we propose a simple method to derive the truncation errors from the exact, central-difference type, recurrence equations of the TRT scheme. They also supply its equivalent three-time-level discretization form. Two different relationships of the two relaxation rates nullify the third (advection) and fourth (pure diffusion) truncation errors, for any linear equilibrium and any velocity set. However, the two relaxation times alone cannot remove the leading-order advection-diffusion error, because of the intrinsic fourth-order numerical diffusion. The truncation analysis is carefully verified for the evolution of concentration waves with the anisotropic diffusion tensors. The anisotropic equilibrium functions are presented in a simple but general form, suitable for the minimal velocity sets and the d2Q9, d3Q13, d3Q15 and d3Q19 velocity sets. All anisotropic schemes are complemented by their exact necessary von Neumann stability conditions and equivalent finite-difference stencils. The sufficient stability conditions are proposed for the most stable (OTRT) family, which enables modeling at any Peclet numbers with the same velocity amplitude. The heuristic stability analysis of the fourth-order truncated corrections extends the optimal stability to larger relationships of the two relaxation rates, in agreement with the exact (one-dimensional) and numerical (multi-dimensional) stability analysis. A special attention is put on the choice of the equilibrium weights. By combining accuracy and stability predictions, several strategies for selecting the relaxation and free-tunable equilibrium parameters are suggested and applied to the evolution of the Gaussian hill.

PACS: 02.60.Lj, 02.30.Jr, 66.10.c

Key words: Two-relaxation-times Lattice Boltzmann scheme, AADE, truncation errors, von Neumann stability analysis, numerical diffusion, heuristic stability analysis.

*Corresponding author. *Email address:* irina.ginzburg@cemagref.fr (I. Ginzburg)

1 Introduction

The two-relaxation-times (TRT) Lattice Boltzmann model is suitable for solving hydrodynamic equations [16–19], and the anisotropic, linear or non-linear, advection-diffusion equations (AADE), [12–15, 44–46]. This paper further investigates the role of the free-tunable relaxation and equilibrium parameters, with the objective to find the best balance between error minimization and robustness. So far, this work extends the mathematical analysis [7, 8, 36] of the multiple-relaxation-times (MRT) operators, TRT operator [12, 17, 20, 34, 44], single-relaxation-time BGK operator [26, 43] and high-order equilibrium BGK schemes [6, 49]. In fact, the TRT model combines the simplicity and efficiency of the BGK operator [41] with a specific capability of the multiple-relaxation-times operators [4, 22, 23, 27–29] to control their numerical solutions with the help of the “free” relaxation parameters [1, 11, 29, 36, 37]. The TRT model has only one free eigenvalue function, say Λ^- for the anti-symmetric modes modeling the Navier-Stokes equations, and Λ^+ for the symmetric modes modeling the AADE. The viscous and diffusion coefficients are then defined by Λ^+ and Λ^- , respectively. The rigorous analysis of the exact form of the steady state conservation equations undoubtedly shows that the LBE schemes need the distinguished relaxation rates for the different parity eigenmodes, to avoid a non-linear dependence of the truncation spatial errors on the selected transport coefficients [30]. The TRT operator is the minimal scheme which allows a full control of the *steady state* hydrodynamic and advection-diffusion solutions by the non-dimensional physical parameters, as Reynolds and Peclet numbers, provided that the free product $\Lambda = \Lambda^+ \Lambda^-$ is fixed. The BGK subclass of the TRT scheme lacks this feature since $\Lambda^- = \Lambda^+$. However, in addition to non-dimensional governing numbers, the *steady state* TRT solutions are controlled by Λ . For example, the permeability of a porous media calculated with a fixed Λ is independent of the viscosity coefficient and depend only on the assigned value of Λ , [5, 11, 18]. Even if the observed variation of the solutions in reasonable Λ -interval is often comparable with the experimental incertitude [33], the question how to select Λ properly has not only methodological but quite practical interest.

Several specific values could be listed. Two functions,

$$\Lambda = 3\delta^2/4 \quad \text{and} \quad \Lambda = 3\delta^2/2,$$

enable the exact location of solid walls with second-order accurate boundary schemes, for plane and diagonal Poiseuille flow, respectively, when the distance to boundary is equal to δ , with $\delta = \frac{1}{2}$ for the bounce-back rule (see [19] and references herein). Similar solutions can be derived for the pressure or AADE Dirichlet boundary schemes, [9, 13, 18]. The MRT schemes often apply the TRT solutions to relevant eigenvalue relationships, [2, 5, 11, 40, 47]. In bulk, the two particular TRT configurations, $\Lambda = \frac{1}{12}$ for the third-order and $\Lambda = \frac{1}{6}$ for the fourth order, nullify the corresponding coefficients of the *steady state* Chapman-Enskog expansion [17], improving the accuracy and grid convergence of the scheme for any equilibrium. However, the *exact time-dependent recurrence* equations of

the link-wise operators [30] and the asymptotic analysis [32] of the TRT scheme make evident that the time-dependent solutions depend on the two separate eigenvalues. Several known solutions [9, 12, 44] for Λ^\pm remove the leading-order temporal truncation errors and confirm these predictions.

This dependence of the temporal behaviour on the two relaxation parameters becomes crucial for the robustness of ADE TRT schemes. The exact stability curves [34], recently constructed for the d1Q3 model, show that decreasing Λ^- towards zero results in a drastic fall of the stable velocity range when Λ is fixed. Similar situation takes place when $\Lambda \rightarrow 0$ for fixed diffusion coefficient. One remarkable exception is the optimal OTRT subclass $\Lambda = \frac{1}{4}$. Its exact von Neumann stability area is set in the equilibrium parameter space, independently of Λ^\pm for any velocity set. It follows that the OTRT may keep the same stable velocity range for any Peclet number in one and multi-dimensions [20]. The BGK AADE models have much weaker but also quite distinguished stability properties, guaranteed by the non-negativity of all equilibrium distributions [20]. Extension of the exact von Neumann stability analysis into multi-dimensions beyond the OTRT subclass is perhaps impossible, even for isotropic equilibrium. A search for an approach capable to predict the stability of the numerical scheme from its high-order truncation errors motivates this work.

Section 2 is self-consistent. We first reduce the link-wise recurrence equations (RE) [30] of the L-operator [12] to its TRT subclass. The RE provide an exact dependence of the non-equilibrium components on the equilibrium ones, in the form of central link-wise differences in space and central-differences in time. They easily reveal the three-level time discretization form of the TRT scheme, which is exact on the OTRT subclass only. We then develop the Taylor series high-order analysis of the TRT mass conservation equation, sequentially taking into account the intrinsic numerical diffusion which originates from the evolution of the advection equilibrium component. The RE have been already recognized as an efficient mathematical technique for (i) the exact analysis of the invariance properties of the steady state solutions, and (ii) the derivation of the coefficients of the infinite steady state Chapman-Enskog series, [17, 30]. In this work, they are shown as a simple powerful technique for the consistent derivation of the truncation errors for time-dependent conservation laws. This extends the previous results obtained with the Fourier and Taylor series analysis of pure advection and pure diffusion corrections. Derivation of the fourth-order numerical diffusion makes evident that no combination of Λ^- and Λ^+ is able to cancel the whole fourth-order advection-diffusion error.

Section 3 further develops the anisotropic techniques suitable for the AADE modeling with the MRT, TRT or BGK operators. We present the common weighted-type anisotropic equilibrium distribution, suitable for all the minimal schemes, the d2Q9, d3Q13, d3Q15 and d3Q19 models, and derive their principal necessary stability conditions. The largest stable velocity amplitude (for an arbitrary velocity direction) at given equilibrium and the pair of relaxation rates is referred to as “necessary velocity boundary”. It consists of the diffusion-dominant and advection-dominant branches. The *diffusion-dominant* conditions are imposed by linear von Neumann stability analysis on the *symmetric equilibrium*

components. They are independent of the relaxation rates. The *advection-dominant* stability branch can be also obtained by the von Neumann stability analysis in the hydrodynamic limit $\vec{k} \rightarrow 0$, or, alternatively, by requiring that the effective second-order diffusion is positive semi-definite in the presence of the *second-order* numerical diffusion. Under this condition, the advection stability branch is also independent of the two eigenvalues. This last approach was called the *heuristic stability argument* in a seminal work by C. W. Hirt [25]. The analysis of the truncation errors is much simpler than the von Neumann analysis since it avoids the inspection of the roots of high-order characteristic polynomials, and it can be extended to the non-linear equations [25]. The necessary conditions are not sufficient in general, and the *necessary and sufficient* boundary depends on the two relaxation rates, except for the OTRT subclass. The stability areas are also delineated for other interesting eigenvalue relationships, with the help of the exact and numerical stability analysis, and compared with the optimal OTRT bounds.

Section 4 combines the results of the two previous sections and develops heuristic stability analysis of the *fourth-order truncated correction*. The matrix form of the truncation errors greatly simplifies their interpretation. The idea is to delineate those fourth-order advection-diffusion forms which are able to factorize the effective second-order diffusion form. One specific relationship of the two relaxation rates,

$$\Lambda = \Lambda^{(ext.)}(\Lambda^-),$$

is shown to be responsible for the stability of the scheme in the advection limit. This combination defines the so-called “extended optimal subclass”, discovered by means of the exact von Neumann stability analysis of the d1Q3 scheme [34]. In one dimension, $\Lambda = \frac{1}{4}$ may decrease to $\Lambda = \Lambda^{(ext.)}(\Lambda^-) \in]\frac{1}{8}, \frac{1}{4}]$ without any deterioration of stability. We investigate when this is possible in multi-dimensions, in the presence of anisotropy. This allows us to list the best equilibrium and eigenvalue candidates for optimal stability, and to explain results of the numerical stability analysis.

Section 5 validates the truncation errors and stability analysis by numerical simulations for the evolution of concentration waves, using the anisotropic d2Q9 TRT scheme. Applying the most accurate and/or most stable eigenvalue strategies, we first examine analytically the amplitude, boundness and isotropy of the relative truncated errors, along with their dependence on the advection velocity and the equilibrium weights, for the largest permissible spectre of the anisotropic factors. These predictions are then checked by efficient measurements of the numerical errors. Throughout the paper, the evolution of the Gaussian hill illustrates the stability and accuracy analysis.

Section 6 summarizes the results. Appendix A provides the intermediate steps for derivation of the truncation errors, then illustrates them for two simplest orientations of the velocity and wave vectors, and links the obtained results to the previous (Fourier) solutions. Appendices B and C contain the technical details on the von Neumann and heuristic stability analysis, respectively. Appendix D builds equivalent finite-difference stencils for the proposed anisotropic advection-diffusion equilibrium.

2 The TRT scheme: Recurrence equations and truncation errors

2.1 Fourth-order accurate mass conservation equation

We consider the TRT operator:

$$f_q(\vec{r} + \vec{c}_q, t+1) = [f_q + g_q^+ + g_q^-](\vec{r}, t), \quad g_q^\pm = \lambda^\pm (f_q^\pm - e_q^\pm), \quad \lambda^\pm \in]-2, 0[,$$

$$\text{with } f_q^\pm = \frac{f_q \pm f_{\bar{q}}}{2}, \quad \vec{c}_q = -\vec{c}_{\bar{q}}, \quad q = 0, \dots, Q_m. \quad (2.1)$$

Two equilibrium values, $e_q^+ = e_{\bar{q}}^+$ and $e_q^- = -e_{\bar{q}}^-$ are prescribed for each pair of the opposite velocities $\{\vec{c}_q, \vec{c}_{\bar{q}}\}$, called a link. The transport coefficients of the second-order macroscopic equations are related to two positive eigenvalue functions, $\Lambda^\pm = -(1/\lambda^\pm + \frac{1}{2})$, where Λ^+ defines the bulk and kinematic viscosities for Navier-Stokes equation, while all the coefficients of the diffusion tensor are proportional to Λ^- , [12, 16]. Their product, the so-called magic parameter: $\Lambda = \Lambda^+ \Lambda^-$, may take *a priori* any positive value. However, this parameter is responsible for the physical consistency of the obtained steady state solutions on the one hand [17, 30], and the stability of the TRT scheme, on the other hand, [20, 34, 44]. The BGK operator is recovered with $\lambda^+ = \lambda^- = -1/\tau$, and thus, the “magic” parameter, symbol Λ_{bgk} hereafter, is fixed for the BGK subclass: $\Lambda_{bgk} = \Lambda^{-2} = \Lambda^{+2} = (2\tau - 1)^2/4$.

The recurrence equations [30] (Eq. (53) there, RE hereafter) present specific linear combinations of the evolution equations. They exactly relate the post-collision non-equilibrium components $\{g_q^\pm\}$ to the variation of the equilibrium and non-equilibrium components. The RE readily fit the link-wise L-operators [12, 15], with two proper eigenvalues per link. Reducing them to the TRT operator (2.1), they are read as

$$g_q^\pm(\vec{r}, t) = \left[\bar{\Delta}_t e_q^\pm + \bar{\Delta}_q e_q^\mp - \Lambda^\mp (\Delta_q^2 - \Delta_t^2) e_q^\pm + \left(\Lambda^\pm - \frac{1}{4} \right) (\Delta_q^2 - \Delta_t^2) g_q^\pm \right](\vec{r}, t)$$

$$- \left[\left[\frac{1}{2} \Delta_t^2 + (\Lambda^\pm + \Lambda^\mp) \bar{\Delta}_t \right] g_q^\pm \right](\vec{r}, t), \quad (2.2)$$

with the central time-differences:

$$\bar{\Delta}_t \phi(\vec{r}, t) = (\phi(\vec{r}, t+1) - \phi(\vec{r}, t-1))/2,$$

$$\Delta_t^2 \phi(\vec{r}, t) = \phi(\vec{r}, t+1) - 2\phi(\vec{r}, t) + \phi(\vec{r}, t-1),$$

and the central differences along the link:

$$\bar{\Delta}_q \phi(\vec{r}, t) = (\phi(\vec{r} + \vec{c}_q, t) - \phi(\vec{r} - \vec{c}_q, t))/2,$$

$$\Delta_q^2 \phi(\vec{r}, t) = \phi(\vec{r} + \vec{c}_q, t) - 2\phi(\vec{r}, t) + \phi(\vec{r} - \vec{c}_q, t),$$

$\forall \phi = \{e_q^\pm, g_q^\pm\}$. The steady state recurrence equations are read as [17, 30]:

$$g_q^\pm = \bar{\Delta}_q e_q^\mp - \Lambda^\mp \Delta_q^2 e_q^\pm + \left(\Lambda^\pm - \frac{1}{4}\right) \Delta_q^2 g_q^\pm.$$

The local source quantities M^\pm can be easily incorporated into the TRT scheme replacing $e_q^\pm(\vec{r}, t)$ with $e_q^\pm(\vec{r}, t) - M_q^\pm / \lambda^\pm$, [16]. The exact conservation relations equate the moments of the distribution $\{g_q^\pm(\vec{r}, t)\}$ to the prescribed moments M^\pm of the set $\{M_q^\pm(\vec{r}, t)\}$. Formally putting the source distribution into the equilibrium one avoids any ambiguity associated with treating its variation, e.g., in space [17]. In this paper we omit the mass source term and employ the time-dependent equations (2.2) to build the fourth-order accurate approximation of the exact mass-conservation equation. Substituting RE (2.2) into mass conservation relation: $\sum_{q=0}^{Q_m} g_q^+(\vec{r}, t) = 0$ with $\sum_{q=0}^{Q_m} e_q^+ = \sum_{q=0}^{Q_m} f_q = s$, and noting that the contributions $\sum_{q=0}^{Q_m} \bar{\Delta}_t g_q^+ = \bar{\Delta}_t \sum_{q=0}^{Q_m} g_q^+$ and $\sum_{q=0}^{Q_m} \Delta_t^2 g_q^+ = \Delta_t^2 \sum_{q=0}^{Q_m} g_q^+$ vanish, the exact mass conservation equation of the TRT scheme is read as

$$T(\vec{r}, t) + C(\vec{r}, t) = \Lambda^- D(\vec{r}, t) + \left(\Lambda - \frac{1}{4}\right) \sum_{q=1}^{Q_m} \Delta_q^2 g_q^+(\vec{r}, t), \tag{2.3}$$

where the temporal $T(\vec{r}, t)$, convective $C(\vec{r}, t)$ and diffusive $\Lambda^- D(\vec{r}, t)$ terms are given via the exact finite-difference operators of the equilibrium components:

$$\begin{aligned} T(\vec{r}, t) &= \bar{\Delta}_t s(\vec{r}, t) + \Lambda^- \Delta_t^2 s(\vec{r}, t) \\ &= \left(\Lambda^- + \frac{1}{2}\right) s(\vec{r}, t+1) - 2\Lambda^- s(\vec{r}, t) + \left(\Lambda^- - \frac{1}{2}\right) s(\vec{r}, t-1), \end{aligned} \tag{2.4}$$

$$C(\vec{r}, t) = \sum_{q=1}^{Q_m} \bar{\Delta}_q e_q^-(\vec{r}, t), \quad \text{and} \quad \Lambda^- D(\vec{r}, t) = \Lambda^- \sum_{q=1}^{Q_m} \Delta_q^2 e_q^+(\vec{r}, t). \tag{2.5}$$

Remarkably, the T -operator is a *three-level time difference*, and then the combination of the T , C and $\Lambda^- D(\vec{r}, t)$ is similar (but not identical owing to freedom in selecting Λ^-) to the LFCCDF schemes [35]. These schemes can be rewritten as a leap-frog difference (LF) for the temporal derivative, centred difference (CC) for the convective term and the Du Fort-Frankel approximation (DF) [10] for the diffusion term. The LFDF schemes are unconditionally stable for the pure diffusion linear equation. In this last case, the TRT schemes are stable provided that the equilibrium distribution $\{E_q^+ = e_q^+ / s\}$ is non-negative [20]. Any value of the diffusion coefficient can then be adjusted with Λ^- . A similarity between the one-dimensional BGK model and the Du Fort-Frankel scheme has been discovered by Ancona [3] and very recently adapted by Suga [49] for construction of the multi-level finite-differences in $1d$. We emphasize that the T -operator *exactly* describes the TRT evolution in time only if $\Lambda = \frac{1}{4}$, and then the non-equilibrium contribution $(\Lambda - \frac{1}{4}) \sum_{q=0}^{Q_m} \Delta_q^2 g_q^+(\vec{r}, t)$ vanishes in relation (2.3). In this case, the characteristic

equation (A.12) becomes quadratic for the amplification factor, as for any linear three-time-level difference scheme. This possibility is available for the BGK scheme only when $\Lambda^\pm = \frac{1}{2}$ ($\tau=1$), when the T -operator in turn reduces to the forward-time central difference scheme.

We prescribe that the equilibrium, then the non-equilibrium, depends linearly on s :

$$e_q^\pm(\vec{r}, t) = [E_q^\pm]s(\vec{r}, t), \quad \sum_{q=0}^{Q_m} E_q^+ = 1, \quad g_q^\pm(\vec{r}, t) = [\mathcal{G}_q^\pm]s(\vec{r}, t). \quad (2.6)$$

Substituting these relations into RE (2.2), and expanding $\sum_{q=0}^{Q_m} \mathcal{G}_q^\pm = 0$ into a Taylor series, the fourth-order approximation takes the following form (the intermediate steps are gathered in Section A.1):

$$\partial_t s = (R_1 + R_2 + R_3 + R_4)s, \quad R_1 = -S_1, \quad R_2 = \Lambda^- D_2, \quad D_2 = S_2 - S_1^2. \quad (2.7)$$

In fact, when the temporal variation is expressed via the spatial one with the help of the previous-order macroscopic relations, the terms R_k are all expressed via the E_q^\pm -weighted link-wise differential operators:

$$S_{2k-1} = \sum_{q=1}^{Q_m} E_q^- \partial_q^{2k-1}, \quad S_{2k} = \sum_{q=1}^{Q_m} E_q^+ \partial_q^{2k}, \quad \partial_q = (\nabla \cdot \vec{c}_q), \quad k \geq 1. \quad (2.8)$$

The second-order approximation is read as: $\partial_t s + S_1 s = \Lambda^- D_2 s$. Namely, the $S_1 s$ is the convective term, and the $\Lambda^- D_2 s$ is the *effective* diffusion term, a sum of the modeled diffusion form $\Lambda^- S_2 s$ and the second-order numerical diffusion form $-\Lambda^- S_1^2 s$. The third-order truncated term $R_3 s$ is read as

$$R_3 = c_{3,1} R_{3,1} + c_{3,2} R_{3,2}, \quad (2.9)$$

with

$$R_{3,1} = D_2 S_1, \quad R_{3,2} = S_1^3 - S_3, \quad c_{3,1} = 2\Lambda_{bgk} + \Lambda - \frac{1}{4}, \quad c_{3,2} = \Lambda - \frac{1}{12}.$$

The fourth-order truncated term $R_4 s$ is read as

$$R_4 = c_{4,1} D_2^2 + c_{4,2} D_2 S_1^2 + c_{4,3} R_{4,3} + c_{4,4} R_{4,4}, \quad (2.10)$$

with

$$\begin{aligned} R_{4,3} &= S_4 - S_1 S_3, & R_{4,4} &= S_1^4 - S_1 S_3, \\ c_{4,1} &= -\Lambda^- \left(\Lambda_{bgk} + \Lambda - \frac{1}{4} \right), & c_{4,2} &= \Lambda^- \left(4\Lambda_{bgk} + \Lambda - \frac{3}{4} + \frac{\Lambda(4\Lambda-1)}{4\Lambda_{bgk}} \right), \\ c_{4,3} &= \Lambda^- \left(\Lambda - \frac{1}{6} \right), & c_{4,4} &= \frac{\Lambda^-}{4} \left(8\Lambda - 1 + \frac{\Lambda(4\Lambda-1)}{4\Lambda_{bgk}} \right). \end{aligned}$$

This form of the coefficients has been obtained by D. d’Humières [31] with the help of the Fourier analysis. The links with the previous high-order analysis [12] for the advection and pure diffusion equations are provided in Section A.3. All the coefficients of the truncated terms, R_3 and R_4/Λ^- , are expressed via the two auxiliary functions: Λ_{bgk} and Λ . We recognize that there is no solution for Λ^\pm where the four coefficients $c_{4,1}-c_{4,4}$ vanish. In the next section we specify several solutions which either nullify the third-order error R_3 , or the pure diffusion fourth-order error $R_4(E_q^- \equiv 0)$, or improve the stability of the scheme.

Indeed, three terms are related to the *fourth-order* numerical diffusion of the scheme, namely: (i) $c_{4,2}D_2S_1^2$, (ii) $-c_{4,3}S_1S_3$ and (iii) $c_{4,4}R_{4,4} = c_{4,4}(S_1^4 - S_1S_3)$. Together, they only vanish for pure diffusion equation ($E_q^- \equiv 0$, then $S_1=S_3=0$). The positive semi-definiteness of the effective second-order diffusion form D_2 determines the principal stable velocity range in the presence of the second-order numerical diffusion $-S_1^2$. The two first terms, namely, D_2^2 and $D_2S_1^2$ and also (with some restrictions for the anisotropy) $R_{4,3}$, vanish on the nullspace of D_2 . Then $c_{4,4}R_{4,4}$ becomes the main term responsible for the stability of the scheme in the advection-dominant zone (when $\vec{k} \rightarrow 0$ in terms of Fourier analysis). This analysis is developed in Section 4.

2.2 Particular solutions for two relaxation parameters

We distinguish four eigenvalue configurations, hereafter referred to as “optimal advection” (2.11), “optimal diffusion” (2.13), “optimal stability” (2.14) and “extended optimal stability” (2.15). Each one of them is valid for any velocity scheme and any sets $\{E_q^\pm\}$. They are compared for effective accuracy in Section 3.4 (see Figs. 5- 7) and Section 5 (see Figs. 11-18), and stability in Section 3.5 (see Figs. 8-10).

“**Optimal advection**”. The R_3 vanishes only for the following (BGK) set-up:

$$\Lambda_{bgk} = \Lambda = \frac{1}{12} \quad \text{then} \quad R_3 = 0$$

$$\text{and} \quad \{c_{4,1}, c_{4,2}, c_{4,3}, c_{4,4}\} = -\frac{\Lambda^-}{12} \{-1, 6, 1, 3\}, \quad \text{with} \quad \Lambda^- = \sqrt{\frac{1}{12}}. \quad (2.11)$$

This choice, providing the best advection properties for the TRT scheme, has been first recognized with the help of the Fourier analysis [12] (relations (B.12)-(B.15) there) and the Chapman-Enskog analysis [44] (relation (22) with (14) and (23) there). The link to the Fourier analysis is provided by relation (A.13) in Section A.3. The choice $\Lambda = \frac{1}{12}$ cancels the coefficient $a_3 = 1 + 6(\Lambda - \frac{1}{4})$ of the third-order term in the steady state Chapman-Enskog expansion (see relation (40) in [17]). This fixes the BGK solution [26] (relation (11) for τ_3 there) and the term C_3 [6], obtained from the Taylor series and multi-scale Chapman-Enskog analysis, respectively.

“Optimal diffusion”. When the anti-symmetric equilibrium component vanishes, $E_q^- \equiv 0$ and $R_3 \equiv 0$, the term R_4 is read as

$$R_4(E_q^- \equiv 0) = c_{4,1}S_2^2 + c_{4,3}S_4. \tag{2.12}$$

The two coefficients $c_{4,1}$ and $c_{4,3}$ vanish only for the following (TRT) configuration:

$$\Lambda = \frac{1}{6}, \quad \Lambda_{bgk} = \frac{1}{12} \quad \text{then} \quad R_4(E_q^- \equiv 0) = 0. \tag{2.13}$$

This choice has the best accuracy for the pure diffusion TRT scheme, previously derived with the help of the Fourier analysis [12] (relations (B.4) with (B.6) there). The link to the Fourier analysis is provided by relation (A.15). This solution has been referred as the “advective thermics at fourth-order” for the d2Q9 scheme, [8]. The separate choice $\Lambda = \frac{1}{6}$ cancels the coefficient $a_4 = 1 + 12(\Lambda - \frac{1}{4})$ of the fourth-order term in the steady state Chapman-Enskog expansion for any equilibrium (see relation(40) in [17]), and hence, any weights. Then this choice is also suitable for the hydrodynamic models, in agreement with already obtained solution for the BGK scheme [26] (see relation (11) for τ_4 there).

“Optimal stability”. The choice $\Lambda = \frac{1}{4}$ defines the OTRT subclass [20], where the Q th-order characteristic equation (A.12) reduces to a second-order one, in agreement with a three-time level effective discretization of the TRT scheme. The OTRT family is stable provided that $\mathcal{A}^2 + \mathcal{B}^2 \leq 1$ for $\forall \vec{k}$, with

$$\mathcal{A} = \sum_{q=0}^{Q_m} \cos[\vec{k} \cdot \vec{c}_q] E_q^+ \quad \text{and} \quad \mathcal{B} = \sum_{q=1}^{Q_m} \sin[\vec{k} \cdot \vec{c}_q] E_q^-.$$

When $E_0 \geq 0$ and $\{E_q^+ > 0\}$ for all q , the sufficient OTRT condition is $\sum_{q=1}^{Q_m} (E_q^-)^2 / E_q^+ \leq 1$. The non-negativity condition: $\{E_q = E_q^+ + E_q^- \geq 0\}$ is stronger and hence sufficient for stability of the OTRT subclass. Also, the non-negativity has been proved as sufficient for stability of the linear mass conserving BGK models [20]. However, this condition is not sufficient for the TRT model, in general [20, 34]. Section 3.3 discusses the sufficient OTRT stability conditions for the *anisotropic* equilibrium distributions. The OTRT does not cancel the truncated coefficients, on the one hand:

$$\begin{aligned} \text{OTRT:} \quad & \Lambda = \frac{1}{4} \quad \text{or} \quad \frac{\lambda^- + \lambda^+}{2} = -1, \quad \text{then} \quad \{c_{3,1}, c_{3,2}\} = \left\{ 2\Lambda_{bgk}, \frac{1}{6} \right\} \\ \text{and} \quad & \{c_{4,1}, c_{4,2}, c_{4,3}, c_{4,4}\} = \Lambda^- \left\{ -\Lambda_{bgk}, \frac{(8\Lambda_{bgk} - 1)}{2}, \frac{1}{12}, \frac{1}{4} \right\}, \quad \forall \Lambda^-. \end{aligned} \tag{2.14}$$

On the other hand, the term

$$\Lambda^- \frac{\Lambda(4\Lambda - 1)}{4\Lambda_{bgk}} = \frac{\Lambda}{\Lambda^-} \left(\Lambda - \frac{1}{4} \right)$$

in $c_{4,2}$ and $c_{4,4}$ becomes unbounded in the advection-limit $\Lambda^- \rightarrow 0$ when Λ is fixed, except for $\Lambda = \frac{1}{4}$. One may conjecture that this reduces the stability of the scheme, unless the relevant fourth-order terms vanish or get suitable signs on the nullspace of the diffusion form D_2 . The exact, heuristic and numerical stability analysis will examine these suggestions for multi-dimensional models and in the presence of anisotropy.

“Extended optimal stability”. The last term $c_{4,4}R_{4,4}$ in relation (2.10) consists from the advection operators. The coefficient $c_{4,4}$ vanishes only if Λ is related to Λ_{bgk} in a specific way:

$$c_{4,4} = 0 \quad \text{if} \quad \Lambda = \Lambda^{(ext.)}(\Lambda_{bgk}), \quad \forall \Lambda_{bgk}, \tag{2.15}$$

where

$$\Lambda^{(ext.)}(\Lambda_{bgk}) = \frac{1}{8}(1 - 8\Lambda_{bgk}) + \frac{1}{8}\sqrt{64\Lambda_{bgk}^2 + 1}.$$

Then

$$\begin{aligned} \Lambda^{(ext.)}(\Lambda_{bgk}) &\in \left[\frac{1}{6}, \frac{1}{4} \left[\text{when } \Lambda_{bgk} \in \right] 0, \frac{1}{6} \right], \\ \Lambda^{(ext.)}(\Lambda_{bgk}) &\approx \frac{1}{4} - \Lambda_{bgk} + \mathcal{O}(\Lambda_{bgk}^2), \quad \Lambda_{bgk} \rightarrow 0, \\ \Lambda^{(ext.)}(\Lambda_{bgk}) &\rightarrow \frac{1}{8}, \quad \text{if } \Lambda_{bgk} \rightarrow \infty. \end{aligned}$$

The exact von Neumann stability analysis [34] shows that the d1Q3 TRT model keeps the optimal stability of the OTRT subclass when $\Lambda \geq \Lambda^{(ext.)}(\Lambda_{bgk})$, i.e., when $c_{4,4} \geq 0$ and Λ either belongs to the interval $[\Lambda^{(ext.)}(\Lambda_{bgk}), \frac{1}{4}]$ or $\Lambda \geq \frac{1}{4}$. The BGK model satisfies these two conditions when $\Lambda_{bgk} \geq \frac{1}{6}$. The numerical stability analysis for $\Lambda = \Lambda^{(ext.)}$ has been performed in [34] for the minimal, d2Q9 and d3Q15 isotropic schemes, and it is extended in Section 3.5 for anisotropic schemes. The simplest situations are illustrated in Figs. 8 and 10. Sections 4 and Appendix C relate the advanced stability properties observed for $c_{4,4} = 0$, and partly for $c_{4,4} \geq 0$, to the behaviour of the R_4 -form on the second-order stability line in multi-dimensions. Otherwise, when $\Lambda < \Lambda^{(ext.)}(\Lambda_{bgk})$, the stable velocity amplitude may become proportional to Λ^- (depending on the equilibrium parameters) such that the available Peclet numbers become limited even in the limit $\Lambda^- \rightarrow 0$. This directly follows from the exact stability curves [34] of the d1Q3 model.

“Optimal advection-diffusion”. A particular BGK model nullifies the three (the last ones) coefficients of R_4 :

$$\begin{aligned} \Lambda_{bgk} = \Lambda = \frac{1}{6}, \quad \text{then} \quad \{c_{3,1}, c_{3,2}\} &= \left\{ \frac{1}{4}, \frac{1}{12} \right\}, \\ \text{and} \quad \{c_{4,1}, c_{4,2}, c_{4,3}, c_{4,4}\} &= -\frac{\Lambda^-}{12} \{1, 0, 0, 0\}, \quad \text{with } \Lambda^- = \sqrt{1/6}. \end{aligned} \tag{2.16}$$

This choice belongs to the “extended optimal stability” family. We examine it in Sections 3.5 and 5, with respect to both stability and accuracy.

3 Anisotropic advection-diffusion equation

3.1 Equilibrium distribution

We apply the TRT scheme (2.1) for modeling of the linear advection-diffusion equation with the velocity \vec{U} and full anisotropic diffusion tensor $\Lambda^- \mathcal{D}_{\alpha\beta}$. The TRT operator needs *anisotropic* equilibrium set $\{E_q^+\}$ in order to describe anisotropy, and thus, these components may differ when their velocities \vec{c}_q have the same amplitude [12, 15].

3.1.1 Second-order equation

In this paper, we extend the E-model [12] (given there in the projection MRT-form) and the “weighted” anisotropic d2Q9 and d3Q15 equilibrium forms [34] to the d3Q13 and d3Q19 models, and give them all in a common form:

$$\begin{aligned} E_q^- &= t_q^{(a)}(\vec{U} \cdot \vec{c}_q), \quad E_0 = 1 - \sum_{q=1}^{Q_m} E_q^+ \quad \text{with} \quad U^2 = \sum_{\alpha} U_{\alpha}^2, \quad \bar{U}^2 = \frac{U^2}{d}, \\ E_q^+ &= t_q^{(m)} c_e + g^{(a)} E_q^{(anis)} + g^{(u)} E_q^{(u)}(\vec{U}), \end{aligned} \quad (3.1)$$

where

$$\begin{aligned} E_q^{(anis)} &= w_q^{(m)} \sum_{\alpha=1}^d (\mathcal{D}_{\alpha\alpha} - c_e) c_{q\alpha}^2 + \sum_{\alpha \neq \beta} \frac{g_{\alpha\beta}^{(a)} \mathcal{D}_{\alpha\beta} c_{q\alpha} c_{q\beta}}{\sum_{j=1}^{Q_m} c_{j\alpha}^2 c_{j\beta}^2}, \\ E_q^{(u)}(\vec{U}) &= t_q^{(u)} \bar{U}^2 + w_q^{(u)} \sum_{\alpha=1}^d (U_{\alpha}^2 - \bar{U}^2) c_{q\alpha}^2 + \sum_{\alpha \neq \beta} \frac{g_{\alpha\beta}^{(u)} U_{\alpha} U_{\beta} c_{q\alpha} c_{q\beta}}{\sum_{j=1}^{Q_m} c_{j\alpha}^2 c_{j\beta}^2}. \end{aligned}$$

After substitution of relations (3.1) into $S_1 = \sum_{q=1}^{Q_m} E_q^- \partial_q$ and $S_2 = \sum_{q=1}^{Q_m} E_q^+ \partial_q^2$, and restricting all weight families $t_q^{(\cdot)}$ and $w_q^{(\cdot)}$ to isotropic condition:

$$\sum_{q=1}^{Q_m} t_q^{(\cdot)} c_{q\alpha} c_{q\beta} = \delta_{\alpha\beta} \quad \text{and} \quad \sum_{q=1}^{Q_m} w_q^{(\cdot)} c_{q\alpha} c_{q\beta} = \delta_{\alpha\beta}, \quad \forall \{\alpha, \beta\}, \quad (3.2)$$

the second-order approximation of Eq. (2.7) is read as

$$\partial_t s + S_1 s = \Lambda^- D_2 s, \quad D_2 = \nabla^T \cdot \mathcal{D}^{(eff)} \cdot \nabla = S_2 - S_1^2,$$

where

$$\begin{aligned} S_1 &= \nabla^T \cdot \vec{U} = \nabla^T \cdot \mathcal{M}_u \cdot \vec{1}, \quad \mathcal{M}_u = \{U_{\alpha} \delta_{\alpha\beta}\}, \\ S_1^2 &= \nabla^T \cdot \mathcal{M}_{u^2} \cdot \nabla, \quad \mathcal{M}_{u^2} = \vec{U} \otimes \vec{U} = \{U_{\alpha} U_{\beta}\}, \quad S_2 = \nabla^T \cdot \mathcal{D}^+ \cdot \nabla, \end{aligned}$$

and

$$\begin{aligned} \mathcal{D}_{\alpha\beta}^+ &= \sum_{q=1}^{Q_m} E_q^+ c_{q\alpha} c_{q\beta} \\ &= \left(c_e + g^{(a)} (\mathcal{D}_{\alpha\alpha} - c_e) + g^{(u)} U_\alpha^2 \right) \delta_{\alpha\beta} + \left(g_{\alpha\beta}^{(a)} \mathcal{D}_{\alpha\beta} + g_{\alpha\beta}^{(u)} U_\alpha U_\beta \right) (1 - \delta_{\alpha\beta}). \end{aligned} \quad (3.3)$$

Here, the modeled tensor is $\Lambda^- \mathcal{D}_{\alpha\beta}$. The total tensor build by the set $\{E_q^+\}$ is $\Lambda^- \mathcal{D}^+$. The tensor of the numerical diffusion is

$$\Lambda^- \mathcal{D}^{(num)} = -\Lambda^- \mathcal{M}_{u^2} = -\Lambda^- \{U_\alpha U_\beta\},$$

see, e.g., [12, 20, 44]. The effective diffusion tensor is $\Lambda^- \mathcal{D}^{(eff)} = \Lambda^- (\mathcal{D}^+ + \mathcal{D}^{(num)})$. The non-negative parameter c_e is equal to mean trace value $\frac{1}{d} \sum_{\alpha=1}^d \mathcal{D}_{\alpha\alpha}$. The equilibrium flags $\{g^{(a)}, g_{\alpha\beta}^{(a)}\}$ and $\{g^{(u)}, g_{\alpha\beta}^{(u)}\}$ are equal to zero or one. When $g^{(a)} = 1$, the anisotropic component $\{E_q^{(anis)}\}$ introduces the anisotropy of the diagonal diffusion entries. When $g^{(a)} g_{\alpha\beta}^{(a)} = 1$, the diagonal links describe the cross-diffusion entries $\mathcal{D}_{\alpha\beta}$. When $g^{(u)} = 1$, the correction $\{E_q^{(u)}\}$ builds the anti-numerical-diffusion tensor. It removes the diagonal elements $\mathcal{D}_{\alpha\alpha}^{(num)}$ for all velocity sets. The full models remove the cross-diffusion entries $\mathcal{D}_{\alpha\beta}^{(num)}$ when $g^{(u)} g_{\alpha\beta}^{(u)} = 1$. In what follows, we say “isotropic” model when the modeled tensor is isotropic: $\mathcal{D}_{\alpha\beta} = c_e \delta_{\alpha\beta}$ and $\{E_q^{(anis)} \equiv 0\}$, with or without anisotropic correction $\{E_q^{(u)}\}$.

3.1.2 Equilibrium weights

The three full velocity sets: d2Q9, d3Q15 and d3Q19, have three independent families of weights: $\{t_q^{(m)}\}$, $\{t_q^{(a)}\}$, and $\{t_q^{(u)}\}$. We restrict them to be non-negative, isotropic (they have one value, $t_c^{(\cdot)} \in [0, \frac{1}{2}]$ or $t_d^{(\cdot)}$, for all the coordinate or the diagonal links, respectively), and obey the *isotropic weight* relation (3.2).

The “same” weight families. We will often concentrate on the configuration where all the weights are the same:

$$t_q^{(m)} = t_q^{(a)} = t_q^{(u)} = t_q = \{t_c, t_d\}. \quad (3.4)$$

The same weights have good stability properties for isotropic tensors, [20]. We show in Section 4 that they are also the first candidates for retention of the optimal stability when $\Lambda = \Lambda^{(ext.)}(\Lambda_{bgk})$ (see relation (2.15)), at least, for diagonal tensors.

The minimal models dDQ(2D+1). Their weights are all the same, with $t_c = \frac{1}{2}$, $t_d = 0$. They allow the largest anisotropy of the diagonal entries, $\mathcal{D}_{\alpha\alpha} \in [0, dc_e]$, with the non-negative values $E_{q,c}^+(\vec{U}=0)$. However, the minimal TRT models are restricted to diagonal

tensors, $\mathcal{D}_{\alpha\beta} = 0$ if $\alpha \neq \beta$. This limitation is relaxed with the help of more complicated collision operators [42, 51]. The non-negativity of the immobile component: $E_0 \geq 0$, is necessary for stability of the minimal TRT schemes, [20]. Then, necessarily: $c_e \in [0, c_e^{(nec)} = 1/d]$.

The d2Q9 and d3Q15 schemes. Their diagonal links do not contribute to anisotropy of the diagonal elements, and then $w_c^{(m)} = w_c^{(u)} = \frac{1}{2}$, and $w_d^{(m)} = w_d^{(u)} = 0$. The minimal schemes d2Q5 and d3Q7 are their respective submodels when $t_c = \frac{1}{2}$ and all the diagonal flags are equal to zero: $g_{\alpha\beta}^{(a)} = g_{\alpha\beta}^{(u)} = 0$. The principal necessary conditions are given by relations (3.16) where $E_0 \geq 0$ is necessary for stability of the d3Q15 TRT scheme but not for the d2Q9 scheme. However, we enforce $E_0 \geq 0$ for the d2Q9 scheme in the presence of the off-diagonal elements. For both schemes, enforcing $E_{q,c}^+ \geq 0$, the largest possible disparity of the diagonal entries $\mathcal{D}_{\alpha\alpha}$ is for $t_c^{(m)} = \frac{1}{2}$ (see in Section 3.1.3). The choice $t_c^{(u)} = \frac{1}{2}$ is recommended for the d3Q15 scheme when the numerical diffusion is canceled, at least (see [20] and conditions (3.19)).

The d3Q19 scheme. The d3Q19 model has an additional weight family: $\{w_q^{(m)}\}$, and thus $\{w_q^{(u)}\}$. These weights enable the d3Q19 model to redistribute the deviations of the diagonal elements, $\{\mathcal{D}_{\alpha\alpha} - c_e\}$ or $\{U_\alpha^2 - \bar{U}^2\}$, between the coordinate and the diagonal links freely. They are related to available freedom for projections on the fourth-order basis vectors, $\{(3c_q^2 - 5)p_q^{(xx)}\}$ and $\{(3c_q^2 - 5)p_q^{(ww)}\}$, where $\{p_q^{(xx)} = 3c_{qx}^2 - c_q^2\}$ and $\{p_q^{(ww)} = c_{qy}^2 - c_{qz}^2\}$ are the second-order basis vectors. The fourth-order vectors are absent for all other considered velocity sets (see the MRT basis in [20, 29]). The natural choice is to take the projections on the fourth- and second-order vectors proportional to each other, and then to parametrize them via the weights, as $\{w_q^{(m)}\}$ and $\{w_q^{(u)}\}$, which obey condition (3.2). To be contrasted with the d2Q9 and d3Q15 schemes, the d3Q19 model may prescribe $\{E_{q,c}^+ \geq 0\}$ for any anisotropy of the diagonal entries with any $t_c^{(m)} \in [0, \frac{1}{2}]$, providing that $w_c^{(m)} \in [0, t_c^{(m)}]$. The d3Q7 and d3Q13 models are particular subclasses of the d3Q19 model (3.4) where $t_c = w_c^{(m)} = w_c^{(u)} = \frac{1}{2}$ and $t_c = w_c^{(m)} = w_c^{(u)} = 0$, respectively. Otherwise, we distinguish between two configurations: (i) $t_c^{(m)} = w_c^{(m)}$ and (ii) $w_c^{(m)} = w_c^{(m)*}$:

$$w_c^{(m)*} = \frac{3 + 2t_c^{(m)}}{8}, \quad \text{and} \quad t_c^{(m)} = w_c^{(m)*} \quad \text{if only} \quad t_c^{(m)} = \frac{1}{2}. \quad (3.5)$$

This choice has interesting equivalent discretization properties (see in Section 3.1.2). Moreover, the interval $w_c^{(m)} \in [0, w_c^{(m)*}]$, along with $w_c^{(m)} = \frac{1}{4}$, allows for the largest stable anisotropic diagonal factors (see after Eqs. (3.16)). In turn, the interval $w_c^{(m)} \in [0, t_c^{(m)}] \in [0, w_c^{(m)*}]$ allows for the largest anisotropy of the diagonal entries when the set of coordinate values $\{E_{q,c}^+\}$ is non-negative and thus, this choice is recommended, along with $w_c^{(u)} \in [0, t_c^{(u)}] \in [0, (3 + 2t_c^{(u)})/8]$.

The “hydrodynamic” weights t_q^* . They obey the additional constraint [41]:

$$3 \sum_{q=1}^{Q_m} t_q^* c_{q\alpha}^2 c_{q\beta}^2 = 1 \quad \text{where} \quad \alpha \neq \beta.$$

Their coordinate values are: $t_c^* = \frac{1}{3}$ for the d2Q9 and d3Q15 models, and $t_c^* = \frac{1}{6}$ for the d3Q19 model. The hydrodynamic weights t_q^* are often applied for the mass and advection terms solving the ADE. Indeed, the hydrodynamic weights are not the most stable for the ADE [20] but, as we will show, they improve the anisotropy of the third and, partly, fourth-order truncated corrections (see in Section 5). Next, the hydrodynamic non-linear equilibrium term $\{E_q^* = \frac{t_q^*}{2} (3(\vec{U} \cdot \vec{c}_q)^2 - U^2)\}$ is the particular case of $\{E_q^{(u)}\}$ in Eqs. (3.1) with $t_c^{(u)} = \{\frac{1}{6}, 0, 0\}$ for the d2Q9, d3Q15 and d3Q19 schemes, respectively. Hence, by combining the hydrodynamic weights and E_q^* , one does not obey relation (3.4) and stability may diminish (see examples [34]).

The “best” weights. Several weight families interesting for their stability properties are derived for isotropic tensors and summarized in Tables 1 and 2 in [34]. When $g^{(u)} = 0$, the same weights (3.4) belong to most stable weight families, [20]. Extending previous analysis, the following weight combinations have good stability properties when $g^{(u)} = 1$ (see also in Sections 3.2 and C.3):

$$t_c^{(u)} = d t_c^{(a)} - (d-1) t_c^{(m)}, \quad d = 1, 2, 3. \tag{3.6}$$

This relationship implies the same weight families (3.4) when any two of three weight families are the same. When the numerical diffusion is cancelled, $g^{(u)} g_{\alpha\beta}^{(u)} = 1$, several specific (“best”) advection weight families $t_q^{(a)} = \{t_c^{(a)}, t_d^{(a)}\}$ may reach the stable value $U_a^2 = 1$ when $c_e \rightarrow 0$:

$$\begin{aligned} \text{d2Q9:} \quad & t_c^{(a)} = \frac{1}{4}, \forall t_c^{(u)}, & \text{d3Q15:} \quad & t_c^{(a)} = \frac{1}{4}, \quad t_c^{(u)} = \frac{1}{2}, \\ \text{d3Q19:} \quad & t_c^{(a)} = t_c^{(u)} = w_c^{(u)} = 0, & \text{when} \quad & w_c^{(m)} = t_c^{(m)}. \end{aligned} \tag{3.7}$$

They are valid for the isotropic or anisotropic equilibrium since the structure of the diffusion tensor does not play any role in the limit $c_e \rightarrow 0$. These weights reach the highest Peclet numbers with the largest velocity amplitudes on the OTRT subclass, at least.

The weights and the finite-difference stencils. The finite-difference equivalents of the convection and diffusion operators (2.5) with the equilibrium (3.1) are constructed in Appendix D. Being combined with the three-level time discretization (2.4), they become equivalent to the OTRT schemes (2.3) where the last (non-equilibrium truncated) term vanishes in Eqs. (2.3). Interestingly, the d2Q9 model describes the anisotropic diagonal elements with the same stencils as the isotropic ones, namely with the factor $2(t_c^{(m)} + t_d^{(m)})$

for the central Laplace operators Δ_α^2 , and factor $2t_d^{(m)}$ for the two neighbor ones, $\Delta_\alpha^{2(\pm\beta)}$ (see relations (D.3)). The link between the d2Q9 weights and the conventional nine-points FTCS scheme [24] is provided by relation (D.9). The same stencils for isotropic and anisotropic diagonal tensors are also available for the d3Q19 model, with the factor $2(t_c^{(m)} + 2t_d^{(m)})$ for the Δ_α^2 and factor $t_d^{(m)}$ for each of the four neighbor operators $\Delta_\alpha^{2(\pm\beta, \pm\gamma)}$, but only when $w_c^{(m)} = w_c^{(m)*}$ as given by Eqs. (3.5).

3.1.3 Pure diffusion: sufficient, non-negativity conditions

Pure diffusion linear TRT model is stable for any eigenvalues when E_0 and $\{E_q^+\}$ are all non-negative, [20]. Condition $E_0 \geq 0$ is independent of the anisotropic factors and it only restricts c_e to interval $[0, c_e^{(0)}(t_c^{(m)})]$ as given by Eqs. (3.20). However, the non-negativity conditions $E_{q,c}^+ \geq 0$ and $E_{q,d}^+ \geq 0$ restrict the available anisotropy for the diagonal and cross-diffusion entries, respectively, [15]. Assuming modeling of the diffusion tensor $\Lambda^- \mathcal{D}_{\alpha\beta}$, let us write the reduced diffusion entries as:

$$\mathcal{D}_{\alpha\alpha} = c_e(1 + a_\alpha), \quad \sum_{\alpha=1}^d a_\alpha = 0, \quad \mathcal{D}_{\alpha\beta} = K_{\alpha\beta} c_e, \quad \alpha \neq \beta, \tag{3.8}$$

where $\{a_\alpha\}$ is limited to the interval $[-1, d-1]$, to assure the non-negativity of the diagonal entries. In turn, the cross-diffusion coefficients $\{K_{\alpha\beta}\}$ are constrained to the positive semi-definiteness of the modeled tensor: $\det[\mathcal{D}_{\alpha\beta}] \geq 0$. Adopting parameters [15] for the TRT operator (we divide them by Λ^-), Eqs. (3.1) can be written in equivalent form:

$$\begin{aligned} E_{q,c}^+ &= \frac{1}{2}(\mathcal{D}_{\alpha\alpha} - s_{\alpha\alpha}), & c_{q\alpha} &\neq 0, \\ E_{q,d}^+ &= \sum_{\alpha \neq \beta} \frac{(s_{\alpha\beta} + \mathcal{D}_{\alpha\beta} c_{q\alpha} c_{q\beta})}{\sum_{j=1}^{Q_m} c_{j\alpha}^2 c_{j\beta}^2}, & s_{\alpha\beta} &= 2c_e \sum_{q=1}^{\frac{Q_m}{2}} E_q^+ c_{q\alpha}^2 c_{q\beta}^2, \end{aligned} \tag{3.9}$$

where

$$\begin{aligned} \text{d2Q9, d3Q15: } & s_{\alpha\beta} = s_{\alpha\alpha} = c_e(1 - 2t_c^{(m)}), \quad w_c^{(m)} = w_c^{(u)} = \frac{1}{2}, \quad \forall \alpha, \beta, \\ \text{d3Q19: } & s_{\alpha\beta} = c_e \left[\frac{1 - 2t_c^{(m)}}{2} - (1 - 2w_c^{(m)}) a_\gamma \right], \quad \gamma \neq \beta \neq \alpha, \end{aligned}$$

and

$$s_{\alpha\alpha} = s_{\alpha\beta} + s_{\alpha\gamma} = c_e [(1 - 2t_c^{(m)}) + (1 - 2w_c^{(m)}) a_\alpha]. \tag{3.10}$$

Altogether, the non-negativity constraints then restrict all considered models to diagonally dominant diffusion tensors:

$$\begin{aligned} 2d: & \quad |D_{xy}| \leq s_{\alpha\alpha} \leq \min\{D_{xx}, D_{yy}\}, \\ 3d: & \quad |D_{\alpha\beta}| \leq s_{\alpha\beta}, \text{ then } |D_{\alpha\beta}| + |D_{\alpha\gamma}| \leq s_{\alpha\alpha} \leq D_{\alpha\alpha}, \quad \alpha \neq \beta \neq \gamma. \end{aligned} \tag{3.11}$$

We recall that the diagonal-dominant condition is sufficient but stronger than necessarily for the positive semi-definiteness of the diffusion matrix. Moreover, the diagonal-dominant condition (3.11) is further constrained, e.g:

$$\begin{aligned}
 \text{d3Q13: } & \quad |\mathcal{D}_{\alpha\beta}| \leq \frac{1}{2}(\mathcal{D}_{\alpha\alpha} + \mathcal{D}_{\beta\beta} - \mathcal{D}_{\gamma\gamma}) \text{ if only } \mathcal{D}_{\gamma\gamma} \leq \mathcal{D}_{\alpha\alpha} + \mathcal{D}_{\beta\beta}, \quad \alpha \neq \beta \neq \gamma, \\
 \text{d3Q15: } & \quad |\mathcal{D}_{\alpha\beta}| + |\mathcal{D}_{\alpha\gamma}| + |\mathcal{D}_{\beta\gamma}| \leq s_{\alpha\alpha} \leq \min_{\alpha}^d \{\mathcal{D}_{\alpha\alpha}\}. \tag{3.12}
 \end{aligned}$$

By combining Eqs. (3.10), (3.11) and (3.12), the available anisotropic factors depend on the weights:

$$\text{d2Q9: } \quad |K_{xy}| \leq 1 - 2t_c^{(m)} \leq 1 - |a|, \text{ where } |a_x| = |a_y| = |a| \leq 2t_c^{(m)}, \tag{3.13}$$

$$\text{d3Q15: } \quad |K_{\alpha\beta}| + |K_{\alpha\gamma}| + |K_{\beta\gamma}| \leq 1 - 2t_c^{(m)} \leq \min_{\alpha}^d (1 + a_{\alpha}), \quad a_{\alpha} \in [-2t_c^{(m)}, 4t_c^{(m)}], \tag{3.14}$$

$$\begin{aligned}
 \text{d3Q19: } & \quad |K_{\alpha\beta}| \leq (1 - 2t_c^{(m)}) \left(\frac{1}{2} - a_{\gamma} \right) = (1 - 2t_c^{(m)}) \frac{\mathcal{D}_{\alpha\alpha} + \mathcal{D}_{\beta\beta} - \mathcal{D}_{\gamma\gamma}}{2c_e}, \\
 & \quad \text{when } t_q^{(m)} = w_q^{(m)}, \quad a_{\gamma} \in [-1, 1/2], \\
 & \quad \text{then } |\mathcal{D}_{\alpha\beta}| + |\mathcal{D}_{\alpha\gamma}| \leq (1 - 2t_c^{(m)})\mathcal{D}_{\alpha\alpha}, \quad \mathcal{D}_{\gamma\gamma} \leq \mathcal{D}_{\alpha\alpha} + \mathcal{D}_{\beta\beta}, \quad \forall \alpha \neq \beta \neq \gamma. \tag{3.15}
 \end{aligned}$$

Summary. Enforcing the non-negativity for the whole set $\{E_q^+\}$, the available anisotropy of the modeled diffusion tensor is limited and weight-dependent:

1. The largest anisotropy of the diagonal entries $a_{\alpha} \in [-1, d-1]$ is available for the d2Q9 and d3Q15 models only when $t_c^{(m)} = \frac{1}{2}$, including the d2Q5 and d3Q7 schemes. The d3Q19 model may achieve this with any weight $t_c^{(m)}$ providing that $w_c^{(m)} \in [0, t_c^{(m)}]$.
2. When $t_c^{(m)} = w_c^{(m)} = \frac{1}{2}$, conditions $\{E_{q,d}^+ \geq 0\}$ enforce $\mathcal{D}_{\alpha\beta} = 0$ for all schemes except d3Q19, and for d3Q19 scheme when $t_q^{(m)} = w_q^{(m)}$, at least.
3. In 2D, Eqs. (3.13) is stronger than necessarily for the diagonal-dominance except when $|a| = 2t_c^{(m)}$. The d2Q9 and d3Q15 schemes, but also the d3Q19 with the same weights $t_q^{(m)} = w_q^{(m)}$, reach the largest cross-diffusion values when $t_c^{(m)} = 0$, including the d3Q13 model.

Finally, we emphasize that conditions (3.13)-(3.15) are the sufficient stability conditions for pure diffusion TRT schemes but they are not necessary conditions.

3.2 Stability conditions

The necessary and sufficient (on periodic solutions) von Neumann stability conditions are satisfied when the amplitudes of all the Q roots $\{\Omega_q\}$ of the characteristic equation (A.12) of the TRT scheme (2.1) with the equilibrium (3.1) are found inside the unit

circle, for any wave vector \vec{k} and any direction of velocity vector \vec{U} . Because of the high order of the characteristic polynomials (see relation (A.12) with (A.11)), the exact stability curves $U^2(c_e)$ are obtained only for the d1Q2 and d1Q3 advection-diffusion models [34, 43] and, in multi-dimensions, only on the OTRT sub-class, for the minimal, d2Q9 and d3Q15 isotropic models, [20].

3.2.1 Diffusion-dominant boundary, $\vec{U} = 0$

The necessary and eigenvalue-independent, *diffusion-dominant* generic conditions restrict the linear combinations of the symmetric components. They are established when the wave vector \vec{k} is parallel to the coordinate and diagonal lattice axes (including the 2D diagonal axis for three-dimensional models), and all non-zero components k_α are equal to π . These conditions are given by relations (B.2)-(B.6). Plugging there the anisotropic equilibrium (3.1), the c_e is necessarily assigned to the interval $[0, c_e^{(nec)}]$:

$$\begin{aligned}
 \text{dDQ}(2D+1): \quad & c_e^{(nec)} = \frac{1}{d}, \quad \forall a_\alpha \in [-1, d-1], \\
 \text{d2Q9}: \quad & c_e^{(nec)} = \min \left\{ \frac{1}{1+|a|}, \frac{1}{4t_c^{(m)}} \right\}, \quad |a_x| = |a_y| = |a| \leq 1, \\
 \text{d3Q15}: \quad & c_e^{(nec)} = c_e^{(0)} = \frac{1}{1+4t_c^{(m)}}, \quad a_\alpha \in [-1, 4t_c^{(m)}], \quad \sum_{\alpha=1}^d a_\alpha = 0, \\
 \text{d3Q19}: \quad & c_e^{(nec)} = \min \left\{ \frac{1}{1+|a_\alpha|}, \frac{1}{6t_c^{(m)}}, c_e^{(nec,3)} \right\}, \\
 & \text{where } c_e^{(nec,3)} = \frac{1}{\max_\alpha \{1+2t_c^{(m)} + a_\alpha(1-4w_c^{(m)})\}}. \tag{3.16}
 \end{aligned}$$

Indeed, $c_e^{(nec,3)} \geq 0$ when $a_\alpha \in [-1, d-1]$ only if $w_c^{(m)} = \frac{1}{4}$ or $w_c^{(m)} \in [0, w_c^{(m)*}]$ (see Eq. (3.5)). When $w_c^{(m)} \in [0, t_c^{(m)}] \in [0, w_c^{(m)*}]$ stability condition (B.6) is satisfied with the non-negative coordinate weights $\forall a_\alpha \in [-1, 2]$. Stability conditions (3.16) are sketched for the d3Q15 and d3Q19 schemes in Fig. 1, and, in the presence of velocity and anisotropy in the left pictures in Figs. 2 and 3, for the minimal and d2Q9 schemes.

Summary. Selecting c_e , conditions (3.16) are necessary to respect for any relaxation rates. The stability boundary is independent of the anisotropy for the minimal models and the d3Q15 scheme. For these schemes, $c_e^{(nec)}$ is set by condition $E_0 \geq 0$ providing that the anisotropic range is limited for the d3Q15 scheme to $a_\alpha \leq 4t_c^{(m)}$ by stability condition (B.5). The stable interval $[0, c_e^{(nec)}]$ shrinks towards the minimal interval $[0, 1/d]$ for the d2Q9 and d3Q19 schemes when one of the diagonal diffusion entries approaches stability limit, $a_\alpha \rightarrow d-1$. The most suitable interval of the d3Q19 scheme is $w_c^{(m)} \in [0, t_c^{(m)}] \in [0, w_c^{(m)*}]$, otherwise the d3Q19 scheme may become unstable when

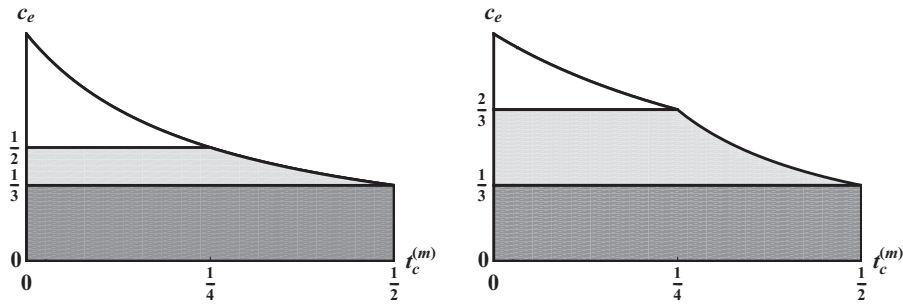


Figure 1: This figure shows necessary stability interval $c_e \in [0, c_e^{(nec)}(t_c^{(m)})]$ given by relations (3.16), for the d3Q15 model when $a_\alpha \leq 4t_c^{(m)}$ (left picture) and the d3Q19 model with $w_c^{(m)} = \frac{1}{4}$ and $a_\alpha = 0$ (right picture). When $a_\alpha \neq 0$, the c_e -interval has to be reduced, if necessary, to $c_e \leq \frac{1}{1 + \max_\alpha |a_\alpha|}$ for the d3Q19 model. The (dark gray) area satisfies conditions (3.16) for any weights and $\forall a_\alpha$.

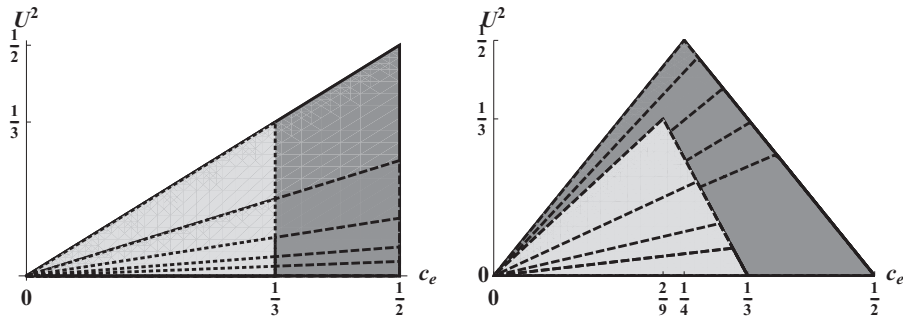


Figure 2: The two diagrams show necessary stability conditions for the d2Q5 and d3Q7 models for $g^{(u)} = 0$ (left picture) and $g^{(u)} = 1$ (right picture), when the minimal diagonal diffusion element reduces from c_e to $c_e/16$ with a ratio $\frac{1}{2}$. The vertical or decreasing boundary is $E_0(c_e) = 0$. The increasing boundary is advection line, (3.22) or (3.23) in 2D. The stable areas below the curves are sufficient on the OTRT subclass for the d2Q5 (gray) and d3Q7 (light gray) models.

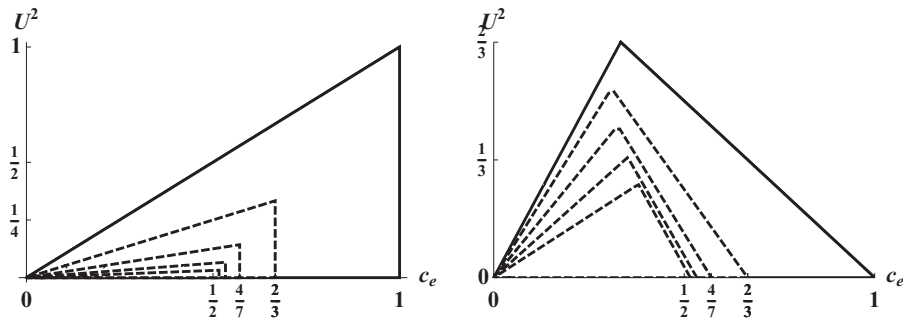


Figure 3: Like the previous picture but for the d2Q9 model with $t_c = \frac{1}{4}$ for all weight families. The advection boundary is the same as for the d2Q5 model but the diffusion boundaries are $c_e^{(nec)} = \frac{1}{1 + |a_\alpha|}$ ($g^{(u)} = 0$) and $U_{d,1}^2 = 1 - c_e(1 + |a_\alpha|)$ ($g^{(u)} = 1$): they narrow down towards the minimal boundary (3.17) when $|a_\alpha| \rightarrow 1$.

$c_e^{(nec,3)} < 0$. In the presence of the cross-diffusion elements $\mathcal{D}_{\alpha\beta}$, $E_0 \geq 0$ is recommended for all schemes.

3.2.2 Diffusion-dominant boundary, $\vec{U} \neq 0, g^{(u)} = 1$

When the numerical diffusion has been corrected, $g^{(u)} = 1$, the set $\{E_0, E_q^+\}$ depends on the velocity. Then the diffusion-dominant conditions (B.2)-(B.6) restrict U^2 , say to the interval $[0, U_{d,nec}^2]$, when $c_e \in [0, c_e^{(nec)}]$ and $c_e^{(nec)}$ is given by Eqs. (3.16):

$$\text{dDQ(2D+1): } U_{d,nec}^2 = \min\{U_{d,1}^2, U_d^2\} = U_d^2 = 1 - dc_e, \tag{3.17}$$

$$\text{d2Q9: } U_{d,nec}^2 = \min\{U_{d,1}^2, U_{d,2}^2\},$$

$$\text{d3Q15: } U_{d,nec}^2 = \min\{U_{d,1}^2, U_d^2, U_{d,3}^2\},$$

$$\text{d3Q19: } U_{d,nec}^2 = \min\{U_{d,1}^2, U_{d,2}^2, U_{d,4}^2\}, \tag{3.18}$$

where

$$\text{all models: } U_{d,1}^2 = 1 - c_e(1 + \max_{\alpha}^d a_{\alpha}), \quad a_{\alpha} \in [-1, d-1],$$

$$\text{d2Q9, d3Q19: } U_{d,2}^2 = \frac{1 - 2dt_c^{(m)}c_e}{2t_c^{(u)}}, \quad t_c^{(u)} \neq 0,$$

$$\text{d3Q15: } U_{d,3}^2 = 3c_e \frac{4t_c^{(m)} - \max_{\alpha}^d a_{\alpha}}{2(1 - 2t_c^{(u)})}, \quad t_c^{(u)} \neq \frac{1}{2},$$

$$\text{d3Q19: } U_{d,4}^2 = \frac{3(1 - \frac{c_e}{c_e^{(nec,3)}})}{1 + 2t_c^{(u)}}, \quad w_c^{(u)} = \frac{1}{4},$$

$$U_{d,4}^2 = \frac{3(1 - \frac{c_e}{c_e^{(nec,3)}})}{2(t_c^{(u)} + 2w_c^{(u)})}, \quad w_c^{(u)} > \frac{1}{4},$$

$$U_{d,4}^2 = \frac{3(1 - \frac{c_e}{c_e^{(nec,3)}})}{3 + 2t_c^{(u)} - 8w_c^{(u)}}, \quad w_c^{(u)} < \frac{1}{4}, \tag{3.19}$$

and

$$\text{d2Q9, d3Q15: } U_d^2 = \frac{d}{1 + 2(d-1)t_c^{(u)}} \left(1 - \frac{c_e}{c_e^{(0)}}\right), \quad c_e^{(0)} = \frac{1}{1 + 2(d-1)t_c^{(m)}},$$

$$\text{d3Q19: } U_d^2 = \frac{2d}{3(1 + 2t_c^{(u)})} \left(1 - \frac{c_e}{c_e^{(0)}}\right), \quad c_e^{(0)} = \frac{2}{3(1 + 2t_c^{(m)})}. \tag{3.20}$$

Hereafter, $U^2 \in [0, U_d^2]$ assures the non-negativity of the immobile component $E_0(c_e, U^2)$ when $c_e \in [0, c_e^{(0)}]$. Note that the diffusion-dominant boundary decreases with c_e except

the $U_{d,3}^2$ -boundary of the d3Q15 scheme, and this increasing (advection-type) constraint vanishes only for $t_c^{(u)} = \frac{1}{2}$. The increasing diffusion branch of the d3Q19 scheme is omitted: it vanishes when $w_c^{(m)} \in [0, w_c^{(m)*}]$ and $w_c^{(u)} \in [0, w_c^{(u)*}]$ (see relation (3.5)).

Summary. The diffusion boundary (3.17) of the minimal schemes lies below the (decreasing) diffusion boundaries of the other schemes, at least when c_e is sufficiently far from zero. Then condition (3.17) can be applied as the simplest sufficient (decreasing) diffusion boundary for all schemes. The increasing diffusion branch vanishes when $t_c^{(u)} = \frac{1}{2}$ for the d3Q15 scheme, and when $w_c^{(m)} \in [0, w_c^{(m)*}]$ and $w_c^{(u)} \in [0, w_c^{(u)*}]$ for the d3Q19 scheme.

3.2.3 Advection-dominant boundary

The diffusion boundary $U_{d,nec}^2$ has to be complemented with the advection-dominant condition, say $U^2 \leq U_a^2(c_e)$. In the presence of the numerical diffusion, this is defined by the k^2 -expansion of the roots of the characteristic equation (A.12) around $k=0$ or, equivalently, requiring the positive semi-definiteness of the effective diffusion tensor $\mathcal{D}^{(eff)}(\vec{U})$ for any velocity direction, [20]. The advection stability line then depends on the dimension of the problem but, to be contrasted with the diffusion conditions, it is independent of the weights. Thus, the advection line $U_a^2(c_e)$ is the same for the d2Q5 and d2Q9 models, on the one hand, and the d3Q7, d3Q15 and d3Q13/d3Q19 schemes, on the other hand. We extend previous analysis to anisotropic diffusion tensors.

When the diffusion tensor is *diagonal*, then $\det[\mathcal{D}^{(eff)}(\vec{U})] \geq 0$ if

$$2D \text{ or } 3D: \quad \sum_{\alpha} \frac{U_{\alpha}^2}{\mathcal{D}_{\alpha\alpha} + g^{(u)}U_{\alpha}^2} \leq 1, \quad \text{if } \mathcal{D}_{\alpha\beta} = 0, \alpha \neq \beta, \mathcal{D}_{\alpha\alpha} \geq 0. \quad (3.21)$$

When $g^{(u)} = 0$, the minimizer \vec{U}_a (the minimum amplitude vector \vec{U}_a which satisfies $\det[\mathcal{D}^{(eff)}(c_e, \vec{U}_a)] = 0$) is parallel to the coordinate axis with the minimal diffusion coefficient, and then

$$U_a^2 = \min_{\alpha}^d \{ \mathcal{D}_{\alpha\alpha} \} = c_e \left(1 + \min_{\alpha}^d a_{\alpha} \right),$$

and $U_a^2 = c_e$ in isotropic case. When $g^{(u)} = 1$ then \vec{U}_a is parallel to a diagonal axis for isotropic tensors, and thus $U_a^2 = \frac{d}{d-1} c_e$, [20]. Figs. 2 and 3 illustrate the reduction in stable velocity amplitude for the diagonal diffusion tensors when the *minimal* diagonal element decreases, from the isotropic value c_e to $c_e/16$ with a factor $\frac{1}{2}$. The necessary stability bounds are plotted for the d2Q5 and d3Q7 models (Fig. 2) and the d2Q9 model (3.4) with $t_c = \frac{1}{4}$ (Fig. 3). The increasing boundary is the advection line. The vertical ($g^{(u)} = 0$) or decreasing ($g^{(u)} = 1$) boundary is set by condition (3.17) for the minimal schemes, and thus it is independent of the anisotropy. This is to be contrasted with the minimum-valued diffusion boundary of the d2Q9 ($t_c^{(m)} = \frac{1}{4}$) scheme, given by $U_{d,1}^2$ in relations (3.19). The

$U_{a,1}^2$ narrows towards the minimal boundary (3.17) when the diagonal elements approach the stability limit.

Next, in the presence of cross-diffusion, the stable velocity amplitude further reduces. Then U_a^2 has to be smaller than the smallest eigenvalue of the diffusion tensor $\{\mathcal{D}_{\alpha\beta}\}$ when $g^{(u)}=0$, and the minimizer is parallel to the corresponding nullspace eigenvector:

$$\begin{aligned}
 g^{(u)}=0: \quad U_a^2 &= \min_{\alpha=1}^d \{\lambda_\alpha\}, \quad \det[\mathcal{D} - \lambda_\alpha \mathcal{I}] = 0, \quad \text{then} \\
 2\text{D}: \quad U_a^2 &= c_e (1 - \sqrt{a^2 + K_{xy}^2}).
 \end{aligned}
 \tag{3.22}$$

When $g^{(u)}=1$ in the presence of cross-diffusion, \vec{U}_a is parallel to a diagonal axis in 2D and U_a^2 is then given by relation (3.23). In the anisotropic 3D case, the exact solution is complicated and we propose the sufficient estimate (3.24) providing that $\sum_{\alpha \neq \beta} |\mathcal{D}_{\alpha\beta}| < \min_{\alpha}^d \{\mathcal{D}_{\alpha\alpha}\}$

$$g^{(u)}=1, 2\text{D}: \quad U_a^2 = 2c_e \left(\sqrt{1-a^2} - |K_{xy}| \right), \quad |K_{xy}| \leq \sqrt{1-a^2},
 \tag{3.23}$$

$$g^{(u)}=1, 3\text{D}: \quad U_a^2 = \frac{3}{2} \left(\min_{\alpha}^d \{\mathcal{D}_{\alpha\alpha}\} - \sum_{\alpha \neq \beta} |\mathcal{D}_{\alpha\beta}| \right).
 \tag{3.24}$$

Summary. (a) We stress that in the presence of the anisotropy the stable velocity amplitude falls below the isotropic boundaries: $U_a^2 = c_e$ or $U_a^2 = \frac{d}{d-1} c_e$, when $g^{(u)}=0$ or $g^{(u)}=1$, respectively, and it reduces to zero in the limit where $\det[\mathcal{D}^{(eff)}] \rightarrow 0$.

(b) When $g^{(u)} g_{\alpha\beta}^{(u)} = 1$, the effective diffusion tensor of the d1Q3 scheme and full models is positive semi-definite: $\mathcal{D}^{(eff)} = \mathcal{D}$, and the advection boundary U_a^2 is not necessary. The effective advection stability boundary is then set by the next, k^4 -terms in expansion, and is difficult to derive. The weight families where this advection constraint may vanish on the OTRT subclass, like for the d1Q3 model [20], are specified by relations (3.7) and discussed below.

3.3 Sufficient stability conditions on the OTRT subclass

3.3.1 Isotropic diffusion tensor

The sufficiency of the minimum-valued combination of the principal necessary advection and diffusion conditions has been proved for the OTRT isotropic models $\{\mathcal{D}_{\alpha\beta} = c_e \delta_{\alpha\beta}\}$, e.g., when $g^{(u)}=0$ and the mass/advection weights are the same, [20]. When $g^{(u)}=1$, the sufficiency of the advection line has been proved for weights (3.6), with the help of the sufficient OTRT stability criterion mentioned before relation (2.14), and provided that the symmetric weights E_q^+ and E_0 are all non-negative, [20]. The non-negativity conditions can be relaxed for the principal weight families. They are summarized in Table 2 [34], along with their stability conditions for isotropic tensors.

3.3.2 Anisotropic diffusion tensor

The sufficient OTRT stability conditions for the *diagonal tensors* are also suggested as the minimum-valued combination of the principal necessary advection-dominant and diffusion-dominant conditions, $U^2 \leq \min\{U_a^2, U_{d,nec}^2\}$ when $c_e \in [0, c_e^{(nec)}]$. This suggestion is confirmed by the numerical stability analysis. However, because of the cross-diffusion which is not accounted by the diffusion-dominant conditions (B.2)-(B.6), we reduce the diffusion boundary $U_{d,nec}^2$ to $U_{d,suf}^2$ enforcing of the non-negativity condition of the immobile component, $U^2 \leq U_d^2$ for the d2Q9 and d3Q19 schemes:

$$\begin{aligned} g^{(u)} = 0: & \quad U^2 \leq U_a^2, \quad \text{when } 0 \leq c_e \leq c_e^{(\max)} = \min\{c_e^{(nec)}, c_e^{(0)}\}, \\ g^{(u)} = 1, g_{\alpha\beta}^{(u)} = 0: & \quad U^2 \leq \min\{U_a^2, U_{d,suf}^2\}, \quad \text{when } c_e \in [0, c_e^{(\max)}], \end{aligned} \tag{3.25}$$

where

$$\begin{aligned} \text{d2Q9:} & \quad U_{d,suf}^2 = \min\{U_{d,1}^2, U_d^2\}, \quad \forall a_\alpha \in [-1, 1], \\ \text{d3Q15:} & \quad U_{d,suf}^2 = \min\{U_{d,1}^2, U_d^2, U_{d,3}^2\}, \quad a_\alpha \in [-2t_c^{(m)}, 4t_c^{(m)}] \in [-1, 2], \\ \text{d3Q19:} & \quad U_{d,suf}^2 = \min\{U_{d,1}^2, U_d^2, U_{d,4}^2\}, \quad \forall a_\alpha \in [-1, 2]. \end{aligned} \tag{3.26}$$

In fact, it can be shown that $c_e \in [0, c_e^{(\max)}]$ with $c_e^{(\max)} = \min\{c_e^{(nec)}, c_e^{(0)}\}$ becomes sufficient for stability of the pure diffusion d2Q9 OTRT model in the presence of cross-diffusion. The additional restriction $a_\alpha \in [-2t_c^{(m)}, 4t_c^{(m)}]$ for the d3Q15 model guarantees $E_{q,c}^+(\vec{U} = 0) \geq 0$ (see Eqs. (3.14)) and dominates the necessary conditions (3.16) for this scheme. A sufficiency of the conditions (3.25) may be readily proved with the help of relation (3.21) and techniques [20, 24] for the minimal models, where \mathcal{D}^+ is diagonal and $U_{d,suf}^2$ reduces to relation (3.17). The necessary conditions of the minimal models are illustrated in Fig. 2. They are sufficient on their OTRT subclass. When $g^{(u)} = 1$, we mainly restrict the weights (3.4) with $t_c = \frac{1}{2}$ to modeling of the diagonal diffusion tensors, where they respect the non-negativity conditions (3.13). Similarly, the limit weights $t_c = 0$ are mainly restricted to isotropic diagonal elements. Quite likely, the limitation for the diagonal tensor can be relaxed for the d3Q15 model with $t^{(a)} = \frac{1}{2}$, along with the d3Q13 limitation for isotropic diagonal elements.

The sufficiency of conditions (3.25)-(3.26) is verified by extensive numerical stability analysis following [34]. Here, we examine condition $\max_q \{|\Omega_q(\vec{U})|\} \leq 1$ on the suggested stability boundary $U^2(c_e)$ when $t_c = \{0, \frac{1}{8}, \frac{1}{6}, \frac{1}{4}, \frac{1}{3}, \frac{1}{2}\}$, by prescribing a very large discrete variation for \vec{U} and \vec{k} . The anisotropic factors, $\{a_\alpha\}$ and $\{K_{\alpha\beta}\}$, vary in their available intervals, which are only restricted to the positive semi-definiteness in 2D. In 3D, we mostly restrict the cross-diffusion elements to the diagonal-dominant conditions, or impose condition (3.24).

Summary. When $g_{\alpha\beta}^{(u)} g^{(u)} = 0$, stability conditions (3.25)-(3.26) have to be respected for any choice of two eigenvalues, and they are expected to be sufficient on the OTRT

subclass, e.g., when the weights are the same. When $g_{\alpha\beta}^{(u)} g^{(u)} = 1$, the advection boundary U_a^2 established for $g^{(u)} = 1$, $g_{\alpha\beta}^{(u)} = 0$ is sufficient, in general, and it vanishes for the “best” weights (3.7). This is demonstrated in the left diagram in Fig. 8 for isotropic tensor: the whole triangle $U^2 \leq 1$, $c_e \in [0, 1]$, is stable for the d2Q9 model (3.7); this area reduces for the two limit weights values and for the hydrodynamic weights but the effective (increasing) stability boundary lies above the advection line $U_a^2 = 2c_e$ (cf. condition (3.23)). In the presence of the anisotropy, the numerical stability analysis confirms the sufficiency of the diffusion boundary alone for the d2Q9 model (3.7) for different values $t_c^{(m)}$ and $t_c^{(u)}$. In particular, $t_c^{(m)} = t_c^{(a)} = t_c^{(u)} = \frac{1}{4}$ is very suitable for the d2Q9 OTRT model, with or without numerical diffusion. The diffusion boundary $U_{d,suf}^2$ alone is sufficient for the selected d3Q15 and d3Q19 models (3.7) only when the cross-diffusion elements are reduced, e.g., to the non-negativity condition $\{E_{q,d}^+ \geq 0\}$. In all cases (3.7), the minimal diffusion boundary (3.17) alone suffices for any anisotropy.

3.4 Evolution of the Gaussian hill with the d2Q9 scheme

Truncated corrections are carefully examined in Section 5 and validated for the evolution of concentration waves. This will show that the fourth-order pure diffusion error is weight-independent for $\Lambda = \frac{1}{6}$, while the third-order advection error is velocity-independent for $\Lambda = \frac{1}{12}$, provided that the numerical diffusion has been corrected. Under this condition, the advection-diffusion fourth-order correction becomes velocity independent only when $\Lambda = \Lambda_{bgk} = \frac{1}{6}$, as given by relation (2.16). Along with the results of stability analysis, these findings are summarized in Section 6. In this section we illustrate the proposed schemes for the evolution of the two-dimensional Gaussian hill using the d2Q9 model. In all cases, we prescribe the isotropic initial distribution for the variance: $\sigma_{\alpha\beta}^2 = 4^2 \delta_{\alpha\beta}$, the equilibrium initial distribution for the populations and periodic boundary conditions.

3.4.1 Pure diffusion

First, the pure diffusion test in Fig. 4 confirms that stable solutions can be reached in the two anisotropic limits: (i) $a = 1$ and (ii) $K_{xy} = 1$. The stable results are obtained with $\Lambda = \{\frac{1}{4}, \frac{1}{6}\}$ in a wide range of the diffusion functions Λ_{bgk} , when $c_e = \frac{1}{2} \leq \frac{1}{1+|a|} \forall |a| \in [0, 1]$ (see relations (3.16), (3.17) and (3.25)). Namely, $\Lambda = \frac{1}{6}$ with $t_c^{(m)} = \{\frac{1}{3}, \frac{1}{2}\}$ and $\Lambda = \frac{1}{4}$ with $t_c^{(m)} = \{0, \frac{1}{3}, \frac{1}{2}\}$ produce the accurate solutions when $a = 1$. However, the stability is lost for $\Lambda = \frac{1}{6}$ with $t_c^{(m)} = 0$. When $K_{xy} = 1$, then $\Lambda = \frac{1}{6}$ with $t_c^{(m)} = \{0, \frac{1}{3}\}$ and $\Lambda = \frac{1}{4}$ with $t_c^{(m)} = 0$ produce accurate solutions. However, the solution is unstable for $\Lambda = \frac{1}{6}$ with $t_c^{(m)} = \frac{1}{2}$. At the same time, solution is stable but loses accuracy when $\Lambda = \frac{1}{4}$ with $t_c^{(m)} = \{\frac{1}{3}, \frac{1}{2}\}$. This agrees with the error estimate for $\Lambda = \frac{1}{4}$ when $K_{xy} = 1$ and $t_c^{(m)} \neq 0$ (cf. after relation (5.11)).

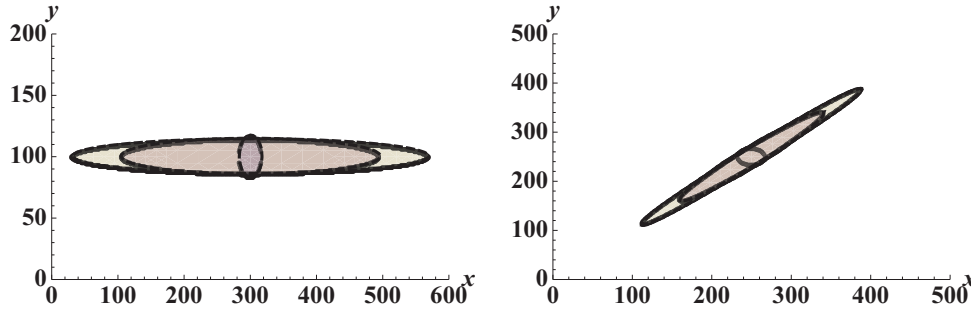


Figure 4: Contour plots $s > 10^{-5}$ illustrate the pure diffusion of the 2D Gaussian hill for two anisotropic limits: $a = 1, K_{xy} = 0$ (left picture, $t = 0, 10^3, 2 \times 10^3$) and $a = 0, K_{xy} = 1$ (right picture, $t = 0, 4 \times 10^2, 10^3$). The analytical solution (dashed) is plotted together with the numerical results (dotted). They are obtained with the d2Q9 model when $c_e = \frac{1}{2}$ and $\Lambda_{bgk} = \frac{25}{12}$. The numerical and analytical solutions practically coincide.

The stable results are also obtained with $\Lambda = \frac{1}{12}$ but only provided that the $\{E_q^+\}$ are all non-negative, i.e., when $t_c^{(m)} = \frac{1}{2}$ for $a = 1$ and $t_c^{(m)} = 0$ for $K_{xy} = 1$.

Summary. These tests recommend, in agreement with the results of the numerical stability analysis below, to respect the non-negativity constraint $E_q^+ \geq 0$ when Λ does not belong to the interval $[\frac{1}{6}, \frac{1}{4}]$, and to avoid the limit weight values, $t_c^{(m)} = 0$ and $t_c^{(m)} = \frac{1}{2}$, when the diagonal or cross-diffusion elements are large, respectively. In agreement with the predictions for the extrema of the fourth-order errors in Section 5.1, $\Lambda = \{\frac{1}{6}, \frac{1}{4}\}$ have a similar accuracy when the diffusion tensor is diagonal but $\Lambda = \frac{1}{6}$ is more accurate than $\Lambda = \frac{1}{4}$ when $K_{xy} = 1$, except when $t_c^{(m)} = 0$.

3.4.2 Advection

Second, the advection limit is illustrated in Fig. 5 when $Pe \approx 31$ (the left diagram) and $Pe \approx 345$ (the right diagram). Hereafter, Pe is the grid Peclet number, $Pe = \frac{|U|}{c_e \Lambda}$. We first set $c_e = 10^{-1}$, $\Lambda_{bgk} = \frac{1}{12}$, $t_c = \{\frac{1}{4}, \frac{1}{3}\}$ and prescribe the minimal diffusion boundary (3.17) for velocity: $U^2 = 1 - 2c_e$ (see left diagram). This choice is expected to be quite stable when $g^{(u)} g_{\alpha\beta}^{(u)} = 1$ and $\Lambda = \{\frac{1}{6}, \frac{1}{4}\}$ (see Fig. 8), but it very closely approaches or even slightly exceeds the stability curves when $\Lambda = \frac{1}{12}$ (see the right diagram in Fig. 9). The left diagram in Fig. 5 shows that $\Lambda = \Lambda_{bgk} = \frac{1}{12}$ produces very accurate solutions for the two weight families, while the solutions obtained with $\Lambda = \frac{1}{4}$ are noticeably less accurate. In turn, when $\Lambda = \frac{1}{4}$, the hydrodynamic weights $t_c = \frac{1}{3}$ are more accurate than the most stable choice (3.7): $t_c = \frac{1}{4}$. The accuracy of $\Lambda = \frac{1}{6}$ is only slightly inferior to $\Lambda = \frac{1}{12}$ in this test. Then c_e is reduced by a factor 10 and velocity is increased to $U^2 = 1 - c_e$ with $c_e = 10^{-2}$. The right diagram in Fig. 5 confirms that, in agreement with the predictions, this configuration remains stable for $\Lambda = \frac{1}{6}$ and $t_c^{(m)} = \frac{1}{4}$ where, however, the solution is still less accurate than for $\Lambda = \frac{1}{4}$. We observe that when c_e approaches zero, $U^2 = 1 - c_e$ is unstable for $\Lambda = \frac{1}{12}$

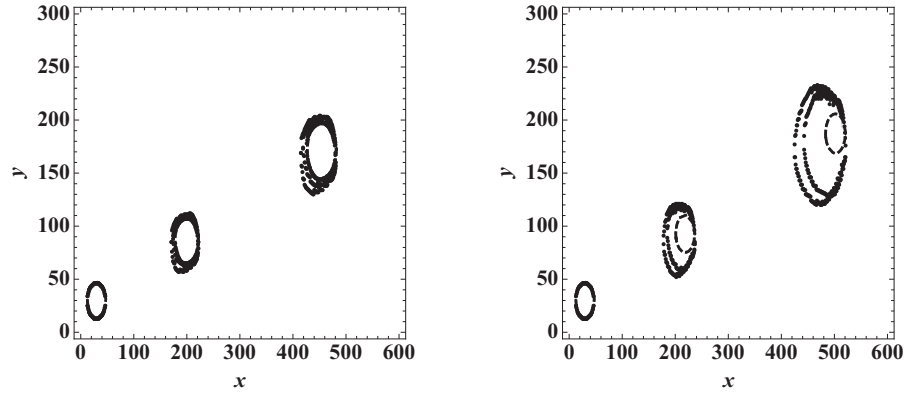


Figure 5: Contour plots $s > 10^{-5}$ for the evolution of the 2D Gaussian hill in the advection limit, when $\Lambda_{bgk} = \frac{1}{12}$, $U_y/U_x = \frac{1}{3}$ and $t=0,200,500$. The analytical contour is dashed. Left diagram: $c_e=10^{-1}$, $U^2=1-2c_e$, $U_x \approx 0.85$, $U_y \approx 0.28$, $Pe = 8\sqrt{15} \approx 31$, $\Lambda = \frac{1}{12}$ (best, solid line, coincides with the analytical contour), $\Lambda = \frac{1}{4}$ with $t_c = \frac{1}{3}$ (intermediate) and $t_c = \frac{1}{4}$ (worst). Right diagram: $c_e=10^{-2}$, $U^2=1-c_e$, $U_x \approx 0.94$, $U_y \approx 0.32$, $Pe = 60\sqrt{33} \approx 345$, $\Lambda = \frac{1}{4}$ with $t_c = \frac{1}{3}$ (best) and $t_c = \frac{1}{4}$ (worst). Solutions with $\Lambda = \frac{1}{6}$ are similar to $\Lambda = \frac{1}{4}$; $\Lambda = \frac{1}{12}$ is unstable.

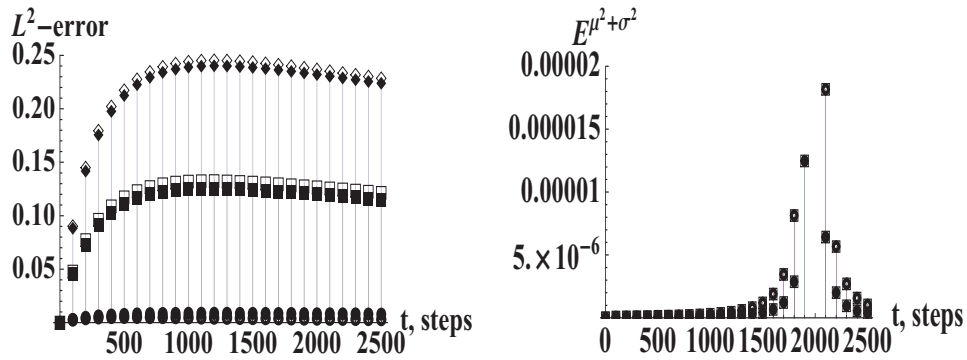


Figure 6: The L^2 -error (left diagram) and the relative error on the second raw moment (right diagram) are plotted versus the number of the time steps for the evolution of the Gaussian hill with the isotropic diffusion tensor when $U_y/U_x = \frac{1}{3}$ and $U^2 = 1/16$. The results are obtained with the d2Q9 model for $t_c^{(m)} = \frac{1}{4}$, $c_e = 0.046875$, when $\Lambda_{bgk} = \frac{1}{12}$ ($Pe = 18.5$) and $\Lambda_{bgk} = \frac{1}{6}$ ($Pe = 13.1$), for $\Lambda = \{\frac{1}{12}, \frac{1}{6}, \frac{1}{4}\}$. Left picture: the error is set by Λ , with diamonds for $\Lambda = \frac{1}{4}$, squares for $\Lambda = \frac{1}{6}$, and circles for $\Lambda = \frac{1}{12}$, the open symbols are for $\Lambda_{bgk} = \frac{1}{12}$. Right picture: the error is set by Λ_{bgk} , with the largest amplitude for $\Lambda_{bgk} = \frac{1}{12}$ (open symbols).

(any weights) and $\Lambda = \frac{1}{6}$ (e.g., $t_c = \frac{1}{3}$). This agrees with the stability diagram in Fig. 9 (right picture).

Actually, a very significant loss of accuracy and weight-dependence of the error observed for both $\Lambda = \frac{1}{4}$ and $\Lambda = \frac{1}{6}$ when $c_e \leq 10^{-2}$ suggest that the error originates from the third-order advection error, examined in Section 5.2. We observe there that similar errors behind the front in Fig. 16 disappear for the special advection solution (5.14). This solution removes the third-order correction for any Λ when $U^2 = 1 - c_e$ and $\Lambda_{bgk} = \frac{1}{12}$ but,

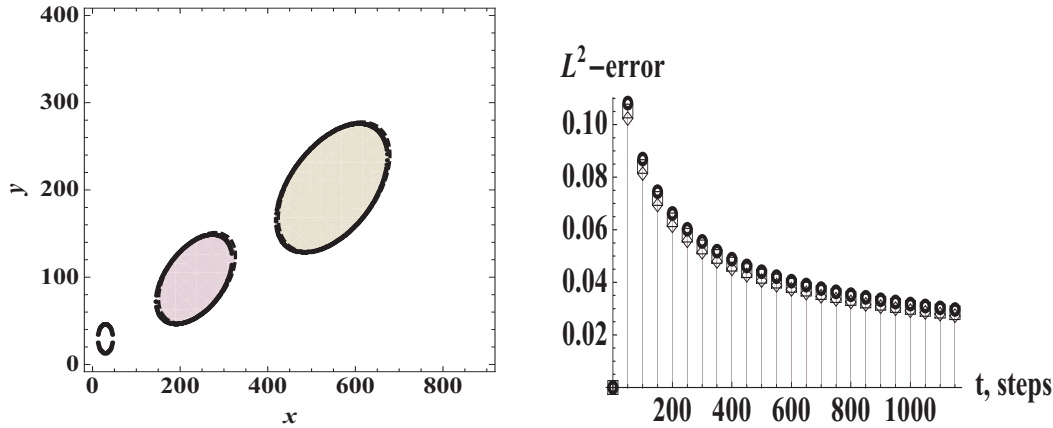


Figure 7: Contour plots $s > 10^{-5}$ for the 2D evolution of the Gaussian hill with the anisotropic tensor when $\Lambda_{bgk} = 25/12$, $a = \frac{1}{2}$ and $K_{xy} = \frac{1}{2}\sqrt{(1-a^2)} = \sqrt{3}/4$, $c_e = 0.348915$, $U_y/U_x = \frac{1}{3}$ and $U^2 = 0.302169$. The results are obtained with $t_c^{(m)} = \frac{1}{3}$ when $\Lambda = \{\frac{1}{12}, \frac{1}{6}, \frac{1}{4}\}$ (circles, triangles, diamonds). The solution is plotted for $\Lambda = \frac{1}{4}$ when $t = \{0, 4 \times 10^2, 2 \times 10^3\}$ time steps.

a-priori, only in 1D. Indeed, even prescribing relations (5.14), the error rapidly increases in the 2D when c_e decreases towards zero (right diagram in Fig. 5). The left diagram in Fig. 6 shows that the L^2 -distribution error is also controlled by Λ , in advection-dominant regime at least, when Pe varies from 13.1 to 18.5. Note that this situation may change, in principle, with the more accurate initial distribution. At the same time, the errors on the second moments, raw or central, are controlled by Λ_{bgk} and they are almost independent of Λ .

Summary. On the one hand, these simulations confirm the ability of the d2Q9 model with $\Lambda = \{\frac{1}{6}, \frac{1}{4}\}$ to reach very high Peclet numbers Pe with the high velocities ($U^2 \approx 1 - c_e$) for small c_e (see Fig. 8). The TRT scheme may then increase Pe as $\frac{1}{c_e \Lambda^-}$, reducing both c_e and Λ^- . On the other hand, the solutions become inaccurate when $c_e \lesssim 10^{-2}$, unless for the 1D solution (5.14). The “optimal advection” relationship $\Lambda = \Lambda_{bgk} = \frac{1}{12}$ produces very accurate solutions but the stable velocity drastically falls when the Peclet number grows, either when $c_e \rightarrow 0$, or when $\Lambda^- \rightarrow 0$, or both (see the right diagram in Fig. 8). The Peclet number increases only as $\approx 1/\sqrt{c_e}$ when $c_e \in]0, 10^{-2}]$ and $\Lambda_{bgk} = \frac{1}{12}$, and still slower when Λ_{bgk} reduces. This may put a limit on the efficient modeling of the high Peclet numbers with the advanced accuracy, unless the balance between the $\Lambda = \{\frac{1}{6}, \frac{1}{4}\}$ and $\Lambda = \frac{1}{12}$ is established.

3.4.3 Advection-diffusion

Finally, Fig. 7 illustrates the intermediate situation where the middle-range anisotropic factor $a = \frac{1}{2}$ is applied together with $K_{xy} = \sqrt{1-a^2}/2 = \sqrt{3}/4$, and the c_e is the bisection of the advection line (3.23) and the minimal diffusion line (3.17): $c_e = 0.348915$ and $U^2 \approx$

0.3. Note that the restriction to the advection line is not necessary in principle, since the numerical diffusion is completely removed. Here, the contour plots are accurate and very similar for all three Λ values. This is confirmed by the L^2 -error in the right diagram.

Summary. Altogether, these three situations indicate that the same weights (3.4), e.g., with $t_c = \{\frac{1}{3}, \frac{1}{4}\}$, are suitable for the middle-range anisotropic simulations with the d2Q9 model when $\Lambda = \{\frac{1}{12}, \frac{1}{6}, \frac{1}{4}\}$, but a special attention has to be paid for the choice of the equilibrium weights and all parameters: $c_e, \Lambda_{bgk}, \Lambda$ and $U^2(c_e, \Lambda_{bgk}, \Lambda)$, in the anisotropic and advection limits, and especially when $\Lambda^- \rightarrow 0$ or $c_e \rightarrow 0$.

3.5 Stability boundaries when $\Lambda \neq \frac{1}{4}$

The minimum-valued combination of the advection and diffusion boundaries is not sufficient when $\Lambda \neq \frac{1}{4}$, in general. The exact stability curves of the d1Q3 model show a drastic velocity reduction when $\Lambda \rightarrow 0, \forall \Lambda_{bgk}$, even when the numerical diffusion has been corrected, [34]. Moreover, when $\Lambda < \Lambda^{(ext.)}(\Lambda_{bgk})$ and $\Lambda^- \rightarrow 0$, the available Peclet numbers are *bounded* when $c_e < 1 - 4\Lambda$, with $Pe^{max} \in [10, 20]$, unless in the limit $c_e \rightarrow 0$. In this section we examine stability areas for several distinguished relationships, such as (2.11), (2.13), (2.15) and (2.16), against the d2Q9 OTRT scheme.

3.5.1 “Optimal advection” solution (2.11), $\Lambda = \Lambda_{bgk} = \frac{1}{12}$

The effective stability boundaries are illustrated on the right diagrams in Figs. 8 and 9 for isotropic diffusion tensor. We first observe in Fig. 9 (the two diagrams) that the diffusion boundary $c_e = c_e^{(max)}$ noticeably narrows the stable area, except for the two limit weights: $t_c = 0$ and $t_c = \frac{1}{2}$ where it is set by the non-negativity condition of the immobile weight. Next, the left diagram in Fig. 9 shows the same decrease of the isotropic stability boundary $U^2 = c_e$ for the three weight families (3.4): $t_c = \{\frac{1}{4}, \frac{1}{3}, \frac{1}{2}\}$, and a slightly stronger decrease for $t_c^{(m)} = 0$. When $g^{(u)} g_{\alpha\beta}^{(u)} = 1$, the right diagram shows a very noticeable velocity fall towards zero in the neighborhood of $c_e = 0$, in comparison with the stability of the OTRT subclass (see the left picture in Fig. 8). This is also observable for $c_e \in]0, 10^{-1}]$ on the right diagram in Fig. 8 where the “optimal advection” solution is significantly less stable than the “optimal advection-diffusion” BGK solution (2.16): $\Lambda = \Lambda^{(ext.)}(\Lambda_{bgk} = \frac{1}{6}) = \frac{1}{6}$. This shows that the solution (2.11) only slightly exceeds $U^2 = c_e$ when $c_e \lesssim 10^{-2}$.

3.5.2 “Optimal diffusion” (2.13) and “optimal advection-diffusion” (2.16)

The two choices give $\Lambda_{bgk} = \frac{1}{6}$, with $\Lambda = \frac{1}{12}$ and $\Lambda = \frac{1}{6}$. The diffusion boundary only slightly displaces for $t_c = \frac{1}{4}$, from $c_e^{(nec)} = 1$ to $c_e^{(max)} \approx \frac{9}{10}$ (data is not shown). Further analysis indicates that when $\Lambda = \frac{1}{6}$ and $\Lambda_{bgk} \lesssim 4$, the interval $c_e^{(max)} = \min\{c_e^{(nec)}, c_e^{(0)}\}$ remains sufficient for the pure diffusion anisotropic d2Q9 scheme with $t_c^{(m)} = \{\frac{1}{4}, \frac{1}{3}\}$ in the whole range $|a| \leq 1$ and $K_{xy}^2 \leq 1 - a^2$. This is also valid for the two limit weights, enforcing the non-negativity condition (3.13), at least. The right diagram in Fig. 8 shows

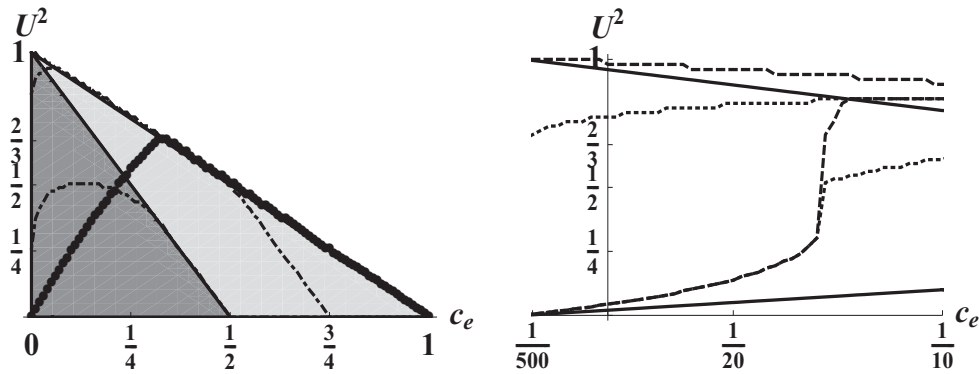


Figure 8: The left diagram shows the stable areas (below the curves) of the d2Q9 OTRT subclass when the second-order numerical diffusion is canceled ($g^{(u)}g_{xy}^{(u)}=1$) and the modeled tensor is isotropic, for four weight families: $t_c^{(m)}=0$ (circles), $t_c^{(m)}=\frac{1}{4}$ (the whole triangle $U^2 \leq 1-c_e$), $t_c^{(m)}=\frac{1}{3}$ (dotted-dashed) and $t_c^{(m)}=\frac{1}{2}$ (dotted). The right diagram compares stability boundaries when $c_e \in [0, 10^{-1}]$ for two BGK models: $\Lambda = \Lambda^{(ext.)}(\Lambda_{bgk}=\frac{1}{6})=\frac{1}{6}$ (two top curves) and $\Lambda = \Lambda_{bgk}=\frac{1}{12}$ (two bottom curves), with $t_c=\frac{1}{4}$ (dashed) and $t_c=\frac{1}{3}$ (dotted). The solid lines are $U^2=1-2c_e$ (both pictures) and $U^2=c_e$ (right picture).

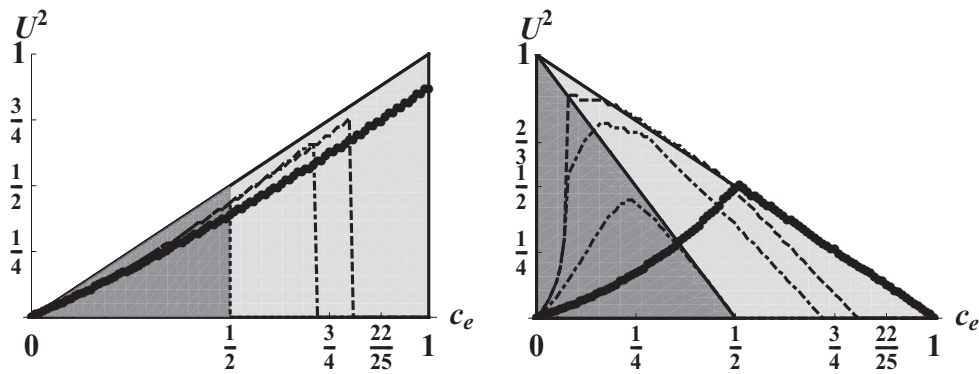


Figure 9: The two diagrams show the stable areas of the isotropic d2Q9 model for the “optimal advection” solution (2.11): $\Lambda_{bgk}=\Lambda=\frac{1}{12}$, when $g^{(u)}=0$ (left picture) and $g^{(u)}g_{xy}^{(u)}=1$ (right picture). Like the previous figure: $t_c^{(m)}=0$ (circles), $t_c^{(m)}=\frac{1}{4}$ (dashed), $t_c^{(m)}=\frac{1}{3}$ (dotted-dashed) and $t_c^{(m)}=\frac{1}{2}$ (dotted).

that the solution (2.16) retains the optimal stability of the OTRT subclass, with $U^2=1-c_e$ for $t_c=\frac{1}{4}$. On the whole, the both solutions only slightly reduce the stable areas with respect to choice $\Lambda=\frac{1}{4}$, with or without numerical diffusion.

3.5.3 “Extended optimal stability” (2.15)

A sufficiency of the optimal stable areas when Λ reduces to $\Lambda^{(ext.)}(\Lambda_{bgk})$ has been analytically confirmed for the d1Q3 model, and observed for the optimal advection lines in case of the minimal models or several full models, [34]. The limit case $\Lambda = \Lambda^{(ext.)}(\Lambda_{bgk}=\frac{1}{6})=\frac{1}{6}$ confirms this when the weights are the same, at least. The left picture in Fig. 10 demon-

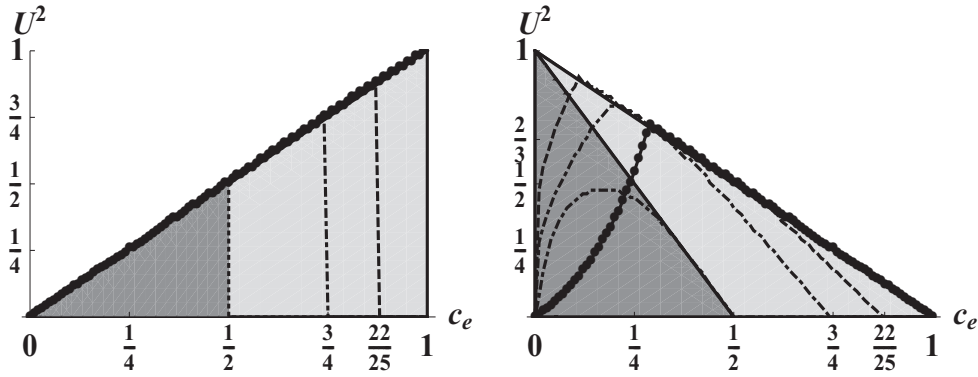


Figure 10: The two diagrams show the stable areas of the isotropic d2Q9 model when $\Lambda = \Lambda^{(ext.)}(\Lambda_{bgk}) = 0.13(3) < \frac{1}{6}$ and $\Lambda_{bgk} = 1$, with $g^{(u)} = 0$ (left diagram) and $g^{(u)}g^{(u)}g^{(xy)} = 1$ (right diagram). Like the previous figure: $t_c^{(m)} = 0$ (circles), $t_c^{(m)} = \frac{1}{4}$ (dashed), $t_c^{(m)} = \frac{1}{3}$ (dotted-dashed) and $t_c^{(m)} = \frac{1}{2}$ (dotted). The optimal stable area is retained when $g^{(u)} = 0$ but it reduces when the numerical diffusion is canceled. When $\Lambda = \Lambda^{(ext.)}(\Lambda_{bgk}) \in [\frac{1}{6}, \frac{1}{4}]$, the optimal advection boundary is kept in the two cases.

states that the optimal isotropic advection boundary $U^2 = c_e$ is kept for all four weight families (3.4) when $\Lambda_{bgk} = 1$ and $\Lambda = \Lambda^{(ext.)}(\Lambda_{bgk}) < \frac{1}{6}$. Similar results are obtained when $g^{(u)} = 1$ but $g^{(xy)} = 0$: the optimal boundary $U^2 = 2c_e$ is retained when $\Lambda = \Lambda^{(ext.)}(\Lambda_{bgk})$ except for $t_c = 0$ (when Λ_{bgk} is not too small). Indeed, the stable area drastically reduces when $t_c^{(m)} = 0$ and $\Lambda_{bgk} \rightarrow \infty$ (then $\Lambda \rightarrow \frac{1}{8}$), quite likely because of the anisotropic diagonal terms U_α^2 in the modeled tensor \mathcal{D}^+ . Note that $U^2 = 2c_e$ also declines when $\Lambda = \Lambda^{(ext.)}(\Lambda_{bgk})$ but the weights are not equal, e.g., applying the “hydrodynamic” form E_q^* where $t_c^{(u)} = \frac{1}{6}$ when $t_c^{(a)} = t_c^{(a)} = \frac{1}{3}$ (see Fig. 11 in [34]).

When the numerical diffusion is canceled, the optimal stability is retained only when $\Lambda = \Lambda^{(ext.)}(\Lambda_{bgk}) \in [\frac{1}{6}, \frac{1}{4}]$, i.e. when $\Lambda_{bgk} \leq \frac{1}{6}$. The anisotropic advection lines (3.22) and (3.23) then keep their sufficiency, enforcing the non-negativity condition (3.13) for the limit weights. Otherwise, the effective advection boundary rapidly deteriorates. This is demonstrated for the isotropic tensor in the right diagram in Fig. 10 when $\Lambda_{bgk} = 1$ and $\Lambda = \Lambda^{(ext.)}(\Lambda_{bgk}) < \frac{1}{6}$. Moreover, when $\Lambda_{bgk} > \frac{1}{6}$ and $\Lambda = \Lambda^{(ext.)}(\Lambda_{bgk}) \in [\frac{1}{8}, \frac{1}{6}]$, the anisotropy has to be reduced towards the sufficient non-negativity conditions (3.13) for pure diffusion equation. The advection boundaries (3.22) and (3.23) are then sufficient only for the diagonal tensors. The d3Q15 model may keep the optimal stable area in the presence of cross-diffusion even for $\Lambda_{bgk} \geq \frac{1}{6}$ provided that the increasing boundary $U_{d,3}^2(c_e)$ dominates the advection line.

3.5.4 Summary

Numerical observations indicate that the optimal stability lines (3.22) and (3.23) can be retained by the d2Q9 scheme with the same weights (3.4) when $\Lambda_{bgk} \leq \frac{1}{6}$ and $\Lambda =$

$\Lambda^{(ext.)}(\Lambda_{bgk}) \in [\frac{1}{6}, \frac{1}{4}]$, in the presence of anisotropy. This includes the “optimal-diffusion” solution (2.13). When $\Lambda \geq \frac{1}{6}$, the stable diffusion areas $c_e \in [0, c_e^{(max)}]$ are approximately valid. However, when $\Lambda_{bgk} > \frac{1}{6}$ and $\Lambda = \Lambda^{(ext.)}(\Lambda_{bgk}) \in [\frac{1}{8}, \frac{1}{6}]$, the advection boundaries only suffice for the diagonal-dominant tensors, restricting anisotropic factors to the non-negativity conditions (3.13). The “optimal advection” choice (2.11) lies beyond the extended optimal interval and it significantly decreases stable velocity amplitude. In the advection limit $c_e \rightarrow 0$, the available Peclet numbers vary from $Pe \approx \frac{1}{c_e \Lambda}$ when $\Lambda = \Lambda^{(ext.)}(\Lambda_{bgk}), \forall \Lambda^-$, to $Pe \approx 1/\sqrt{12c_e}$ for solution (2.11) when the numerical diffusion has removed. Next section aims to explain the optimal stability when $\Lambda = \Lambda^{(ext.)}(\Lambda_{bgk})$ and $\Lambda_{bgk} \leq \frac{1}{6}$, for isotropic or anisotropic tensors, and depending on weight relationships.

4 Heuristic stability analysis

One of our objectives is to examine when the extended optimal subclass (2.15): $\Lambda = \Lambda^{(ext.)}(\Lambda_{bgk})$ retains the advection stability line $U^2 = U_a^2$ given by relations (3.22) and (3.23) in 2D. The advection line corresponds to the minimum amplitude velocity vector \vec{U}_a which gives $\det[\mathcal{D}^{(eff)}(\vec{U}_a)] = 0$. In fact, if the diffusion form D_2 vanishes: $D_2 = \nabla^T \cdot \mathcal{D}^{(eff)} \cdot \nabla = 0$, then $\nabla^T \cdot \mathcal{D}^{(eff)} \cdot \mathcal{M} \cdot \nabla = 0$ for any $[d \times d]$ matrix \mathcal{M} . Our heuristic argument consists of conjecture that those truncated terms which factorize $\mathcal{D}^{(eff)}$ with some matrix \mathcal{M} do not perturb the sufficient advection line. We point out that this analysis will not cover two other principal limits: (i) when the second-order numerical diffusion is removed and $\mathcal{D}^{(eff)}$ is positive semi-definite, and (ii), the diffusion-dominant boundary since it does not satisfy condition $D_2 = 0$.

The matrix form of the truncation errors allows for an easier inspection of their factorization by $\mathcal{D}^{(eff)}$. The auxiliary matrix operators are given by Eqs. (3.3) and (C.1)-(C.2). The matrix form of the third-order term R_3 (cf. relation (2.9)) is build from three following components:

$$\begin{aligned}
 S_1^3 &= \nabla^T \cdot [\mathcal{M}_u \cdot \mathcal{M}_\nabla^{(1)} \cdot \mathcal{M}_{u^2}] \cdot \nabla, & D_2 S_1 &= \nabla^T \cdot [\mathcal{M}_u \cdot \mathcal{M}_\nabla^{(1)} \cdot \mathcal{D}^{(eff)}] \cdot \nabla, \\
 S_3 &= \nabla^T \cdot [\mathcal{M}_u \cdot \mathcal{M}_a^{(1)}] \cdot \nabla = \sum_{\alpha=1}^d U_\alpha \partial_\alpha^3 + w \sum_{\alpha \neq \beta} U_\alpha \partial_\alpha \partial_\beta^2.
 \end{aligned}
 \tag{4.1}$$

Hereafter, we assume that w is related to the corresponding equilibrium weights by relations (C.2). The operator S_3 factorizes the Laplace operator $\Delta = \sum_{\alpha=1}^d \partial_\alpha^2$ only for the hydrodynamic weights, since they give $w = 1$ (see relations (C.2)), then $S_3 = (\nabla^T \cdot \vec{U}) \Delta$. The two components of the advection-based fourth-order operator $R_{4,4} = S_1^4 - S_1 S_3$ are

$$S_1 S_3 = \nabla^T \cdot [\mathcal{M}_{u^2} \cdot \mathcal{M}_a^{(2)}] \cdot \nabla, \quad \text{and} \quad S_1^4 = \nabla^T \cdot [\mathcal{M}_{u^2} \cdot \mathcal{M}_\nabla^{(2)} \cdot \mathcal{M}_{u^2}] \cdot \nabla.
 \tag{4.2}$$

The two fourth-order operators $D_2 S_1^2$ and D_2^2 factorize the matrix $\mathcal{D}^{(eff)}$:

$$\begin{aligned} D_2 S_1^2 &= \nabla^T \cdot [\mathcal{D}^{(eff)} \cdot \mathcal{M}_{\nabla}^{(2)} \cdot \mathcal{M}_{u^2}] \cdot \nabla, \\ D_2^2 &= \nabla^T \cdot [\mathcal{D}^{(eff)} \cdot \mathcal{M}_{\nabla}^{(2)} \cdot \mathcal{D}^{(eff)}] \cdot \nabla. \end{aligned} \tag{4.3}$$

The remaining operator $R_{4,3} = S_4 - S_1 S_3$ is the most complicated. Writing the operator S_4 in the matrix form: $S_4 = \nabla^T \cdot \mathcal{M}_4 \cdot \nabla$ we obtain

$$R_{4,3} = S_4 - S_1 S_3 = \nabla^T \cdot \mathcal{M}_{4,3} \cdot \nabla, \quad \text{where} \quad \mathcal{M}_{4,3} = \mathcal{M}_4 - \mathcal{M}_{u^2} \cdot \mathcal{M}_a^{(2)}, \tag{4.4}$$

$$\begin{aligned} \mathcal{M}_4 &= c_e \mathcal{M}_m^{(2)} + g^{(u)} \bar{U}^2 \mathcal{M}_u^{(2)} + g^{(a)} \{(\mathcal{D}_{\alpha\beta} - c_e) \delta_{\alpha\beta}\} \cdot \mathcal{M}^{(2)}|_w + g^{(u)} \{(U_\alpha^2 - \bar{U}^2) \delta_{\alpha\beta}\} \cdot \mathcal{M}^{(2)}|_w \\ &\quad + [g^{(a)} g_{\alpha\beta}^{(a)} \{\mathcal{D}_{\alpha\beta} (1 - \delta_{\alpha\beta})\} + g^{(u)} g_{\alpha\beta}^{(u)} \{U_\alpha U_\beta (1 - \delta_{\alpha\beta})\}] \cdot \mathcal{M}_0^{(2)}. \end{aligned} \tag{4.5}$$

These relations are valid for the d2Q9 model with any w owing to the last relation (C.3), and hence for the d2Q5 scheme. The matrix form (4.5) is also suitable for the d3Q7 model with the diagonal tensor ($w=0$) and the full d3Q15 and d3Q19 models with the isotropic tensor \mathcal{D}^+ (i.e., only when $g^{(u)} = g^{(a)} = 0$). Relations (C.4)-(C.5) provide further corrections when the \mathcal{D}^+ is anisotropic. When the \mathcal{D}^+ is diagonal, the corrections vanish for the d3Q7 model and the d3Q19 model with $w_c^{(m)} = w_c^{(m)*}$ (see relation (3.5)). The matrix $\mathcal{M}_{4,3}$ factorizes $\mathcal{D}^{(eff)}$ in the two cases:

$$\begin{aligned} \{g^{(u)}, g^{(a)}\} &= \{0, 1\}: \quad \text{if } t_c^{(m)} = t_c^{(a)} = t_c^{(u)} = t_c, \\ \text{then } \mathcal{M}_{4,3} &= \mathcal{D}^{(eff)} \cdot \mathcal{M}^{(2)}|_{w=w^*(1-2t_c)}, \quad \forall t_c. \end{aligned} \tag{4.6}$$

$$\begin{aligned} g_{\alpha\beta}^{(a)} = 1 \text{ or } g_{\alpha\beta}^{(u)} g_{\alpha\beta}^{(a)} = 1: \quad &\text{if } t_c^{(m)} = t_c^{(a)} = t_c^{(u)} = 0, \\ \text{then } \mathcal{M}_{4,3} &= \mathcal{D}^{(eff)} \cdot \mathcal{M}_0^{(2)}. \end{aligned} \tag{4.7}$$

The first relation (4.6) is only valid for the *diagonal* tensors \mathcal{D}^+ ($g_{\alpha\beta}^{(u)} = g_{\alpha\beta}^{(a)} = 0$) and when all the weights are equal (relation (3.4)). In this case, the operator S_4 reduces to $\mathcal{D}^+ \Delta^2$ for the d2Q9 and d3Q19 ($w_c^{(m)} = w_c^{(m)*}$) schemes only if their weights $t_q^{(m)}$ and $t_q^{(u)}$ take the hydrodynamic values t_q^* . Taking into account relations (4.2), the operator $R_{4,3} = S_4 - S_1 S_3$ factorizes the Laplace operator: $R_{4,3} = \mathcal{D}^{(eff)} \Delta^2$ when all the weights: $t_q^{(m)}$, $t_q^{(u)}$ and $t_q^{(a)}$ take the hydrodynamic values. In the presence of cross-diffusion, only the d2Q9 model factorizes $\mathcal{D}^{(eff)}$ if the coordinate weights are all set equal to zero (relation (4.7)).

Diagonal tensors: summary. By gathering all the components of R_4 , we conclude that its two first terms, $c_{4,1} D_2^2$ and $c_{4,2} D_2 S_1^2$, factorize $\mathcal{D}^{(eff)}$ (cf. relation (4.3)) but the term $R_{4,3}$ does it only under conditions (4.6) and (4.7), in general. Furthermore, the operator $c_{4,4} R_{4,4}$ does not factorize $\mathcal{D}^{(eff)}$. The heuristic analysis then supports the observed retention of the advection line for the d2Q9 model if (i) $c_{4,3}$ and $c_{4,4}$ vanish together on the solution (2.16), or (ii) $\Lambda = \Lambda^{(ext.)}(\Lambda_{bgk})$ (and thus $c_{4,4} = 0$) when the tensor is diagonal and

the weights obey relation (3.4). Further extensions include the d3Q15 and d3Q19 models, e.g., when the modeled tensor is isotropic and $g^{(u)} = 0$, or when $g^{(u)} = 1$ and thus \mathcal{D}^+ becomes anisotropic but the corrections (C.4) vanishes on the optimal line (diagonal axis). In particular, this explains the numerical observations [34] for the d3Q15 model.

Full tensors: summary. In order to explain the observed sufficiency of the optimal advection lines in the presence of cross-diffusion elements, e.g., for $\Lambda_{bgk} \leq \frac{1}{6}$ when $\Lambda = \Lambda^{(ext.)}(\Lambda_{bgk}) \in [\frac{1}{6}, \frac{1}{4}]$ and thus $c_{4,3} \geq 0$, we examine the sign of the operator $R_{4,3}(\vec{v}_e, \vec{U}_a)$ by combining the analytical and numerical tools. The details are gathered in Section C.3. This confirms that $R_{4,3}(\vec{v}_e, \vec{U}_a) \leq 0$ when $U^2 \leq U_a^2$, e.g., for the d2Q9 model with the same weights (3.4) and any anisotropy. We then conjecture that $c_{4,3}R_{4,3}(\vec{v}_e, \vec{U}_a)$ does not violate the sufficiency of the advection line when $c_{4,3} \geq 0$.

Extensions. The next step would naturally consist to extend these properties to a larger interval $\Lambda \in [\Lambda^{(ext.)}(\Lambda_{bgk}), \frac{1}{4}]$ or $\Lambda \geq \Lambda^{(ext.)}(\Lambda_{bgk})$ where $c_{4,4} \geq 0$. The sign of the operator $R_{4,4}(\vec{v}_e, \vec{U}_a)$ is examined in Section C.4. This shows that $R_{4,4}(\vec{v}_e, \vec{U}_a) \leq 0$ for most of the relevant situations. In particular, the 1D analytical solution [34] is recovered. Here, $R_{4,4} \leq 0$ when $U^2 \leq 1$ and $R_{4,3} = \partial^4(c_e + g^{(u)}U^2 - U^2)$, then $R_{4,3} = 0$ on the 1D advection line: $U^2 = c_e$ ($g^{(u)} = 0$) or $c_e = 0$ ($g^{(u)} = 1$). This explains why, in one dimension, the optimal advection lines are retained in the whole semi-interval $\Lambda \geq \Lambda^{(ext.)}(\Lambda_{bgk})$. In multi-dimensions, the numerical stability analysis suggests to avoid $\Lambda > \frac{1}{4}$ for very small Λ_{bgk} , at least. Further work is needed in order to understand stability when $\Lambda > \frac{1}{4}$. However, we consider this interval as irrelevant because of the deterioration of accuracy there.

Summary. We expect the optimal advection lines given in Section 3.2.3 to remain *essentially* sufficient when the weights are the same, $\Lambda \in [\Lambda^{(ext.)}(\Lambda_{bgk}), \frac{1}{4}]$ in the multi-dimensions, for any Λ_{bgk} in the case of the diagonal tensors (where, for diffusion boundary, the anisotropy has to be reduced towards non-negativity conditions when Λ_{bgk} is large and $\Lambda < \frac{1}{6}$), and then when $\Lambda_{bgk} \leq \frac{1}{6}$ in the presence of cross-diffusion or when numerical diffusion is removed.

5 Concentration wave

In this section we validate the truncation errors (2.9)-(2.10) for the evolution of concentration waves. The computational domain has length L_α along the α -axis, with periodic boundary conditions for all ends. The evolution of concentration wave $s(\vec{r}, 0) = s_0 \cos(\vec{k} \cdot \vec{r})$ in time should obey

$$s(\vec{r}, t) = s_0 \cos(\vec{k} \cdot (\vec{r} - \vec{U}t)) \exp(-\Omega(\vec{k})t), \quad \Omega(\vec{k}) = \Lambda^{-1} \sum_{\alpha, \beta} \mathcal{D}_{\alpha\beta} k_\alpha k_\beta,$$

$$k_\alpha = \frac{2\pi}{L_\alpha} n_\alpha, \quad n_\alpha = 1, 2, \dots \quad (5.1)$$

The two integrals $I_s(t)$ and $I_c(t)$:

$$I_s(t) = \frac{1}{L_x L_y} \int_0^{L_x} \int_0^{L_y} s(\vec{r}, t) \sin(\vec{k} \cdot \vec{r}), \quad I_c(t) = \frac{1}{L_x L_y} \int_0^{L_x} \int_0^{L_y} s(\vec{r}, t) \cos(\vec{k} \cdot \vec{r}),$$

are computed on the obtained solution $s(\vec{r}, t)$. Their predicted values are:

$$I_s(t) = \frac{\sin(\vec{k} \cdot \vec{U}t)}{2} \exp(-\Omega t), \quad I_c(t) = \frac{\cos(\vec{k} \cdot \vec{U}t)}{2} \exp(-\Omega t).$$

From their numerical values, we derive the effective values for $\Omega^{num}(\vec{k})/k^2$ and $(\vec{k} \cdot \vec{U}^{num})$:

$$\begin{aligned} \frac{\Omega^{num}(\vec{k})}{k^2} &= \frac{1}{k^2 t_a} (\log[I(t_a)] - \log[I(t+t_a)]), \quad \text{where } I^2(t) = I_s^2(t) + I_c^2(t), \\ (\vec{k} \cdot \vec{U}^{num}) &= \frac{1}{t_a} \left(\arctan \left[\frac{I_s(t+t_a)}{I_c(t+t_a)} \right] - \arctan \left[\frac{I_s(t)}{I_c(t)} \right] \right). \end{aligned} \tag{5.2}$$

The numerical estimates (5.2) are obtained using t_a in the interval $[5, 50]$ time steps, $s_0 = 100$ and $L_\alpha = 50$. Replacing formally ∂_α with k_α for operators (2.8), the fourth-order solution (2.10) prescribes:

$$\begin{aligned} \Omega^{num}(\vec{k}) &= R_2(\vec{k}) - R_4(\vec{k}) + \mathcal{O}(k^6), \\ (\vec{k} \cdot \vec{U}^{num}) &= -R_1(\vec{k}) + R_3(\vec{k}) + \mathcal{O}(k^5), \end{aligned}$$

where the diffusion form $R_2(\vec{k}) = \Lambda^- \sum_{\alpha, \beta} \mathcal{D}_{\alpha\beta}^{(eff)} k_\alpha k_\beta$ and the advection term $-R_1(\vec{k}) = (\vec{k} \cdot \vec{U}^{num})$. We compare the relative numerical errors to their predicted values:

$$\frac{E^{(r,4)}}{k^2} = \frac{\Omega^{num}(\vec{k}) - R_2(\vec{k})}{k^2 R_2(\vec{k})} \approx - \frac{R_4(\vec{k})}{k^4 \Lambda^- \sum_{\alpha, \beta} \mathcal{D}_{\alpha\beta}^{(eff)} \hat{k}_\alpha \hat{k}_\beta}, \quad k^2 = \|\vec{k}\|^2, \tag{5.3}$$

$$\frac{E^{(r,3)}}{k^2} = \frac{(\vec{k} \cdot \vec{U}^{num}) - (-R_1(\vec{k}))}{k^2 (-R_1(\vec{k}))} \approx \frac{R_3(\vec{k})}{k^3 (\vec{k} \cdot \vec{U})}, \quad \text{with } \vec{\hat{k}} = \frac{\vec{k}}{k}, \quad k = \|\vec{k}\|. \tag{5.4}$$

This technique has been efficiently applied in order to validate the truncation errors estimates for the anisotropic d3Q15 model, [12]. We extend this analysis taking into account the fourth-order numerical diffusion of the scheme, and using the d2Q9 model. Numerical analysis is concentrated on the weight distribution (3.4) where we examine the two limit weight families: $t_c = 0$ and $t_c = \frac{1}{2}$, along with the ‘‘hydrodynamic’’ choice $t_c = \frac{1}{3}$ and the ‘‘best advection’’ choice (3.7) $t_c = \frac{1}{4}$. When $g^{(u)}_{\alpha\beta} = 1$, the diagonal links build the equilibrium elements $U_\alpha U_\beta$ (the anti-numerical diffusion) for any weights. This distinguishes the limit scheme $t_c = \frac{1}{2}$ from the d2Q5 model. We mainly restrict the numerical validation of the truncation errors to $\Lambda^- \in [10^{-2}, \approx 1]$.

5.1 Truncation error of the pure diffusion equation (d2Q9 scheme)

In the pure diffusion case $E_q^- \equiv 0$, the second-order diffusion form $\Lambda^- D_2 (\vec{U}=0)$ reduces to $\Lambda^- S_2$, $S_2 = \sum_{q=1}^{Q_m} E_q^+ \partial_q^2$. The truncated fourth-order correction R_4 is then described by relation (2.12):

$$R_4 = c_{4,1} S_2^2 + c_{4,3} S_4, \quad S_4 = \sum_{q=1}^{Q_m} \partial_q^4 E_q^+.$$

These relations allow to compute R_4 for any velocity set. Alternatively, one may compute R_4 in the matrix form, combining relations (4.3) and (4.4):

$$R_4(\vec{U}=0) = \nabla^T \cdot \mathcal{M}_4^{diff} \cdot \nabla, \quad \mathcal{M}_4^{diff} = c_{4,1} \mathcal{D} \cdot \mathcal{M}_{\nabla}^{(2)} \cdot \mathcal{D} + c_{4,3} \mathcal{M}_4, \quad (5.5)$$

or, equivalently (we set all $g^{(a)} g_{\alpha\beta}^{(a)}$ equal to 1):

$$\begin{aligned} \mathcal{M}_4^{diff} = & (c_e c_{4,1} + c_{4,3}) \mathcal{D} \cdot \mathcal{M}_{\nabla}^{(2)} + c_{4,1} \left(\mathcal{D} \cdot \mathcal{M}_{\nabla}^{(2)} \cdot \mathcal{D} - c_e \mathcal{I} \cdot \mathcal{M}_{\nabla}^{(2)} \cdot \mathcal{D} \right) \\ & + c_{4,3} c_e \left(\mathcal{M}_m^{(2)} - \mathcal{M}_{\nabla}^{(2)} \right) + c_{4,3} \{ \mathcal{D}_{\alpha\beta} (1 - \delta_{\alpha\beta}) \} \cdot \left(\mathcal{M}_0^{(2)} - \mathcal{M}_{\nabla}^{(2)} \right). \end{aligned} \quad (5.6)$$

Let us examine several eigenvalue strategies.

(i) **“Optimal diffusion” solution** (2.13): $\Lambda = \frac{1}{6}$ and $\Lambda_{bgk} = \frac{1}{12}$, then $c_{4,1} = c_{4,3} = 0$ and thus $R_4(\vec{U}=0) \equiv 0$. This choice is expected to be the most accurate for any weights, c_e and anisotropy. However, it is necessarily to assign the modeled mean trace value $\Lambda^- c_e$ to the interval $[0, (c_e^{(nec)} \sqrt{12}) / 12]$ where, according to the numerical stability analysis in Section 3.5, $c_e^{(nec)} = \{1, \approx \frac{9}{10}, \approx \frac{3}{4}, \frac{1}{2}\}$ when $t_c^{(m)} = \{0, \frac{1}{4}, \frac{1}{3}, \frac{1}{2}\}$, respectively. Indeed, these boundaries are only slightly inferior to the OTRT results for isotropic diffusion tensors. Fig. 11 confirms that the relative error (5.3) is very small on the “optimal diffusion” solution, for isotropic or anisotropic tensors.

(ii) **Strategy D.1**: $\Lambda = \frac{1}{6}$, and thus $c_{4,3} = 0$. Here, Λ_{bgk} is a free-tunable parameter and any diffusion coefficient can be obtained when c_e is fixed. According to the numerical stability analysis, the non-negativity conditions $E_0 \geq 0$ and $\{E_q^+ \geq 0\}$ become relevant for $\Lambda = \frac{1}{6}$ only when Λ_{bgk} is sufficiently large, $\Lambda_{bgk} > \approx 4$. The fourth-order correction $R_4 (\vec{U}=0, \Lambda = \frac{1}{6})$ and the relative error (5.3) are read as

$$\Lambda = \frac{1}{6}: \quad R_4(\vec{k}) = - \frac{(\Lambda_{bgk} - \frac{1}{12})}{\Lambda^-} R_2^2(\vec{k}).$$

Then

$$\begin{aligned} \frac{E^{(r,4)}}{k^2} &= \left(\Lambda_{bgk} - \frac{1}{12} \right) c_e F_1(\theta, a, K_{xy}), \quad \vec{k} = k(\cos\theta, \sin\theta), \\ F_1 &= \frac{R_2(\vec{k})}{k^2 c_e \Lambda^-} = \frac{(1+a)k_x^2 + (1-a)k_y^2 + 2K_{xy}k_x k_y}{k^2} \\ &= 1 + a \cos[2\theta] + K_{xy} \sin[2\theta], \quad F_1 \geq 0, \quad \text{and} \quad \max_{\theta, a, K_{xy}} F_1 = 2. \end{aligned} \tag{5.7}$$

The term $E^{(r,4)}$ linearly increases with c_e but it is independent of the weights $t_q^{(m)}$. This errors scales with the $(\Lambda_{bgk} - \frac{1}{12})$. Notice: $F_1 \geq 0$ owing to the positive semi-definiteness of the modeled tensor $\mathcal{D}_{\alpha\beta}$. The term $E^{(r,4)}$ is isotropic on the isotropic tensors where $F_1 \equiv 1$. In the anisotropic diagonal case, $\max_{\theta} F_1$ reaches $1 + |a|$ when \vec{k} is parallel to the axis with the largest diffusion coefficient $c_e(1 + |a|)$. In the presence of cross-diffusion, $\max_{\theta} F_1 = 1 + \sqrt{a^2 + K_{xy}^2}$ and this is reached when $\tan[2\theta] = K_{xy}/a$. The worst anisotropic error is $\max_{\theta, a, K_{xy}} F_1 = 2$. Altogether, the term $E^{(r,4)}$ varies from $(\Lambda_{bgk} - \frac{1}{12})c_e k^2$ on isotropic tensors to $2(\Lambda_{bgk} - \frac{1}{12})c_e k^2$.

These predictions are validated as shown in Fig. 11. The left diagram is computed for an isotropic tensor, when \vec{k} is parallel to the x -axis and using $t_c^{(m)} = \frac{1}{4}$ for five c_e values: $c_e = \{c_e^{(0)}/10, \frac{1}{3}, \frac{1}{2}, c_e^{(0)} = \frac{3}{5}, c_e^{(\max)} = 1\}$, when $\Lambda_{bgk} = \{10^{-4}, \frac{1}{12}, \frac{1}{4}, 1\}$. The numerical results confirm $F_1 \approx 1$ for the different combinations of $t_q^{(m)}$, c_e and Λ_{bgk} , and the isotropy of $E^{(r,4)}$ with respect to θ . The right diagram in Fig. 11 shows the reduced relative error versus the anisotropic factor $a \in [0, 2t_c^{(m)}]$ when $K_{xy} = 1 - 2t_c^{(m)}$. This obeys the non-negativity condition (3.13). We set: $c_e = \frac{1}{2}$, $k_y = 2k_x$, $\Lambda_{bgk} = \frac{1}{6}$, as given by relation (2.16). The results are in good agreement with the predictions (5.7), giving $F_1(\theta, a, K_{xy}) \approx 2$ in the two anisotropic limits. Similar as in Fig. 4, the limit case $a=1, K_{xy}=0$ is stable for all the examined weights, but $K_{xy} = 1, a=0$ is unstable for $t_c^{(m)} = \frac{1}{2}$.

Thus, the numerical results fit very accurately the fourth-order predictions in the pure diffusion case. We then verify if the scale factor $(\Lambda_{bgk} - \frac{1}{12})c_e$ applies to the relative errors obtained for the second central moment, modeling the diffusion of the Gaussian hill with the isotropic tensor. The left diagram in Fig. 12 is computed with $c_e = 10^{-1}$ when Λ_{bgk} varies. The diffusion coefficient $\Lambda^- c_e$ is fixed in the right diagram when both c_e and Λ^- vary. These tests are less precise (because of the time dependence of the error), and they are difficult to conduct for large variations of Λ_{bgk} because of the disparity in transition and evolution times. Altogether, we find that the scale factor is reasonably retained, especially when c_e is fixed (see the left diagram).

(iii) **Strategy D.2:** $\Lambda = \frac{1}{4} - \Lambda_{bgk}$ when $\{\Lambda, \Lambda_{bgk}\} \in]0, \frac{1}{4}[$, and thus $c_{4,1} = 0$. Here, the mean trace magnitude is restricted to the interval $]0, c_e^{(\max)}/2[$. A nearly optimal advection stability is expected when $\Lambda \in [\frac{1}{6}, \frac{1}{4}]$ since this choice gives the leading-order approximation

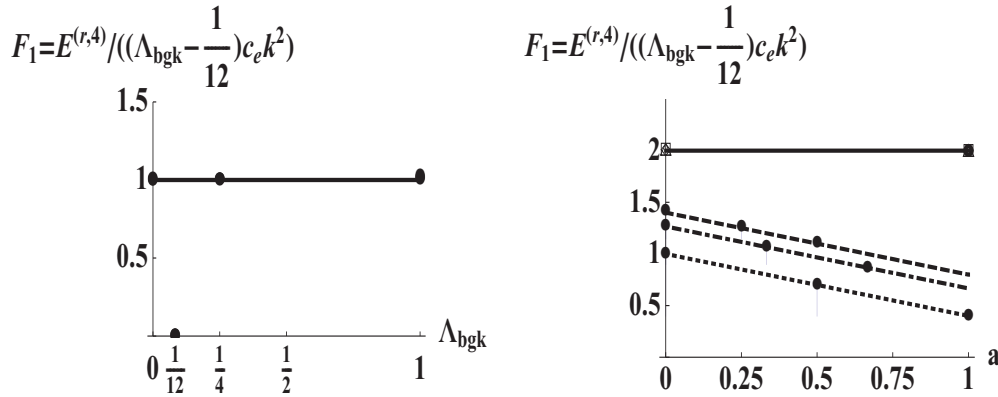


Figure 11: **Strategy D.1:** $\Lambda = \frac{1}{6}$. The numerical results (5.3) (symbols) are plotted along with the predicted solution (5.7) (lines). All results are divided by $(\Lambda_{bgk} - \frac{1}{12})c_e$, except when $\Lambda_{bgk} = \frac{1}{12}$. The left diagram is computed with the isotropic tensor and five c_e values for each Λ_{bgk} , $\Lambda_{bgk} \in [10^{-4}, 1]$. The right diagram is computed with $t_c^{(m)} = \frac{1}{4}$ (dashed), $t_c^{(m)} = \frac{1}{3}$ (dotted-dashed) and $t_c^{(m)} = \frac{1}{2}$ (dotted) when $K_{xy} = 1 - 2t_c^{(m)}$, $|a| \in [0, 2t_c^{(m)}]$. The two limit cases give $F_1(\theta, a, K_{xy}) \approx 2$. They are computed with: (i) $a=1, K_{xy}=0, t_c^{(m)} = \{0, \frac{1}{3}, \frac{1}{4}, \frac{1}{2}\}$, $k_y=0$ and (ii), $a=0, K_{xy}=1, t_c^{(m)} = \{0, \frac{1}{3}, \frac{1}{4}\}$, $k_x = k_y$.

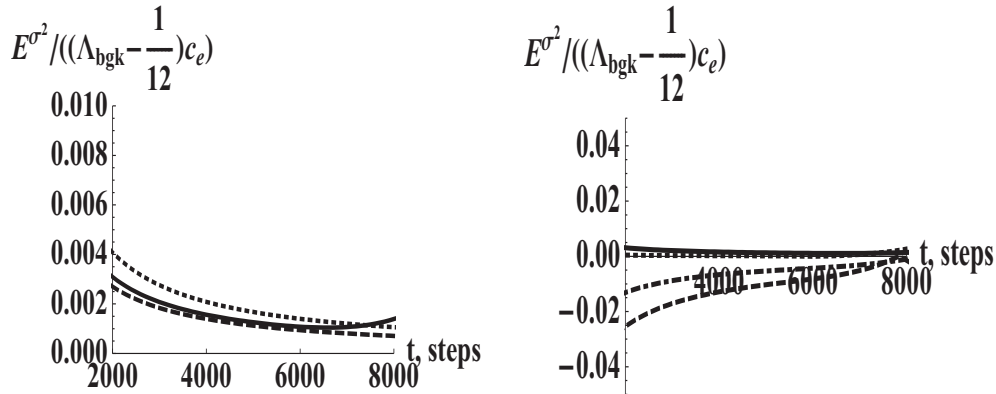


Figure 12: The relative error of the second moment $\sigma^2 + 2c_e\Lambda^{-1}t$ is rescaled with the factor $(\Lambda_{bgk} - \frac{1}{12})c_e$ and plotted versus the number of time steps for evolution of the Gaussian hill with the isotropic diffusion tensor, using the d2Q9 model with $\Lambda = \frac{1}{6}$ and $t_c^{(m)} = \frac{1}{4}$. Left diagram: $c_e = 10^{-1}$, $\Lambda_{bgk} = \{\frac{25}{12}, \frac{5}{6}, \frac{1}{3}\}$, Right diagram: $c_e\Lambda^{-1} = \frac{25}{12}$ with $c_e = \{10^{-1}, \frac{3}{10}, \frac{3}{5}, \frac{6}{10}\}$. Lines: solid, dotted, dashed and dot-dashed, respectively.

for relation (2.15) when $\Lambda_{bgk} \rightarrow 0$. The fourth-order relative error becomes

$$\begin{aligned} \Lambda = \frac{1}{4} - \Lambda_{bgk}: \quad R_4(\vec{U}=0) &= c_{4,3}S_4, \\ \frac{E^{(r,4)}}{k^2} &= \left(\Lambda_{bgk} - \frac{1}{12}\right) F_2(t_c^{(m)}, \theta, a, K_{xy}), \\ F_2 &= \frac{3(1 - t_c^{(m)}) + (3t_c^{(m)} - 1)\cos[4\theta] + 2a\cos[2\theta] + 4K_{xy}\sin[2\theta]}{2(1 + a\cos[2\theta] + K_{xy}\sin[2\theta])}. \end{aligned} \tag{5.8}$$

Again, $E^{(r,4)}/k^2$ scales with $(\Lambda_{bgk} - \frac{1}{12})$ since $-c_{4,3}/\Lambda^- = \frac{1}{6} - \Lambda = \Lambda_{bgk} - \frac{1}{12}$. The term $E^{(r,4)}$ is independent of the c_e but, in general, it depends on the weights. When \vec{k} is parallel to a lattice axis, $F_2 \equiv 1$ and $E^{(r,4)} = (\Lambda_{bgk} - \frac{1}{12})k^2$, for any weights. The function F_2 is non-negative for diagonal tensors. However, the term $E^{(r,4)}$ is then anisotropic, except the hydrodynamic weight $t_c^{(m)} = \frac{1}{3}$ where $E^{(r,4)}$ reduces to the isotropic solution $(\Lambda_{bgk} - \frac{1}{12})k^2$. The most accurate weight interval is $t_c^{(m)} \in [\frac{1}{3}, \frac{1}{2}]$ where $\max_{\theta,a} F_2 = 1$. Otherwise, $\max_{\theta,a \neq 0} F_2 = 3(1 - 2t_c^{(m)})$ and this is reached when $|a| = 1$. In the presence of cross-diffusion, and when the non-negativity condition $|a| \in [0, 2t_c^{(m)}]$ is enforced, along with the diagonal-dominant condition $|K_{xy}| \leq 1 - |a|$, the F_2 is limited and the worst error happens when $a = 0$ and $|K_{xy}| = (1 - |a_x|)/2$, with $\max_{\theta,a,K_{xy}} F_2 = 1/2(4 - 3t_c^{(m)})$ when $t_c^{(m)} \in [0, \frac{4}{9}]$, and then

$$\max_{\theta,a,K_{xy}} F_2 = 2 \left(-\sqrt{3t_c^{(m)}(3t_c^{(m)} - 1)} + 3t_c^{(m)} \right), \quad \text{when } t_c^{(m)} \in \left[\frac{4}{9}, \frac{1}{2} \right].$$

On the other hand, $\max_{\theta,K_{xy},a=0} F_2 = 2$ when $t_c^{(m)} = 0$, $a = 0$ and $|K_{xy}| \in [0, 1]$.

These predictions are validated as shown in Fig. 13 when $c_e = \frac{1}{2}$, for the isotropic (left) and the anisotropic full tensor (right), when $k_x = k_y$ or $k_y = 2k_x$, respectively. In isotropic case, we set $\Lambda = \{\approx \frac{1}{4}, \frac{1}{6}, \frac{1}{12}, 10^{-4}\}$, and the solution remains stable for $\Lambda_{bgk} \in \{10^{-4}, \frac{1}{12}, \frac{1}{6}, \approx \frac{1}{4}\}$, respectively, for all four examined weight families. The non-negativity condition (3.13) is enforced in the limit form: $K_{xy} = 1 - 2t_c^{(m)}$ and $a = 2t_c^{(m)}$. The stable solutions are obtained by decreasing Λ to 10^{-2} , at least, in agreement with the predicted sufficiency of the non-negativity conditions for the pure diffusion equation. Otherwise, the stability is attained with $K_{xy} = \sqrt{1 - a^2}$ only for $\Lambda = \{\approx \frac{1}{4}, \frac{1}{6}\}$, as expected.

Altogether, the strategy **D.1** is more accurate than **D.2** because of its scale-factor $c_e \in]0, 1[$ in $E^{(r,4)}$, and **D.1** has the smallest errors in the anisotropic limits. Applying the strategy **D.2**, the ‘‘hydrodynamic’’ choice $t_c^{(m)} = \frac{1}{3}$ results in the most isotropic error distribution. This is to be contrasted with **D.1** where the leading errors are weight-independent. However, **D.2** may become more robust for advection-dominant problems, when $\Lambda^- \rightarrow 0$ and $c_e \rightarrow 0$.

(iv) **Strategy D.3:** $c_{4,1}c_e + c_{4,3} = 0$. The first coefficient in Eq. (5.6) vanishes if

$$c_e = -\frac{c_{4,3}}{c_{4,1}} = \frac{\Lambda - \frac{1}{6}}{\Lambda_{bgk} + \Lambda - \frac{1}{4}}. \tag{5.9}$$

This solution corresponds to formula (B.7) in [20]. Similar relation has been very recently reported by Suga [49] for the d1Q3 BGK model, (Eq. (17) there, replacing w with $-\lambda^-$, a with $c_e/2$ and changing the sign (typos, probably) for two the last terms). This strategy

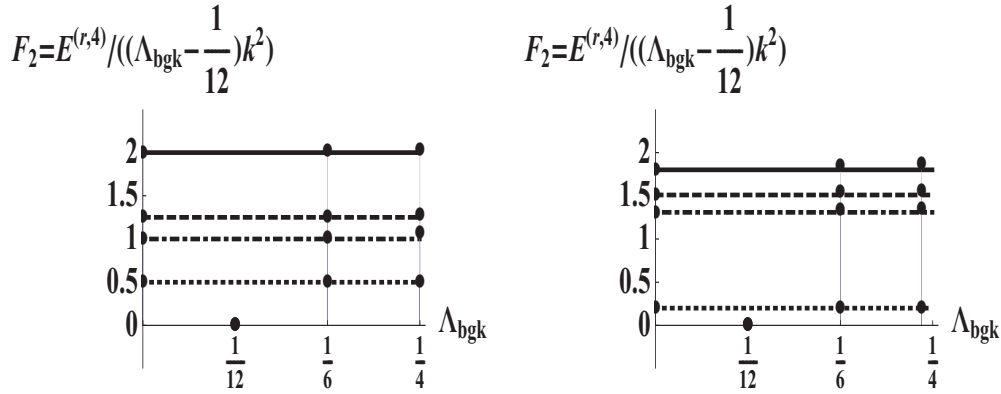


Figure 13: **Strategy D.2:** $\Lambda = \frac{1}{4} - \Lambda_{bgk}$. The predicted solution (5.8) (lines) and the numerical results (symbols) are plotted versus $\Lambda_{bgk} \geq 10^{-4}$ for four different weights: $t_c^{(m)} = 0$ (solid), $t_c^{(m)} = \frac{1}{4}$ (dashed), $t_c^{(m)} = \frac{1}{3}$ (dotted-dashed) and $t_c^{(m)} = \frac{1}{2}$ (dotted). The diffusion tensor is isotropic on the left picture, with $k_x = k_y$, and anisotropic on the right picture, where $a = 2t_c^{(m)}$ and $K_{xy} = 1 - 2t_c^{(m)}$, with $k_y = 2k_x$.

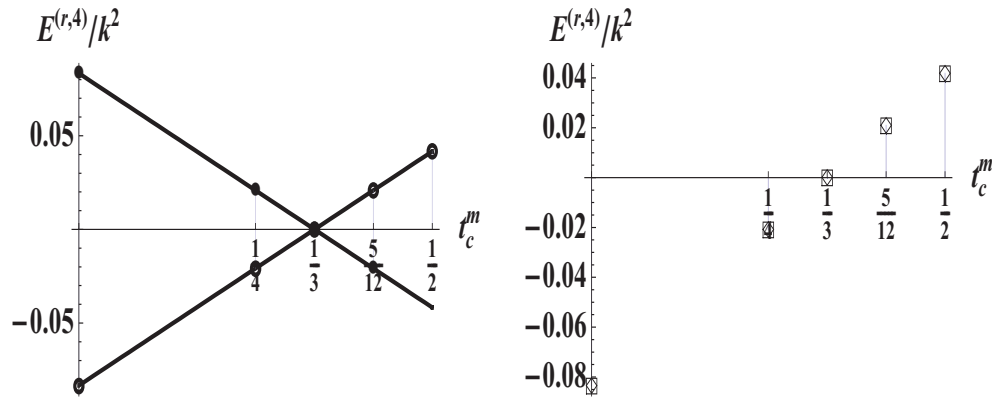


Figure 14: **Strategy D.3.** The left diagram plots the numerical results (symbols) against the predicted solution (5.10) for $\Lambda = \frac{1}{4}$, $\Lambda_{bgk} = \frac{1}{6}$ (increasing line) and $\Lambda = \frac{1}{12}$, $\Lambda_{bgk} = 10^{-4}$ (decreasing line), versus the weight $t_c^{(m)}$. The right diagram shows results for $\Lambda_{bgk} = \frac{1}{6}$ (“squares”) and $\Lambda_{bgk} = 1$ (“diamonds”) when $\Lambda = \frac{1}{4}$. They confirm that the relative error (5.10) is independent of Λ_{bgk} .

yields

$$c_e = \frac{\Lambda - \frac{1}{6}}{\Lambda_{bgk} + \Lambda - \frac{1}{4}} : \quad \frac{E^{(r,4)}}{k^2} = \left(\Lambda - \frac{1}{6} \right) F_3(t_c^{(m)}, \theta, a, K_{xy}),$$

$$F_3 = a \cos[2\theta] + \frac{(3t_c^{(m)} - 1 + K_{xy}^2) \sin^2[2\theta] + \frac{aK_{xy}}{2} \sin[4\theta]}{1 + a \cos[2\theta] + K_{xy} \sin[2\theta]},$$

$$t_c^{(m)} = \frac{1}{3} \text{ or 1D: } F_3 = 0 \text{ if } \mathcal{D}_{\alpha\beta} = c_e \delta_{\alpha\beta}. \tag{5.10}$$

In principle, the error remains the same when Λ^- varies but the diffusion coefficient $\Lambda^- c_e$ and Λ are fixed. The error depends on the weights, and this strategy is best suited for isotropic tensors when $t_c^{(m)} = \frac{1}{3}$, or in 1D, when the fourth-order error (5.6) vanishes. Otherwise, $E^{(r,k)}/k^2$ varies as $(\Lambda - \frac{1}{6})(3t_c^{(m)} - 1)\sin^2[2\theta]$ for isotropic tensors. This prediction is validated as shown in Fig. 14, when \vec{k} is along the diagonal axis. The numerical tests are run with $\Lambda = \frac{1}{4}$ ($c_e = 1/(12\Lambda_{bgk})$) and $\Lambda = \frac{1}{12}$ ($c_e = \frac{1}{12(1/6 - \Lambda_{bgk})} > \frac{1}{2}$) with $\Lambda_{bgk} \in [0, \frac{1}{6}]$. The last choice is not available for the d2Q5 scheme where $c_e^{(\max)} = \frac{1}{2}$. Indeed, Λ_{bgk} and Λ have to be selected such that c_e given by relation (5.10) stays inside the stable interval $[0, c_e^{(\max)}]$. The scale factors of this and the two previous strategies are then related, e.g.: $|\Lambda - \frac{1}{6}| \leq |\Lambda_{bgk} - \frac{1}{12}|$ and $c_e \in [0, 1]$ if only $\Lambda \in [\frac{1}{6}, \Lambda_{bgk} + \frac{1}{12}]$ and $\Lambda_{bgk} \geq \frac{1}{12}$, or when $\Lambda \in [\Lambda_{bgk} + \frac{1}{12}, \frac{1}{6}]$ and $\Lambda_{bgk} \leq \frac{1}{12}$.

In the anisotropic diagonal case, the most accurate weight interval is again $t_c^{(m)} \in [\frac{1}{3}, \frac{1}{2}]$ where $|E^{(r,4)}| \leq |\Lambda - \frac{1}{6}|k^2$. When $t_c^{(m)} = \frac{1}{3}$ then $\max_{\theta} |F_3| = |a|$. The weight interval $t_c^{(m)} \in [0, \frac{1}{3}]$ should be avoided when $|a|$ is large. In the presence of cross-diffusion, $|E^{(r,4)}|$ is smaller than $4/3|\Lambda - \frac{1}{6}|k^2$ when $t_c^{(m)} = \frac{1}{3}$, provided that $|K_{xy}|$ is restricted to the interval $[0, \sqrt{1 - a^2}/2]$. Otherwise, e.g., when $a = 0$ and $t_c^{(m)} = \frac{1}{3}$, the $\max_{\theta, a=0} F_3$ may reach $K_{xy}^2/(1 - |K_{xy}|)$. Moreover, $E^{(r,4)}/k^2$ is unbounded when $t_c^{(m)} = \frac{1}{3}$ for the diagonal-dominant tensors:

$$|K_{xy}| \leq 1 - |a|, \quad |a| \leq 2t_c^{(m)},$$

unless the non-negativity conditions (3.13) reduce the $|K_{xy}|$ to the interval $[0, 1 - 2t_c^{(m)}]$. On the other side, when $t_c^{(m)} = 0$, $a = 0$ and $|K_{xy}| \in [0, 1]$, the $\max_{\theta} |F_3|$ still belongs to the interval $[1, 1 + |K_{xy}|] \in [0, 2]$, like with the previous strategies.

Altogether, this strategy may be profitable in 1D or for isotropic tensors, provided that $t_c^{(m)} = \frac{1}{3}$ and c_e lies in the stable interval, and thus the fourth-order truncation error vanishes. The diffusion error may keep the same magnitude when the diffusion coefficient and Λ are fixed but Λ^- and c_e vary.

(v) **The OTRT subclass** $\Lambda = \frac{1}{4}$ is expected to have the best stability, with the sufficient condition $c_e \in [0, c_e^{(\max)} = \min\{c_e^{(nec)}, c_e^{(0)}\}]$ for any anisotropy and weight values. The error estimate gives

$$\Lambda = \frac{1}{4} : \quad \frac{E^{(r,4)}}{k^2} = -\frac{1}{6} + \Lambda_{bgk}^{(c_e)}(1 + a\cos[2\theta] + K_{xy}\sin[2\theta]) + \frac{1 + 3t_c^{(m)} + 2a\cos[2\theta] + (1 - 3t_c^{(m)})\cos[4\theta]}{24(1 + a\cos[2\theta] + K_{xy}\sin[2\theta])}, \quad \Lambda_{bgk}^{(c_e)} = c_e\Lambda_{bgk}. \quad (5.11)$$

The error $E^{(r,4)}$ depends on Λ_{bgk} only in its product with c_e , unlike the previous strategies.

For isotropic tensors, $E^{(r,4)}/k^2$ reduces to

$$\Lambda_{bgk}^{(c_e)} + \frac{1}{8}(t_c^{(m)} - 1) + \frac{1}{24} \left((1 - 3t_c^{(m)}) \cos[4\theta] \right).$$

The error is isotropic only when $t_c^{(m)} = \frac{1}{3}$, as for the two previous strategies, and then $|E^{(r,4)}/k^2| = |\Lambda_{bgk}^{(c_e)} - \frac{1}{12}|$. In principle, $|E^{(r,4)}|$ may become smaller than $(\Lambda_{bgk} - \frac{1}{12})c_e$ (see strategy **D.1**). The error vanishes when $\Lambda_{bgk}^{(c_e)} = \frac{1}{12}$ in agreement with strategy **D.3**. When $t_c^{(m)} \neq \frac{1}{3}$, the amplitude of the error may exceed $|\Lambda_{bgk}^{(c_e)} - \frac{1}{12}|$, e.g., when $t_c^{(m)} \in [0, \frac{1}{3}]$, $\Lambda_{bgk}^{(c_e)} \in [\frac{1}{12}, \frac{1}{8}]$ and $t_c^{(m)} \in [0, 1 - 8\Lambda_{bgk}^{(c_e)}]$, or when $t_c^{(m)} \in [\frac{1}{3}, \frac{1}{2}]$, $\Lambda_{bgk}^{(c_e)} \in [1/16, \frac{1}{12}]$ and $t_c^{(m)} \in [1 - 8\Lambda_{bgk}^{(c_e)}, \frac{1}{2}]$. On diagonal tensor, the term $E^{(r,4)}$ is anisotropic even if $t_c^{(m)} = \frac{1}{3}$, and $\max_{\theta} E^{(r,4)}/k^2 = \Lambda_{bgk}^{(c_e)} - \frac{1}{12} + |a|\Lambda_{bgk}^{(c_e)}$ is reached either when $\Lambda_{bgk}^{(c_e)} > \frac{1}{12}$, or when $\Lambda_{bgk}^{(c_e)} \in [\frac{1}{24}, \frac{1}{12}]$ and $|a| \in [1/(12\Lambda_{bgk}^{(c_e)}) - 1, 1]$. Accordingly, $\min_{\theta} E^{(r,4)}/k^2 = \Lambda_{bgk}^{(c_e)} - \frac{1}{12} - |a|\Lambda_{bgk}^{(c_e)}$, and this is reached either when $\Lambda_{bgk}^{(c_e)} < \frac{1}{12}$, or when $\Lambda_{bgk}^{(c_e)} > \frac{1}{12}$ and $|a| \in [1 - 1/(12\Lambda_{bgk}^{(c_e)}), 1]$. In the presence of cross-diffusion, $E^{(r,4)}$ may become unbounded for $t_c^{(m)} = \frac{1}{3}$ when $|K_{xy}| \rightarrow 1$ and $a = 0$. However, the diagonal weights $t_c^{(m)} = 0$ keep again the bounded error magnitude which does not exceed

$$E^{(r,4)}/k^2 = \Lambda_{bgk}^{(c_e)}(1 + |K_{xy}|) - \frac{1}{6}$$

when $a = 0$.

In summary, the fourth-order diffusion error depends on the product $\Lambda_{bgk}c_e$ when $\Lambda = \frac{1}{4}$, and thus it varies when the diffusion coefficient $\Lambda^{-}c_e$ is fixed. When Λ_{bgk} and c_e are selected in a special way, e.g., when $\Lambda_{bgk} > \frac{1}{12}$ and $c_e \in [1/(24\Lambda_{bgk} - 1), 1]$ for $t_c^{(m)} = \frac{1}{3}$, the error is smaller than the isotropic error of the **D.1** scheme, as one example. However, the truncation errors may become unbounded in the anisotropic limits where the advanced stability is confirmed as it is shown in Fig. 4 and for the evolution of waves. At the same time, the accuracy deteriorates when $K_{xy} = 1$, except when $t_c^{(m)} = 0$.

5.2 Truncation advection error (d2Q9 scheme)

The third-order advection correction (2.9) of the d2Q9 model is read as (again, we replace ∂_{α} with $k\hat{k}_{\alpha}$):

$$R_3(\vec{k}) = k^3 \left(c_{3,1} \frac{R_2(\vec{k})}{\Lambda^{-}} (\vec{k} \cdot \vec{U}) - c_{3,2} \left(\hat{k}_x^3 U_x + \hat{k}_y^3 U_y + 3(1 - 2t_c^{(a)}) \hat{k}_x \hat{k}_y (\hat{k}_y U_x + \hat{k}_x U_y) - (\vec{k} \cdot \vec{U})^3 \right) \right). \tag{5.12}$$

The coefficients $c_{3,1}$ and $c_{3,2}$ vanish together only on the ‘‘optimal advection’’ solution (2.11): $\Lambda_{bgk} = \Lambda = \frac{1}{12}$. When the numerical diffusion has been corrected, $R_2(\vec{k})/\Lambda^{-}$

reduces to its diffusion solution: $R_2(\vec{k})/\Lambda^- = c_e F_1(\theta, a, K_{xy})$, where F_1 is given by Eq. (5.7). The BGK configuration yields $c_{3,1} = 3c_{3,2} = 3(\Lambda_{bgk} - \frac{1}{12})$. Then $E^{(r,3)}$ scales as $(\Lambda_{bgk} - \frac{1}{12})k^3$. The TRT scheme with c_e , Λ and Λ_{bgk} has the same error as the BGK scheme with c'_e and Λ'_{bgk} when

$$\Lambda'_{bgk} = \Lambda \quad \text{and} \quad c'_e = \frac{c_{3,1}(\Lambda_{bgk}, \Lambda)}{c_{3,1}(\Lambda, \Lambda)} c_e.$$

The TRT scheme with $\Lambda = \frac{1}{4}$ has the same errors as the BGK scheme with $\Lambda'_{bgk} = \frac{1}{4}$ and $c'_e = 4c_e \Lambda_{bgk}$, as one example. The term $E^{(r,3)}$ becomes isotropic with respect to $(\vec{k} \cdot \vec{U})$ only for the hydrodynamic advection weight $t_c^{(a)} = \frac{1}{3}$:

$$t_c^{(a)} = \frac{1}{3} : \quad \frac{E^{(r,3)}}{k^2} = c_{3,1} c_e F_1 + c_{3,2} ((\vec{k} \cdot \vec{U})^2 - 1). \quad (5.13)$$

In isotropic case $\mathcal{D}_{\alpha\alpha} = c_e$ this error becomes independent of Λ on the diffusion stability line $U^2 = 1 - c_e$ of the d1Q3 model (cf. relation (3.17)):

$$t_c^{(a)} = \frac{1}{3} : \quad \frac{E^{(r,3)}}{k^2} = 2(\Lambda_{bgk} - \frac{1}{12})c_e \quad \text{if } (\vec{k} \cdot \vec{U})^2 = 1 - c_e, \quad F_1 = 1, \quad \forall \Lambda. \\ \text{then } R_3 = 0, \quad \text{if } \Lambda_{bgk} = \frac{1}{12}, \quad \forall \Lambda. \quad (5.14)$$

This is also valid in 1D, or when \vec{k} is parallel to the coordinate axis, with $(\vec{k} \cdot \vec{U})^2 = U_\alpha^2$ and for any $t_c^{(a)}$. Fig. 15 shows a very accurate one-dimensional front propagation for $t_c^{(m)} = \frac{1}{3}$, $\Lambda = \Lambda_{bgk} = \frac{1}{12}$ and $U = \frac{1}{4}$ when $c_e = 4.6875 \times 10^{-2}$ (see the left diagram). A small oscillation develops behind the front in the same simulations when $\Lambda = \frac{1}{4}$ (see the right diagram). This oscillation rapidly increases when c_e decreases (see the left diagram in Fig. 16) where c_e is reduced by a factor 10. As with the 2D-simulations in Fig. 5, the simulations in Fig. 15 are accurate for $\Lambda = \frac{1}{6}$ but the both values $\Lambda = \{\frac{1}{6}, \frac{1}{4}\}$ give very similar results when c_e decreases. The right diagram in Fig. 16 illustrates that the discrepancy disappears using solution (5.14) for extremely high velocity $U = 0.997653$. However, the right diagram in Fig. 5 shows that solution (5.14) does not improve the advection error in 2D, as it could be expected.

Altogether, using $\Lambda_{bgk} \in [\frac{1}{6}, \frac{1}{4}]$ in order to improve the stability in multi-dimensions (this includes relations (2.15) when $\Lambda_{bgk} \leq \frac{1}{6}$), one has to avoid very small value of c_e , say $c_e < 10^{-2}$. This clearly limits the ability of the scheme to reach very high Peclet numbers with very high velocity magnitudes $U^2 \approx 1 - c_e$.

When $c_e > \approx 10^{-2}$, the choice $\Lambda = \frac{1}{12}$ (where $c_{3,2} = 0$) becomes one of the most interesting for advection. Provided that the second-order numerical diffusion has been canceled, the advection error is independent of the velocity and weights:

$$\Lambda = \frac{1}{12}, \quad g^{(u)} g_{\alpha\beta}^{(u)} = 1 : \quad \frac{E^{(r,3)}}{k^2} = 2 \left(\Lambda_{bgk} - \frac{1}{12} \right) F_1(\theta, a, K_{xy}). \quad (5.15)$$

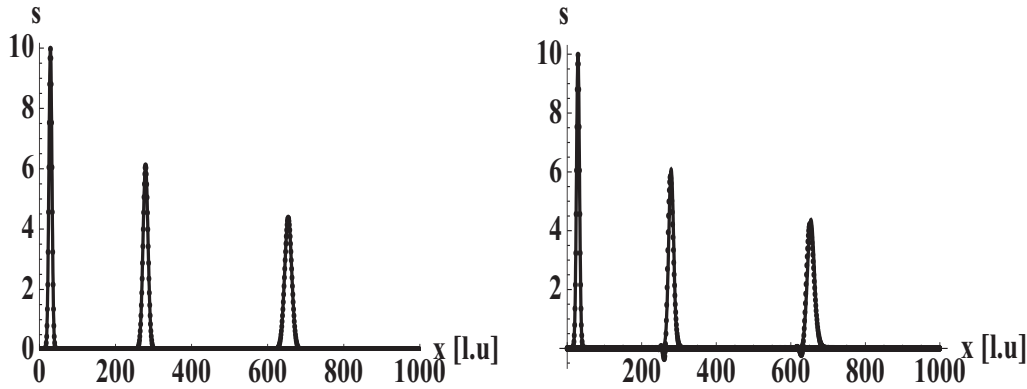


Figure 15: Evolution of the Gaussian hill along the x -axis when $\Lambda_{bgk} = \frac{1}{12}$, $c_e = 4.6875 \times 10^{-2}$, $U = \frac{1}{4}$, $Pe \approx 18.5$, $\Lambda = \frac{1}{12}$ (left diagram) and $\Lambda = \frac{1}{4}$ (right diagram), when $t = 0, 10^3, 2.5 \times 10^3$. One-dimensional solution is independent of the weights.

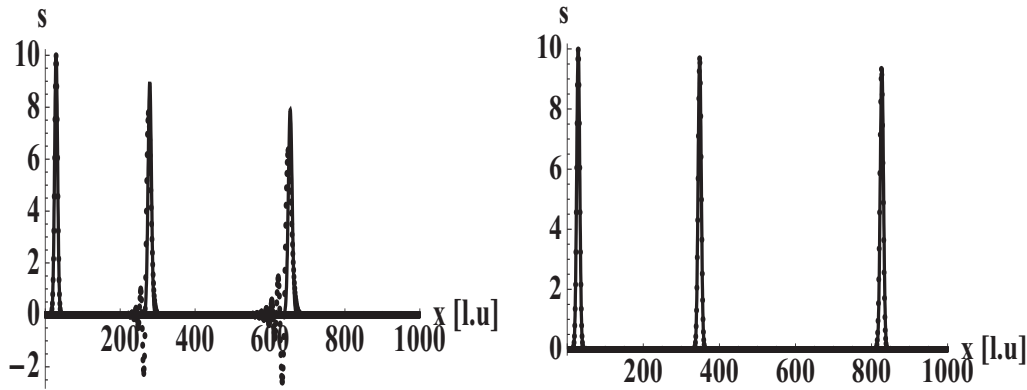


Figure 16: Evolution of the Gaussian hill along the x -axis when $c_e = 4.6875 \times 10^{-3}$, $\Lambda_{bgk} = \frac{1}{12}$ and $\Lambda = \frac{1}{4}$. Left diagram: $U = \frac{1}{4}$, $Pe \approx 185$, $t = 0, 10^3, 2.5 \times 10^3$. Right diagram: $U^2 = 1 - c_e$ (see relation (5.14)), then $U \approx 0.997653$, $Pe \approx 737$, $t = 0, 320, 800$.

The amplitude is twice as high as $|E^{(r,4)} / k^2|$ on the “optimal advection-diffusion” solution (2.16) (cf. relation (5.7)). Fig. 17 illustrates the advection and diffusion errors for $\Lambda = \frac{1}{6}$ and $\Lambda = \frac{1}{12}$. The numerical computations (5.3) and (5.4) are compared to the theoretical predictions for the isotropic diffusion tensor and when \vec{U} and \vec{k} are along the diagonal axis. The left diagram plots $E^{(r,3)} / k^2$ when $\Lambda_{bgk} = \frac{1}{6}$. The right diagram plots $E^{(r,4)} / k^2$ for the optimal advection and advection-diffusion strategies, (2.11) and (2.16). The advection velocity U^2 lies on the diffusion stability line $1 - c_e$ when $t_c^{(m)} = \{\frac{1}{3}, \frac{1}{4}\}$, and it is set close to the stability limits when $t_c^{(m)} = \{0, \frac{1}{2}\}$. In all the cases, $c_e = \frac{1}{4}$ (and then $2c_e = 1 - 2c_e$). The numerical results are found in good agreement with the stability and accuracy predictions using largest stable velocity amplitudes. The horizontal line in the left diagram

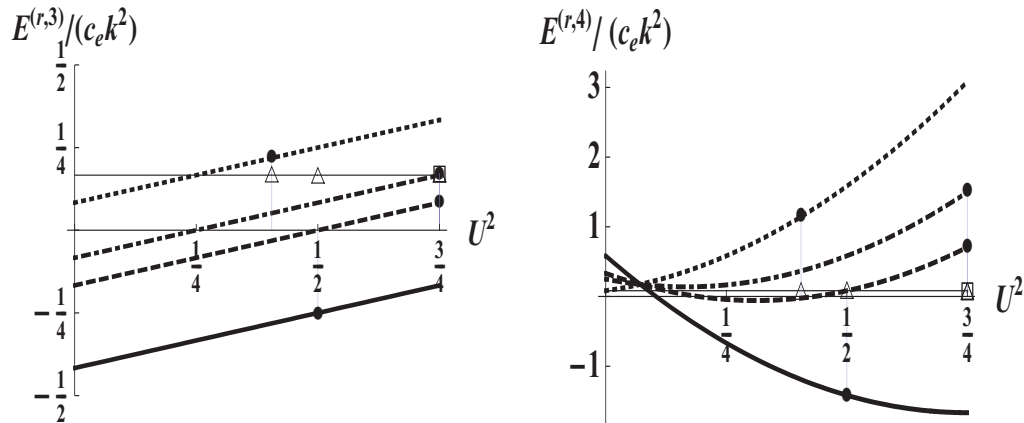


Figure 17: The $E^{(r,3)}/k^2$ (left diagram) and $E^{(r,4)}/k^2$ (right diagram) are shown when $\Lambda = \frac{1}{6}$ and $\Lambda = \frac{1}{12}$. The symbols plot the numerical results for $U^2 = \{1 - 2c_e, 1 - c_e, 1 - c_e, 2 \times 0.45^2\}$ when $t_c^{(m)} = \{0, \frac{1}{3}, \frac{1}{4}, \frac{1}{2}\}$ (solid, dashed, dotted-dashed and dotted), against the analytical predictions (5.12) and (5.7), respectively. Left diagram: $\Lambda_{bgk} = \frac{1}{6}$, $\Lambda = \frac{1}{6}$ (circles) and $\Lambda = \frac{1}{12}$ (triangles). Right diagram: $\Lambda = \Lambda_{bgk} = \frac{1}{6}$ (triangles) and $\Lambda = \Lambda_{bgk} = \frac{1}{12}$ (circles).

is $\frac{E^{(r,3)}}{c_e k^2}(\Lambda_{bgk} = \frac{1}{6}, \Lambda = \frac{1}{12}) \equiv \frac{1}{6} \forall c_e$, and the increasing with c_e lines are for $\Lambda = \Lambda_{bgk} = \frac{1}{6}$. Conversely, the velocity-independent diffusion error $\frac{E^{(r,4)}}{c_e k^2} = \frac{1}{12}$ is for $\Lambda = \Lambda_{bgk} = \frac{1}{6}$, while $|\frac{E^{(r,4)}}{c_e k^2}|$ grows with U^2 when $\Lambda = \Lambda_{bgk} = \frac{1}{12}$ (see right diagram). This error may vanish for particular orientations of \vec{U} and \vec{k} (two different but similar solutions are illustrated by left diagrams in Figs. 19 and 20). When $\Lambda = \Lambda_{bgk} = \frac{1}{12}$, solutions where $R_4(\vec{U} = 0)$ are limited to relatively small value c_e but they are mainly located in stable area (cf. left diagram Fig. 9). In the next section, we further comment on the velocity dependence of the diffusion error.

5.3 Truncation diffusion error in the presence of advection (d2Q9 scheme)

The fourth-order numerical diffusion makes the diffusion error velocity-dependent. This is illustrated by relations (A.8) when \vec{U} and \vec{k} are parallel to the principal axes. Moreover, since the advection-based term $R_{4,4}$ does not factorize D_2 (see in Section 4), the term $E^{(r,4)}$ diverges when $c_e \rightarrow 0$ and $\vec{U} \neq 0$, except when $\Lambda = \Lambda^{(ext.)}(\Lambda_{bgk})$ and $c_{4,4} = 0$ (cf. relations (2.15)). The interesting property of this choice is that it reduces the quadratic velocity dependence of the error to the linear one, provided that the second-order numerical diffusion has been corrected. This is illustrated in Fig. 18 where $\frac{E^{(r,4)}}{c_e k^2}$ is plotted for $\Lambda_{bgk} = \frac{1}{12}$, in order to compare with the “optimal advection” solution (2.11) in Fig. 17. Only when $\Lambda = \Lambda^{(ext.)}(\Lambda_{bgk} = \frac{1}{6}) = \frac{1}{6}$, the pure diffusion and advection-diffusion fourth-order errors coincide. The solution is then given by relation (5.7). We recall that this particular choice is also advantageous for its advanced stability.

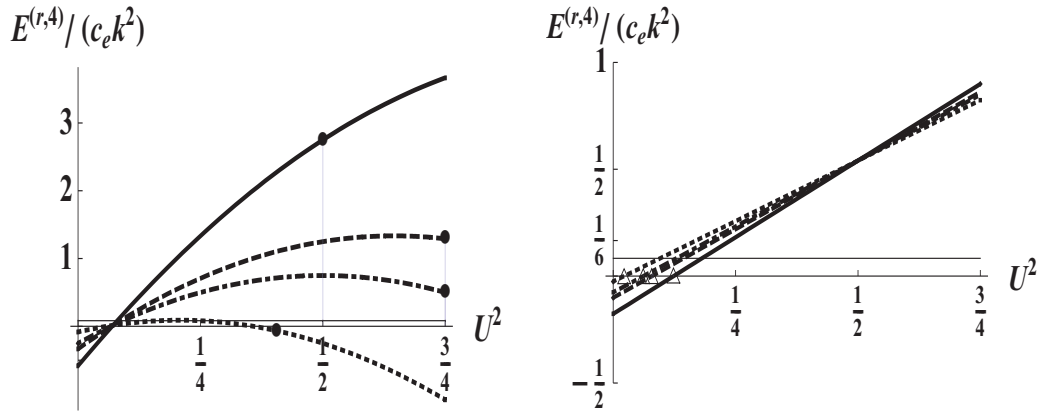


Figure 18: The predictions for $\frac{E^{(r,4)}}{c_e k^2}(U^2)$ are plotted for the isotropic tensor when $\Lambda_{bgk} = \frac{1}{12}$, $c_e = \frac{1}{4}$, the velocity and \vec{k} are along the diagonal, for $\Lambda = \frac{1}{4}$ (the left diagram) and $\Lambda = \Lambda^{(ext.)}(\Lambda_{bgk})$ (the right diagram). The symbols plot numerical results using the same velocity as in Fig. 17 when $\Lambda = \frac{1}{4}$. The velocity is set according to relation (A.10) when $\Lambda = \Lambda^{(ext.)}(\Lambda_{bgk})$, then $E^{(r,4)} = 0$. The horizontal line is $\frac{E^{(r,4)}}{c_e k^2} = \frac{1}{12}$ for $\Lambda = \Lambda^{(ext.)}(\frac{1}{6}) = \frac{1}{6}$.

Otherwise, one may try to remove the term R_4 with the special solutions for \vec{U} . Figs. 19 and 20 illustrate this when \vec{U} and \vec{k} are parallel to a principal lattice axis and the modeled tensor is isotropic. The solution exists for the diagonal orientation in the whole interval $c_e \in [0,1]$ when $\Lambda = \frac{1}{4}$ and $\Lambda_{bgk} \leq \frac{1}{12}$. When $\Lambda = \Lambda^{(ext.)}(\Lambda_{bgk})$, the solution exists when c_e is not too small or when Λ_{bgk} is sufficiently large (the right diagram in Fig. 20). One interesting solution is $U^2(c_e) = \frac{1}{9}$ in 1D when $\Lambda = \Lambda^{(ext.)}(\Lambda_{bgk})$ and $\Lambda_{bgk} \rightarrow 0$, for any t_c . When $\Lambda = \Lambda^{(ext.)}(\Lambda_{bgk})$ and $\Lambda_{bgk} \rightarrow \infty$ (then $\Lambda \rightarrow \frac{1}{8}$), then $R_4(U^2) = 0$ if $U^2 = c_e/4$, for the two orientations. These solutions are mainly located in stable areas. The minimization of the advection-diffusion error is difficult in the presence of all the parameters and arbitrary orientations of \vec{U} and \vec{k} . We suggest that if the velocity is close to delineated limits, $E^{(r,4)}$ remains relatively small. In principle, one may try to optimize the applied advection velocity, c_e and the two eigenvalues giving truncation errors of the problem.

6 Concluding notes

Truncated corrections. Firstly, we show that the Taylor series analysis of the time-dependent exact recurrence equations provides a simple method to derive the high-order approximation of the macroscopic equations. By this means, the generic forms of the third and fourth-order truncated corrections for the mass conservation equation are obtained for the TRT operator. The result is applicable for any velocity set and any linear, isotropic or anisotropic, equilibrium distribution. Secondly, developed heuristic stability analysis undoubtedly shows that there exists the narrow relation between the stability and the fourth-order truncated correction in the advection limit where the effective

second-order diffusion form vanishes. This last condition defines the largest stable velocity amplitude, sufficient providing that the fourth-order correction vanishes or obtains the suitable sign on this stability line.

The stability analysis is then coupled with the inspection of the third and fourth-order truncated corrections, with respect to their magnitude, isotropy, weight and velocity dependence. The analysis is fully supported by the evolution of concentration waves and, to some extent, for the propagation of the Gaussian hill, using the d2Q9 anisotropic scheme. Two particular collision configurations, namely, the BGK model with $\Lambda_{bgk} = \Lambda^{-2} = \frac{1}{12}$ and the TRT model with $\Lambda = \frac{1}{6}$ and $\Lambda_{bgk} = \frac{1}{12}$ remove, respectively, the third-order advection error and the fourth-order pure diffusion error. However, the fourth-order advection-diffusion error R_4 depends on velocity \vec{U} , and it cannot be removed independently of it. We find that velocity solution where R_4 vanishes for the principal lattice directions lie inside the stability intervals for the most interesting eigenvalue relationships. The “best” choice of the equilibrium parameters and relaxation rates depends on the problem (e.g., diffusion or advection-dominant) and the objectives (e.g., stability or advanced accuracy). In particular, the hydrodynamic weights are not the most stable but they produce the most isotropic form for advection and, for the majority of the eigenvalue strategies, diffusion truncation errors.

Anisotropic diffusion. The common equilibrium form is provided for the d2Q9, d3Q15 and d3Q19 TRT schemes, including the minimal schemes and the d3Q13 velocity set as their respective submodels. All of them match the anisotropic diffusion entries with the suitable linear combinations of the symmetric equilibrium components $\{E_q^+\}$, multiplied by the eigenvalue function Λ^- of the anti-symmetric modes. The d3Q19 model may freely redistribute the diagonal anisotropy between the two velocity classes with the additional equilibrium weight. The d3Q27 model has free weights also for the cross-diffusion stencil but the study of this model is out of the scope of this work.

The specific linear E_q^+ -combinations are restricted by the exact von Neumann stability conditions derived in the diffusion-dominant limit (see Eqs. (3.16)-(3.20)). We emphasize that improper choice of the free equilibrium weights for given anisotropic factors may destabilize the scheme. Another critical point is that the stable mean trace magnitude: $c_e \in [0, c_e^{(\max)}(t_q^{(m)})]$ is weight-dependent and it shrinks towards the minimum interval: $c_e \in [0, 1/d]$ when any one of the modeled diagonal elements approaches zero. The minimum interval guarantees stability of the pure diffusion minimal schemes, restricted to modeling of the diagonal tensors using the TRT operator.

Non-negativity conditions. Non-negativity of the immobile component E_0 and all “moving” components $\{E_q^+\}$ is sufficient but not necessary for stability of pure diffusion TRT schemes. In the presence of cross-diffusion elements, $E_0 \geq 0$ is recommended for any weights and eigenvalues. The principal necessary diffusion stability conditions (3.16) become then sufficient, essentially, for the OTRT subclass $\Lambda = \frac{1}{4}$, for any anisotropy. Beyond the optimal subclass, the analytical form of the *necessary and sufficient* diffusion boundary is not known. Non-negativity conditions might be recommended for safety, especially for

large diffusion coefficients and when Λ lies outside the interval $[\frac{1}{6}, \frac{1}{4}]$. One should bear in mind that this constraints the modeled tensor to the diagonal-dominant condition (at the best), where the available anisotropic range depends on the velocity set and mass term weights, as given by Eqs. (3.13)-(3.15). In particular, only the coordinate ($t_c^{(m)} = \frac{1}{2}$) or the diagonal ($t_c^{(m)} = 0$) weights, respectively, may then reach the largest anisotropy of the diagonal and off-diagonal elements for the d2Q9 and d3Q15 models. This first constraint is relaxed for the d3Q19 model. Finally, being sufficient for stability of the pure diffusion schemes, the whole set of the non-negativity conditions $\{E_q = E_q^+ + E_q^- \geq 0\}$ is not sufficient in the presence of advection, except, principally, the OTRT and BGK subclasses.

Advection-dominant boundary. The necessary advection line $U^2 = U_a^2(c_e)$ is derived requiring the positive semi-definiteness of the effective diffusion form in the presence of the velocity-dependent second-order numerical diffusion (or its cross-diffusion entries) and the anisotropy (Eqs. (3.22), (3.23) and (3.24)). The advection line is independent of the weights and eigenvalues, but $U_a^2(c_e)$ falls to zero in the anisotropic limits, unless the second-order numerical diffusion has been suppressed with the help of equilibrium correction $E_q^{(u)}$. Again, the minimum-valued combination of necessary advection and diffusion conditions is not sufficient in general, except, essentially, the OTRT subclass. Moreover, the OTRT subclass may reach the best possible velocity range of the d1Q3 model: $U^2 \in [0, 1 - c_e]$ in multi-dimensions with the special (non-hydrodynamic) weights (3.7). A sufficiency of the advection line is extended for larger relationships of the two eigenvalues given by Eqs. (2.15). A nearly optimal stability then becomes available for any anisotropy in 2D, and for the diagonal-dominant tensors in the 3D, at least. Further analytical work could confirm these results, partly based on the numerical analysis.

Relaxation rates. The most stable advection choices are: (i) $\Lambda = \frac{1}{4} \forall \Lambda^-$, and (ii) $\Lambda \in [\Lambda^{(ext.)}(\Lambda_{bgk}), \frac{1}{4}] \in [\frac{1}{6}, \frac{1}{4}]$ when $\Lambda_{bgk} \leq \frac{1}{6}$. They enable the TRT scheme to reach any Peclet number with the largest stable velocity. The Λ -independent advection accuracy is only obtained in one dimension, when $U^2 = 1 - c_e$. Otherwise, both $\Lambda = \frac{1}{4}$ and $\Lambda = \frac{1}{6}$ demonstrate very reasonable accuracy, except for extremely high velocities $U^2 \approx 1$ in the advection limit $c_e \rightarrow 0$. Next, the BGK set-up with $\Lambda = \Lambda_{bgk} = \frac{1}{6}$ is interesting since it has a nearly optimal stability and makes the fourth-order error: (i) bounded for any anisotropy, (ii) independent of the velocity and weights, (iii) isotropic, at least for the isotropic tensors. However, the relative diffusion error grows then linearly with c_e , while the relative advection error grows with the velocity, and the mean trace magnitude is limited to $\sqrt{1/6}c_e^{(max)}$.

Other eigenvalue strategies overcome some of these artefacts. In particular, $\Lambda = \frac{1}{12}$ may result in velocity independent advection error, with a relative amplitude twice as high as the relative diffusion error with $\Lambda = \frac{1}{6}$. The choice $\Lambda = \Lambda_{bgk} = \frac{1}{12}$ is extremely precise for the advection problems. However, modeling at the high Peclet numbers with the help of small c_e is then limited to relatively small velocity amplitudes, as $U^2 \approx c_e$ when $c_e \in]0, 10^{-2}]$ for isotropic diffusion tensors. At the same time, the stable velocity rapidly drops

for $\Lambda = \frac{1}{12}$ when Λ^- decreases to zero, [34]. This results in limited range Peclet numbers. More stable choice, $\Lambda = \frac{1}{4} - \Lambda_{bgk}$ when $\Lambda_{bgk} \leq \frac{1}{4}$, enables the c_e -independent diffusion error. In turn, the most stable family $\Lambda = \Lambda^{(ext.)}(\Lambda_{bgk})$ results in linear dependency of the fourth-order correction on the velocity provided that the second-order numerical diffusion has been suppressed.

Future work. The proposed eigenvalue configurations need further evaluation. Besides that, the truncated components can be examined with respect to their grid refining behaviour. The derived necessary and sufficient stability conditions can be adapted for the finite-difference anisotropic schemes on the equivalent spatial and temporal stencils, e.g., limiting the OTRT to its BGK component $\Lambda^- = \Lambda^+ = \frac{1}{2}$ (or $\tau = 1$) for the forward-time schemes [24]. It would be very interesting to develop the similar stability analysis of two alternative anisotropic approaches based on the isotropic equilibrium: the L-model with direction-depending relaxation rates of the anti-symmetric modes [12, 15, 38, 48, 52], and the MRT-type minimal anisotropic models, [42, 51]. Finally, the presented methodology allows for extensions of the analysis of the LBE models to non-linear equilibrium functions, [21].

A Details for derivation of the truncated terms

A.1 Fourth-order approximation: Intermediate steps

In the simplest case, when the set $\{E_q^\pm\}$ is time-independent and constant along the link, the recurrence equations (2.2) are read as

$$\mathcal{G}_q^\pm = \mathcal{S}_q^\pm + \mathcal{R}_q^\pm + \mathcal{T}_q^\pm + \mathcal{Z}_q^\pm, \quad q=0, \dots, Q_m, \quad (\text{A.1})$$

where

$$\begin{aligned} \mathcal{S}_q^\pm &= E_q^\mp \bar{\Delta}_q - \Lambda^\mp E_q^\pm \Delta_q^2, \quad \mathcal{R}_q^\pm = \left(\Lambda - \frac{1}{4}\right) \mathcal{G}_q^\pm \Delta_q^2, \quad \mathcal{S}_0^\pm = \mathcal{R}_0^\pm = 0, \\ \mathcal{T}_q^\pm &= E_q^\pm \bar{\Delta}_t + \Lambda^\mp E_q^\pm \Delta_t^2, \\ \mathcal{Z}_q^\pm &= - \left[\left(\Lambda - \frac{1}{4}\right) \mathcal{G}_q^\pm \Delta_t^2 + \frac{1}{2} \mathcal{G}_q^\pm \Delta_t^2 + (\Lambda^\pm + \Lambda^\mp) \mathcal{G}_q^\pm \bar{\Delta}_t \right]. \end{aligned} \quad (\text{A.2})$$

We build the fourth-order approximation (2.7)-(2.10) of the exact mass conservation relation $\sum_{q=0}^{Q_m} \mathcal{G}_q^\pm(\vec{r}, t) = 0$. Plugging the last relation (A.2) into $\sum_{q=0}^{Q_m} \mathcal{Z}_q^\pm(\vec{r}, t)$, and taking into account that $\sum_{q=0}^{Q_m} \mathcal{G}_q^\pm(\vec{r}, t) = 0 \forall \vec{r}$ and $\forall t$, it comes out that

$$\sum_{q=0}^{Q_m} \mathcal{Z}_q^+(\vec{r}, t) = 0.$$

The exact mass conservation equation becomes:

$$\sum_{q=0}^{Q_m} [\mathcal{S}_q^+ + \mathcal{T}_q^+ + \mathcal{R}_q^+] s(\vec{r}, t) = 0.$$

We construct the n th order approximations $\mathcal{S}_{q,n}^+$ and $\mathcal{T}_{q,n}^+$ for $n \geq 1$, then $\mathcal{Z}_{q,n}^+$ for $n \geq 2$ and $\mathcal{R}_{q,n}^+$ for $n \geq 3$, sequentially replacing all the link-wise central differences by their n th order Taylor approximation:

$$\begin{aligned} \bar{\Delta}_q^{(n)} &= \sum_{k=1}^{(n+1)/2} \frac{\partial_q^{2k-1}}{(2k-1)!}, & \Delta_q^{2(n)} &= 2 \sum_{k=1}^{n/2} \frac{\partial_q^{2k}}{(2k)!} \quad \text{with } \partial_q^1 = \partial_q = (\nabla \cdot \vec{c}_q), \\ \bar{\Delta}_t^{(n)} &= \sum_{k=1}^{(n+1)/2} \frac{\partial_t^{2k-1}}{(2k-1)!}, & \Delta_t^{2(n)} &= 2 \sum_{k=1}^{n/2} \frac{\partial_t^{2k}}{(2k)!}. \end{aligned} \tag{A.3}$$

We then obtain the mass conservation equation in the form $\partial_t s = [\sum_{k=1}^n R_k] s$ where R_k are related to operators S_{2k-1} and S_{2k} (defined by relations (2.8)). At the first order $n=1$, and taking into account that $\sum_{q=0}^{Q_m} E_q^+ = 1$, it comes that $R_1 = -S_1$ and thus $\partial_t s = -S_1 s$, as

$$\sum_{q=1}^{Q_m} \mathcal{S}_{q,1}^+ = \sum_{q=1}^{Q_m} E_q^- \partial_q = S_1, \quad \sum_{q=0}^{Q_m} \mathcal{T}_{q,1}^+ = \sum_{q=0}^{Q_m} E_q^+ \partial_t = \partial_t, \quad \mathcal{R}_{q,1}^+ = \mathcal{Z}_{q,1}^+ = 0. \tag{A.4}$$

The key point is to account for the numerical diffusion of the scheme at any order n , replacing ∂_t with $(\sum_{k=1}^{n-1} R_k)$ when $n \geq 2$. At the second order $n=2$, $\mathcal{R}_{q,2}^+ = 0$ and thus $R_2 = \Lambda^- D_2$, $D_2 = S_2 - S_1^2$, as

$$R_2 = - \sum_{q=1}^{Q_m} [\mathcal{S}_{q,2}^+ + \mathcal{T}_{q,2}^+] \Big|_{\partial_t \rightarrow -S_1} = \Lambda^- \left[\sum_{q=1}^{Q_m} E_q^+ \right] \partial_q^2 - \Lambda^- \left[\sum_{q=1}^{Q_m} E_q^+ \right] \partial_t^2 \Big|_{\partial_t \rightarrow S_1^2}. \tag{A.5}$$

Here, S_1^2 is the second-order numerical diffusion of the scheme. Then, at third order, by substituting $\mathcal{G}_{q,1}^+$ into $\mathcal{R}_{q,3}^+$:

$$\mathcal{R}_{q,3}^+ = \left(\Lambda - \frac{1}{4} \right) \sum_{q=1}^{Q_m} \partial_q^2 (E_q^- \partial_q + E_q^+ \partial_t),$$

one obtains

$$R_3 = - \left[\sum_{q=1}^{Q_m} (\mathcal{S}_{q,3}^+ + \mathcal{T}_{q,3}^+ + \mathcal{R}_{q,3}^+) \right] \Big|_{\partial_t \rightarrow (R_1 + R_2)} = -C_3,$$

where

$$C_3 = - \left(2\Lambda_{bgk} + \Lambda - \frac{1}{4} \right) S_1 D_2 + \left(\Lambda - \frac{1}{12} \right) (S_3 - S_1^3),$$

with

$$\begin{aligned} \sum_{q=1}^{Q_m} \mathcal{S}_{q,3}^+ + \mathcal{T}_{q,3}^+ \Big|_{\partial_t \rightarrow (R_1+R_2)} &= -\frac{1}{6}(S_1^3 + 12\Lambda_{b g k} S_1 D_2 - S_3), \\ \sum_{q=1}^{Q_m} \mathcal{R}_{q,3}^+ \Big|_{\partial_t \rightarrow (R_1+R_2)} &= \left(\Lambda - \frac{1}{4}\right) \sum_{q=1}^{Q_m} \partial_q^2 (E_q^- \partial_q + E_q^+ \partial_t) = \left(\Lambda - \frac{1}{4}\right) (S_3 - S_1 S_2). \end{aligned} \quad (\text{A.6})$$

Finally, at fourth order, plugging $\mathcal{G}_{q,2}^+$ into $\mathcal{R}_{q,4}^+$ we obtain

$$\begin{aligned} R_4 &= - \left[\sum_{q=1}^{Q_m} (\mathcal{S}_{q,4}^+ + \mathcal{T}_{q,4}^+ + \mathcal{R}_{q,4}^+) \right] \Big|_{\partial_t \rightarrow \sum_{k=1}^3 R_k} \\ &= c_{4,1} D_2^2 + c_{4,2} D_2 S_1^2 + c_{4,3} (S_4 - S_1 S_3) + c_{4,4} S_1 (S_1^3 - S_3), \end{aligned}$$

with

$$\begin{aligned} \sum_{q=1}^{Q_m} [\mathcal{S}_{q,4}^+ + \mathcal{T}_{q,4}^+] \Big|_{\partial_t \rightarrow \sum_{k=1}^3 R_k} &= \frac{1}{12} \Lambda^- (12\Lambda_{b g k} D_2^2 - 24C_3 S_1 + 6D_2 S_1^2 + S_1^4 - S_4), \\ \sum_{q=1}^{Q_m} \mathcal{R}_{q,4}^+ \Big|_{\partial_t \rightarrow \sum_{k=1}^3 R_k} &= \left(\Lambda - \frac{1}{4}\right) \left[\sum_{q=1}^{Q_m} \partial_q^2 (\mathcal{S}_{q,2}^+ + \mathcal{T}_{q,2}^+ + \mathcal{Z}_{q,2}^+) \right] \Big|_{\partial_t \rightarrow \sum_{k=1}^3 R_k}, \end{aligned}$$

where

$$\begin{aligned} \sum_{q=1}^{Q_m} \partial_q^2 [\mathcal{S}_{q,2}^+ + \mathcal{T}_{q,2}^+] \Big|_{\partial_t \rightarrow \sum_{k=1}^3 R_k} &= -\Lambda^- (S_4 - S_2^2), \\ \mathcal{Z}_{q,2}^+ &= -(\Lambda^- + \Lambda^+) \partial_t \mathcal{G}_{q,1}^+ = -(\Lambda^- + \Lambda^+) (E_q^- \partial_q + E_q^+ \partial_t) \partial_t, \\ \sum_{q=1}^{Q_m} \partial_q^2 \mathcal{Z}_{q,2}^+ \Big|_{\partial_t \rightarrow \sum_{k=1}^3 R_k} &= \sum_{q=1}^{Q_m} \partial_q^2 \mathcal{Z}_{q,2}^+ \Big|_{\partial_t \rightarrow -S_1} = -(\Lambda^- + \Lambda^+) S_1 (S_1 S_2 - S_3). \end{aligned} \quad (\text{A.7})$$

Summing R_1 to R_4 we obtain the solution (2.7)-(2.10).

A.2 Examples of the fourth-order errors

The truncation errors given below are used for the analysis of concentration waves in Section 5. Here, we replace ∂_α with k_α for operators (2.8). When the modeled tensor is isotropic, all the weights are the same and obey relation (3.4), the second-order numerical diffusion has been suppressed ($g^{(u)} g_{\alpha\beta}^{(u)} = 1$), and the two vectors \vec{U} and \vec{k} are either

parallel to the coordinate or the diagonal axis, then $R_4(\vec{U}, \vec{k})$ becomes

$$\begin{aligned}
 (a) \quad \vec{k} \parallel \vec{U} \parallel \{1,0\}: \quad & \frac{R_4(\vec{U}, \vec{k})}{k^4} = c_e(c_e c_{4,1} + c_{4,3}) + (c_e c_{4,2} - c_{4,4})U^2 + c_{4,4}U^4, \\
 (b) \quad \vec{k} \parallel \vec{U} \parallel \{1,1\}: \quad & \frac{R_4(\vec{U}, \vec{k})}{k^4} = c_e(c_e c_{4,1} + (2 - 3t_c)c_{4,3}) \\
 & + (c_e c_{4,2} + \frac{3}{2}t_c c_{4,3} + (3t_c - 2)c_{4,4})U^2 + c_{4,4}U^4. \quad (A.8)
 \end{aligned}$$

These relations define the relative errors (5.3). When $\Lambda = \frac{1}{4}$, $E^{(r,4)}/k^2$ is read as

$$\begin{aligned}
 (a): \quad & \frac{E^{(r,4)}}{k^2} = \frac{1}{12} - c_e \Lambda_{bgk} + \frac{(2c_e(8\Lambda_{bgk} - 1) - 1)U^2 + U^4}{4c_e}, \\
 (b): \quad & \frac{E^{(r,4)}}{k^2} = c_e \Lambda_{bgk} + \frac{t_c}{4} - \frac{1}{6} + \frac{(4(1 + c_e(1 - 8\Lambda_{bgk})) - 7t_c)U^2 - 2U^4}{8c_e}. \quad (A.9)
 \end{aligned}$$

In general, $E^{(r,4)}$ diverges when $c_e \rightarrow 0$ and $U^2 \neq 0$. When $\Lambda_{bgk} \rightarrow 0$, then $R_4(\vec{U}, \vec{k})$ vanishes in 1D when $U^2 = c_e + 1/2 - \sqrt{3}/6 \sqrt{3 + 4c_e(2 + 3c_e)}$. When $\Lambda = \Lambda^{(ext.)}(\Lambda_{bgk})$, then $c_{4,4} = 0$ in relations (A.8) and $E^{(r,4)}/k^2$ is bounded when $c_e \rightarrow 0$. Solution of linear equation $R_4(\vec{U}, \vec{k}) = 0$ then becomes

$$\begin{aligned}
 (a): \quad & U^2(c_e) = \frac{-(1 + 24\Lambda_{bgk} + 3c_e(\gamma - 1) - 3\gamma)}{3(5 + \gamma - 40\Lambda_{bgk})}, \quad \gamma = \sqrt{64\Lambda_{bgk} + 1}, \\
 (b): \quad & U^2(c_e, t_c) = -\frac{2c_e(3c_e(\gamma - 1) + (3\gamma - 24\Lambda_{bgk} - 1)(3t_c - 2))}{3(2c_e(5 + \gamma - 40\Lambda_{bgk}) + t_c - 3(\gamma - 8\Lambda_{bgk})t_c)}. \quad (A.10)
 \end{aligned}$$

When $\Lambda_{bgk} \rightarrow 0$, then $\gamma \rightarrow 1$ and solution (a) reduces to $U^2 = 1/9$, while solution (b) becomes $\frac{2c_e(2 - 3t_c)}{3(6c_e - t_c)}$. The solutions differ for $\Lambda = \frac{1}{4}$ and $\Lambda = \Lambda^{(ext.)}(\Lambda_{bgk})$ when $\Lambda_{bgk} \rightarrow 0$, even if $\Lambda^{(ext.)} \rightarrow \frac{1}{4}$ in this limit, since $c_{4,4}(\Lambda = \frac{1}{4}) = \Lambda^-/4 \neq 0$. When $\Lambda_{bgk} \rightarrow \infty$, the two solutions (A.10) are the same: $U^2 = c_e/4$. The left diagram in Fig. 19 shows the 1D solutions for U^2 where $R_4(U^2) = 0$. The right diagram in Fig. 19 shows similar solution for the diagonal axis when for $\Lambda = \frac{1}{4}$, to compare with the solutions in Fig. 20 for $\Lambda = \frac{1}{12}$ (see the left diagram) and $\Lambda = \Lambda^{(ext.)}(\Lambda_{bgk})$ (see the right diagram). The diagonal solution $U^2 \in [0, 1]$ exists for $\Lambda = \frac{1}{4}$ when $\Lambda_{bgk} \leq \frac{1}{12}$ for all $c_e \in [0, c_e^{(0)}]$, to be contrasted with the solutions in Fig. 20. Here, solution does not exist for small c_e when $\Lambda = \Lambda^{(ext.)}(\Lambda_{bgk})$ and Λ_{bgk} is small (the right diagram), or when $c_e \geq \frac{1}{2}$ and $\Lambda = \Lambda_{bgk} = \frac{1}{12}$ (the left diagram). Altogether, the solutions $U^2(c_e)$ where $R_4(\vec{U}) = 0$ for the principal lattice directions and isotropic tensors stay inside the stability interval for the principal eigenvalue relationships.

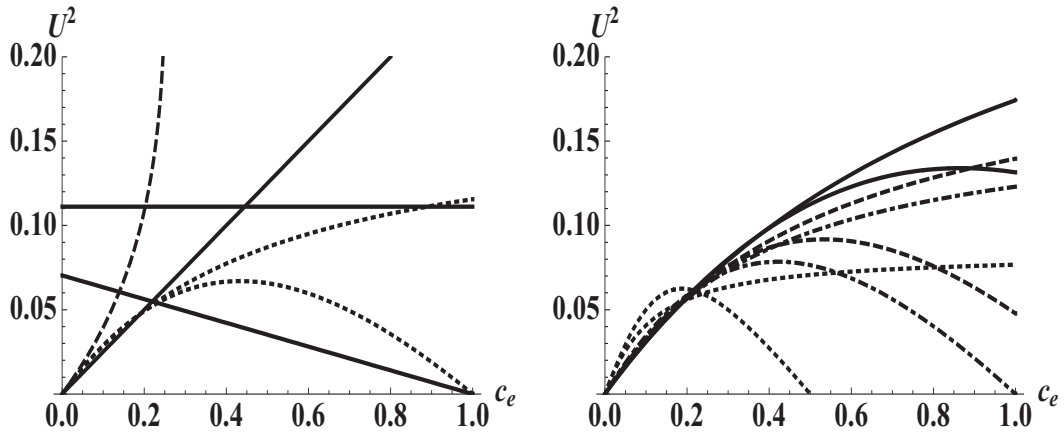


Figure 19: The left diagram plots the solutions for $U^2(c_e)$ where $R_4(\vec{U}, \vec{k})=0$ when \vec{U} and \vec{k} are parallel to a coordinate axis, with (i) $\Lambda = \frac{1}{4}$ (dotted lines, increasing for $\Lambda_{bgk} \rightarrow 0$ and non-monotonic for $\Lambda_{bgk} = \frac{1}{12}$), (ii) $\Lambda = \Lambda^{(ext.)}(\Lambda_{bgk})$ (solid lines): decreasing for $\Lambda_{bgk} = \frac{1}{12}$, $U^2 \equiv \frac{1}{9}$ for $\Lambda_{bgk} \rightarrow 0$, and $U^2 = c_e/4$ when $\Lambda_{bgk} \rightarrow \infty$, and (iii) $\Lambda = \Lambda_{bgk} = \frac{1}{12}$ (dashed, exists when $c_e \leq \frac{1}{4}$). The right diagram plots the solutions for $\Lambda = \frac{1}{4}$ when \vec{U} and \vec{k} are parallel to a diagonal axis for four weight families: $t_c^{(m)} = \{0, \frac{1}{4}, \frac{1}{3}, \frac{1}{2}\}$ (solid, dashed, dotted-dashed and dotted lines, respectively). The four increasing lines are for $\Lambda_{bgk} \rightarrow 0$ and four non-monotonic lines are for $\Lambda_{bgk} = \frac{1}{12}$.

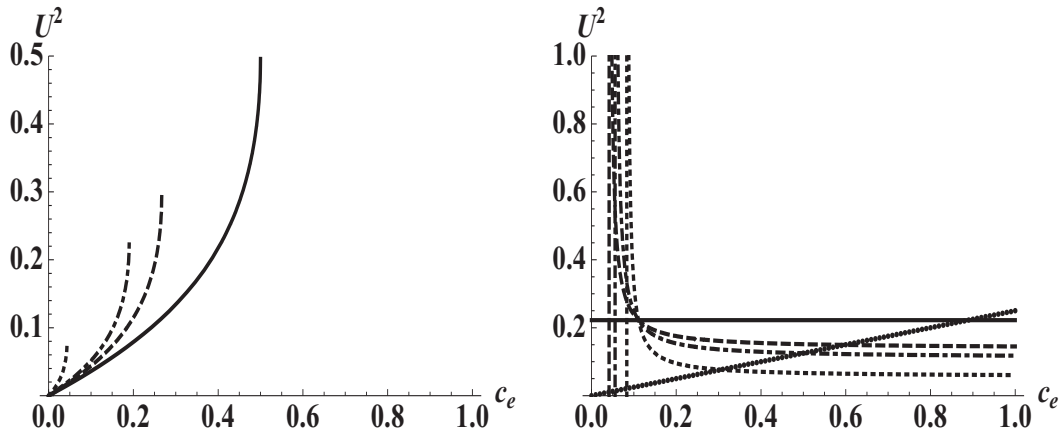


Figure 20: The two diagrams plot solution $U^2(c_e)$ where $R_4(\vec{U}, \vec{k})=0$ when \vec{U} and \vec{k} are parallel to the diagonal axis, for four weight families: $t_c^{(m)} = \{0, \frac{1}{4}, \frac{1}{3}, \frac{1}{2}\}$ (solid, dashed, dotted-dashed and dotted, respectively). Left diagram: $\Lambda = \Lambda_{bgk} = \frac{1}{12}$. Right diagram: $\Lambda = \Lambda^{(ext.)}(\Lambda_{bgk})$. When $\Lambda_{bgk} \rightarrow \infty$ then $U^2 \equiv c_e/4$ for all weights (line of circles). Other curves are for $\Lambda_{bgk} \rightarrow 0$, with $U^2 \equiv \frac{2}{9}$ when $t_c^{(m)} = 0$.

A.3 Links with the Fourier analysis

In a periodic domain, the solution of linear evolution equation is looked in the form $f_q^\pm(\vec{r}, t) = \Omega^t e^{i\vec{r} \cdot \vec{k}} F_q^\pm s(\vec{r}, t)$, where the eigenvectors $\{F_q^\pm\}$ obey the TRT evolution equation

for $q=0, \dots, Q_m$:

$$\Omega(F_q^+ + F_q^-)e^{ikq} = (1 + \lambda^+)F_q^+ + (1 + \lambda^-)F_q^- - \lambda^+E_q^+ - \lambda^-E_q^- . \tag{A.11}$$

A generic form of solution $F_q^+(\Omega)$ of Eq. (A.11) can be found in [20]. The characteristic equation of the mass conservation relation takes the form:

$$\sum_{q=0}^{Q_m} F_q^+ = 1 \quad \text{when} \quad \sum_{q=0}^{Q_m} E_q^+ = 1. \tag{A.12}$$

In the limit $\vec{k} \rightarrow 0$, the root Ω of the characteristic equation can be expanded into series of k :

$$\Omega = \sum_n \exp(w_n k^n), \quad k = ||\vec{k}||.$$

The third-order correction $w_3 k^3$ has been given by formulae (B.13) in [12], assuming the hydrodynamic weights $t_q^{(a)}$ for the advection term $\{E_q^-\}$ and $\vec{k} = \vec{k}/k$:

$$w_3 k^3 = -ik^3 (\vec{U} \cdot \vec{k}) \left[f_2^{(u)}(\lambda_D, \lambda_e) \frac{v(\vec{k})}{\Lambda^-} + g_u(\lambda_D, \lambda_e) ((\vec{U} \cdot \vec{k})^2 - 1) \right]. \tag{A.13}$$

Let us first give the two eigenvalue functions (A.13) in current variables:

$$g_u(\lambda_D, \lambda_e) = \left(\Lambda - \frac{1}{12} \right) = c_{3,1}, \quad f_2^{(u)}(\lambda_D, \lambda_e) = 2\Lambda_{bgk} + \Lambda - \frac{1}{4} = c_{3,2},$$

with $\lambda_D \rightarrow \lambda^-, \lambda_e \rightarrow \lambda^+, \Lambda^2 \rightarrow 4/3\Lambda, \frac{v_D}{c_s^2} \rightarrow \Lambda^-$. (A.14)

Then relation (A.13) can be obtained from the $-iR_3(\vec{k})$ replacing S_1 with $ik(\vec{U} \cdot \vec{k})$ and D_2 with $-v(\vec{k})k^2/\Lambda^-$, then taking the hydrodynamic weights and replacing $(S_1^3 - S_3)$ with $-ik^3(\vec{U} \cdot \vec{k})((\vec{U} \cdot \vec{k})^2 - 1)$ (here, k^2 replaces $-\Delta$ for the hydrodynamic weights, see relations (4.1)). It follows that $v(\vec{k})$ is, indeed, the *effective diffusion form*,

$$v(\vec{k}) = \sum_{\alpha, \beta} \mathcal{D}_{\alpha\beta}^{(eff)} \hat{k}_\alpha \hat{k}_\beta.$$

The pure diffusion fourth-order error has been first prescribed by formulas (B.1)-(B.3) in [20], keeping in mind the d2Q9 and d3Q15 models. The current solution (5.5) with (5.6) reduces to the previous solution with the following transformations:

$$v_D \rightarrow c_s^2 \Lambda^-, \quad c_s^2 \rightarrow c_e \frac{(1 + 6t_c^{(m)})}{3},$$

$$c_s^2 a_e \rightarrow c_e - c_s^2 = 2c_e \left(\frac{1}{3} - t_c^{(m)} \right),$$

$$f_2(\lambda_D, \lambda_e) \Lambda^- \rightarrow -c_{4,1}, \quad g(\lambda_D, \lambda_e) \Lambda^- \rightarrow -c_{4,3},$$

$$f_1(c_s^2, \lambda_D, \lambda_e) \Lambda^- \rightarrow -(c_e c_{4,1} + c_{4,3}). \tag{A.15}$$

The two first terms (B.2) in [20] correspond to two first terms (5.6). Their term $g(\lambda_D, \lambda_e) \times G(\mathcal{D}_{\alpha\beta}, \vec{k})$ is given by the two next terms for the d2Q9 model when $g^{(a)} = g_{\alpha\beta}^{(a)} = 1$. This solution is supplemented by correction

$$c_{4,3} \left(-w \mathcal{M}_{4,dig}(\mathcal{D}_{\alpha\alpha}) + \mathcal{M}_{4,off}(\mathcal{D}_{\alpha\beta}) \right)$$

for the d3Q15 model (cf. relation (C.4)-(C.5) with relations (C.2)).

B Details to von Neumann stability analysis

These conditions are prescribed by extending the von Neumann analysis [20] to the d3Q19 model and anisotropic equilibrium (see their relations (61)-(68)). When \vec{k} is parallel to any one principal lattice axis and its all non-zero components are set equal to π , the characteristic equation (A.12) becomes independent of the anti-symmetric component $\{E_q^-\}$:

$$(1 + \lambda^- + \Omega) \left(\Omega^2 + \Omega \lambda^+ (1 - 2s^+) - (1 + \lambda^+) \right) = 0. \tag{B.1}$$

Applying the Miller's theorem [39] to the second-order polynomial in Eq. (B.1), it comes out that $|\Omega| \leq 1$ provided that $s^+ \in [0, 1]$, where:

$$\vec{k} = \pi \vec{1}_\alpha, \quad \text{all models: } s^+ = \sum_{q=1}^{Q_m} E_q^+ c_{q\alpha}^2 = \mathcal{D}_{\alpha\alpha} + g^{(u)} U_\alpha^2, \tag{B.2}$$

$$\vec{k} = \pi \vec{1}_d, \quad \text{d2Q9, d3Q19: } s^+ = \sum_q E_{q,c}^+, \tag{B.3}$$

$$\vec{k} = \pi \vec{1}_d, \quad \text{d2Q5, d3Q7, d3Q15: } E_0 \in [0, 1], \tag{B.4}$$

$$\vec{k} = \pi \vec{1}_d^{(\gamma)}, \quad \text{d3Q15: } s^+ = \sum_{q:c_{q\gamma}=0} E_{q,c}^+, \quad \forall \gamma = 1, \dots, d, \tag{B.5}$$

$$\vec{k} = \pi \vec{1}_d^{(\gamma)}, \quad \text{d3Q19: } s^+ = \sum_{q:c_{q\gamma}=0} E_{q,c}^+ + \sum_{q:c_{q\gamma} \neq 0} E_{q,d}^+, \quad \forall \gamma. \tag{B.6}$$

The first condition (B.2) is prescribed for any velocity set when \vec{k} is parallel to some coordinate axis. In particular, it restricts E_0 to $[0, 1]$ for the d1Q3 model. The second and third conditions are set when \vec{k} is parallel to the diagonal lattice axis and they are independent of the anisotropy of the modeled tensor. Two last conditions are set when \vec{k} is parallel to the diagonal axis in the plan perpendicular to the γ -axis. Altogether, the diffusion-dominant conditions prescribe c_e to interval $[0, c_e^{(nec)}] \in [0, 1]$, further precised by relations (3.16).

C Details to heuristic stability analysis

C.1 Auxiliary matrix operators

The matrix form of the truncation errors is obtained with the help of the two operators:

$$\begin{aligned} \mathcal{M}^{(1)}|_w &= \mathcal{I}_\nabla + w(\mathcal{M}_\nabla^{(1)} - \mathcal{I}_\nabla) = \{\partial_\alpha \delta_{\alpha\beta} + w\partial_\beta(1 - \delta_{\alpha\beta})\}, \\ \mathcal{M}^{(2)}|_w &= \mathcal{I}_\nabla^2 + w(\mathcal{M}_\nabla^{(2)} - \mathcal{I}_\nabla^2) = \{\partial_\alpha^2 \delta_{\alpha\beta} + w\partial_\alpha \partial_\beta(1 - \delta_{\alpha\beta})\}, \end{aligned} \tag{C.1}$$

where

$$\mathcal{I}_\nabla = \{\partial_\alpha \delta_{\alpha\beta}\}, \quad \mathcal{M}_\nabla^{(1)} = \vec{1} \otimes \vec{\nabla}, \quad \mathcal{I}_\nabla^2 = \{\partial_\alpha^2 \delta_{\alpha\beta}\}, \quad \mathcal{M}_\nabla^{(2)} = \nabla \otimes \nabla.$$

Prescribing particular values for w , we operate with the weight-dependent (anisotropic) operators:

$$\begin{aligned} \mathcal{M}_a^{(1)} &= \mathcal{M}^{(1)}|_{w=w^*(1-2t_c^{(a)})}, \\ \mathcal{M}_a^{(2)} &= \mathcal{M}^{(2)}|_{w=w^*(1-2t_c^{(a)})}, \quad \mathcal{M}_m^{(2)} = \mathcal{M}^{(2)}|_{w=w^*(1-2t_c^{(m)})}, \\ \mathcal{M}_u^{(2)} &= \mathcal{M}^{(2)}|_{w=w^*(1-2t_c^{(u)})}, \quad \mathcal{M}_0^{(2)} = \mathcal{M}^{(2)}|_{w=w^*}, \end{aligned}$$

where d2Q9, d3Q15: $w^* = 3$, and $w = 1$ if only $t_c = \frac{1}{3}$,
 d3Q19: $w^* = \frac{3}{2}$, and $w = 1$ if only $t_c = \frac{1}{6}$. (C.2)

These operators become isotropic only for the hydrodynamic weights: $t_c^{(\cdot)} = \{\frac{1}{3}, \frac{1}{3}, \frac{1}{6}\}$ for the d2Q9, d3Q15 and d3Q19 schemes, respectively. The following relations are valid:

$$\begin{aligned} \nabla^T \cdot \mathcal{M}_\nabla^{(2)} \cdot \nabla &= \Delta^2, \quad \Delta = \sum_{\alpha=1}^d \partial_\alpha^2, \quad \nabla^T \cdot \mathcal{I}_\nabla^2 \cdot \nabla = \sum_{\alpha=1}^d \partial_\alpha^4, \\ \nabla^T \cdot \{\mathcal{M}_{\alpha\beta} \delta_{\alpha\beta}\} \cdot \mathcal{M}^{(2)}|_w \cdot \nabla &= \sum_{\alpha=1}^d \mathcal{M}_{\alpha\alpha} \partial_\alpha^4 + \frac{w}{2} \sum_{\alpha \neq \beta} (\mathcal{M}_{\alpha\alpha} + \mathcal{M}_{\beta\beta}) \partial_\beta^2 \partial_\alpha^2, \quad \forall \mathcal{M}_{\alpha\beta}. \end{aligned} \tag{C.3}$$

The last term vanishes in two dimensions for any traceless matrix as for example, $\{(U_\alpha^2 - \bar{U}^2) \delta_{\alpha\beta}\}$ and $\{(\mathcal{D}_{\alpha\beta} - c_e) \delta_{\alpha\beta}\}$ (cf. relation (3.1)).

C.2 Operator $R_{4,3}$: Corrections for anisotropic d3Q15 and d3Q19 models

The matrix form of the operator $R_{4,3}$ is given by relations (4.5) for the d2Q9 model. This form is also valid for the d3Q7 model and isotropic d3Q15 and d3Q19 models. These two last models need to correct the matrix \mathcal{M}_4 in relations (4.5) when the diagonal entries $\mathcal{D}_{\alpha\alpha}$

are anisotropic :

$$\begin{aligned}
 \text{d3Q15: } & \mathcal{M}_4 \rightarrow \mathcal{M}_4 - w\mathcal{M}_{4,dig}, \\
 \text{d3Q19: } & \mathcal{M}_4 \rightarrow \mathcal{M}_4 + \frac{3}{2}(3 + 2t_c^{(m)} - 8w_c^{(m)})\mathcal{M}_{4,dig}, \\
 & \mathcal{M}_{4,dig} = g^{(a)}\{(\mathcal{D}_{\alpha\beta} - c_e)\delta_{\alpha\beta}\} \cdot (\mathcal{M}_{\nabla}^{(2)} - \mathcal{I}_{\nabla}^2), \\
 & \nabla^T \cdot \mathcal{M}_{4,dig} \cdot \nabla = (c_e - \mathcal{D}_{xx})\partial_y^2\partial_z^2 + (c_e - \mathcal{D}_{yy})\partial_x^2\partial_z^2 + (c_e - \mathcal{D}_{zz})\partial_x^2\partial_y^2. \tag{C.4}
 \end{aligned}$$

Indeed, the correction restores the matrix form of the d3Q7 model (where $w = 0$) for the d3Q15 model, since the two schemes describe the anisotropic diagonal entries on the coordinate links (relation (3.1)). The correction vanishes when $w_c^{(m)} = w_c^{(m)*}$ for the d3Q19 model (relation (3.5)). In any case, $\mathcal{M}_{4,dig} = 0$ on the diagonal axis $\partial_x = \partial_y = \partial_z$. In the presence of cross-diffusion entries, the \mathcal{M}_4 has to be further modified:

$$\begin{aligned}
 & \mathcal{M}_4 \rightarrow \mathcal{M}_4 + \mathcal{M}_{4,off}, \\
 \text{d3Q15: } & \mathcal{M}_{4,off} = 3\{g_{\alpha\beta}^{(a)}\mathcal{D}_{\alpha\beta}(1 - \delta_{\alpha\beta})\} \cdot (\mathcal{M}_{\nabla}^{(2)} - 2\mathcal{I}_{\nabla}^2), \\
 & \nabla^T \cdot \mathcal{M}_{4,off} \cdot \nabla = 6(\mathcal{D}_{xy}\partial_z + \mathcal{D}_{yz}\partial_x + \mathcal{D}_{xz}\partial_y)\partial_x\partial_y\partial_z, \\
 \text{and d3Q19: } & \mathcal{M}_{4,off} = -\frac{3}{2}\{g_{\alpha\beta}^{(a)}\mathcal{D}_{\alpha\beta}(1 - \delta_{\alpha\beta})\} \cdot (\mathcal{M}_{\nabla}^{(2)} - 3\mathcal{I}_{\nabla}^2), \\
 & \nabla^T \cdot \mathcal{M}_{4,off} \cdot \nabla = \frac{3}{2}\left((2\partial_x\partial_y\partial_z^2 - \partial_y\partial_x^3 - \partial_x\partial_y^3)\mathcal{D}_{xy} + (2\partial_x\partial_z\partial_y^2 - \partial_z\partial_x^3 - \partial_x\partial_z^3)\mathcal{D}_{xz} \right. \\
 & \quad \left. + (2\partial_y\partial_z\partial_x^2 - \partial_y\partial_z^3 - \partial_z\partial_y^3)\mathcal{D}_{yz}\right). \tag{C.5}
 \end{aligned}$$

On the contrary with the d2Q9 model, the anisotropic d3Q15 and d3Q19 do not factorize the full matrix \mathcal{D} . When $g^{(u)} = 1$, the additional corrections keep the form (C.4)-(C.5) replacing there $g^{(a)}$ with $g^{(u)}$, $g_{\alpha\beta}^{(a)}$ with $g_{\alpha\beta}^{(u)}$, $\{\mathcal{D}_{\alpha\beta}\}$ with $\{U_\alpha U_\beta\}$, $t_q^{(m)}$ with $t_q^{(u)}$ and $w_q^{(m)}$ with $w_q^{(u)}$.

C.3 The operator $R_{4,3} = S_4 - S_1 S_3$: Links to stability

Our aim is to check whether the optimal advection lines (3.22) and (3.23) may remain sufficient when $\Lambda = \Lambda^{(ext.)}(\Lambda_{bgk})$ (relation (2.15)). We assume that \vec{v}_e is the nullspace eigenvector of the tensor $\mathcal{D}^{(eff)}$, ∇s is parallel to \vec{v}_e (in Fourier space, the wave vector \vec{k} is parallel to \vec{v}_e), and \vec{U}_a minimizes the stability condition: $\det[\mathcal{D}^{(eff)}(\vec{U})] = 0$. We then examine $R_{4,3}$ plugging there \vec{v}_e and \vec{U}_a .

C.3.1 Two dimensions

First, in agreement with Eqs. (4.6) and (4.7), $R_{4,3}(\vec{v}_e, \vec{U}_a)$ vanishes when the weights are the same, for the diagonal tensors and then only when $t_c = 0$ in the presence of cross-diffusion entries. This confirms the extension of the advection line to these two cases.

However, the numerical stability analysis suggests that $\Lambda = \Lambda^{(ext.)}(\Lambda_{bgk})$ may retain the advection line in the presence of cross-diffusion when $t_c \neq 0$. We then suggest that, since the operators R_4 and D_2 have the opposite signs in Fourier space, $c_{4,3}R_{4,3}(\vec{v}_e, \vec{U}_a)$ has to be non-positive when $U^2 \leq U_a^2$. We examine $R_{4,3}(\vec{v}_e, \vec{U}_a)$ for same weights (3.4).

When $g^{(u)} = 0$ the minimizer $\vec{U}_a = \{U_x, U_y\}$ has the following components (assuming $U_x U_y > 0$ (or < 0) when $\mathcal{D}_{xy} < 0$ (or > 0), respectively):

$$\begin{aligned}
 U_x^2 &= \frac{1}{2} \left(\mathcal{D}_{xx} + \frac{\mathcal{D}_{xx}(\mathcal{D}_{yy} - \mathcal{D}_{xx}) - 2\mathcal{D}_{xy}^2}{\sqrt{(\mathcal{D}_{xx} - \mathcal{D}_{yy})^2 + 4\mathcal{D}_{xy}^2}} \right), \\
 U_y^2 &= \frac{1}{2} \left(\mathcal{D}_{yy} + \frac{\mathcal{D}_{yy}(\mathcal{D}_{xx} - \mathcal{D}_{yy}) - 2\mathcal{D}_{xy}^2}{\sqrt{(\mathcal{D}_{xx} - \mathcal{D}_{yy})^2 + 4\mathcal{D}_{xy}^2}} \right),
 \end{aligned}
 \tag{C.6}$$

where $U_a^2 = |\vec{U}_a|^2$ is given by relation (3.22). The non-zero nullspace eigenvectors are:

$$\begin{aligned}
 \vec{v}_e &= \left\{ (\mathcal{D}_{yy} - U_y^2)(\mathcal{D}_{xx} - \mathcal{D}_{xy} + U_x(U_y - U_x)), (\mathcal{D}_{xx} - U_x^2)(\mathcal{D}_{yy} - \mathcal{D}_{xy} + U_y(U_x - U_y)) \right\}, \\
 \text{or } \vec{v}_e &= \left\{ U_x U_y - \mathcal{D}_{xy}, \mathcal{D}_{xx} - U_x^2 \right\}, \quad \text{or } \vec{v}_e = \left\{ \mathcal{D}_{yy} - U_y^2, U_x U_y - \mathcal{D}_{xy} \right\}.
 \end{aligned}
 \tag{C.7}$$

We could verify with the help of the optimization routines [50] that $R_{4,3}(\vec{v}_e, \vec{U}_a) \leq 0$ when $\mathcal{D}_{xx} = \mathcal{D}_{yy}$ and thus, $U_x = \pm U_y$, $U_a^2 = c_e - |\mathcal{D}_{xy}|$ and \vec{v}_e is along the diagonal axis. When the diagonal elements differ, we confirm that $R_{4,3}(\vec{v}_e, \vec{U}_a) \leq 0$ with the help of the intensive numerical variation of the anisotropic factors. Then $c_{4,3}R_{4,3}(\vec{v}_e, \vec{U}_a) \leq 0$ only when $\Lambda_{bgk} \geq \frac{1}{6}$ where optimal stability is confirmed by numerical observations.

When $g^{(u)} = 1$, then \vec{U}_a is parallel to the diagonal axis: $U_x = U_y$ when $\mathcal{D}_{xy} < 0$, or $U_x = -U_y$ when $\mathcal{D}_{xy} > 0$, and U_a^2 is given by relation (3.23). The nullspace eigenvectors \vec{v}_e are

$$g^{(u)} = 1: \quad \vec{v}_e = \left\{ \mathcal{D}_{yy}(\mathcal{D}_{xx} - \mathcal{D}_{xy} + U_x U_y), \mathcal{D}_{xx}(\mathcal{D}_{yy} - \mathcal{D}_{xy} + U_x U_y) \right\}.
 \tag{C.8}$$

Writing $\mathcal{D}_{\alpha\alpha} = c_e(1 \pm a)$ and $\mathcal{D}_{xy} = K'_{xy} c_e \sqrt{1 - a^2}$, $|a_\alpha| \leq 1$, it comes out

$$R_{4,3}(\vec{v}_e, \vec{U}_a) = -48c_e^9 (a^2 - 1)^3 \left(a^2 - 2 \left(1 - \frac{K'_{xy}}{|K'_{xy}|} \sqrt{1 - a^2} \right) \right) |K'_{xy}| t_c, \quad \forall K'_{xy} \in [-1, 1].
 \tag{C.9}$$

Then $R_{4,3}(\vec{v}_e, \vec{U}_a) \leq 0$, and $R_{4,3}(\vec{v}_e, \vec{U}_a) = 0$ when $c_e = 0$ (this is advection line of the d1Q3 model), or when $t_c = 0$, in agreement with relation (4.7).

Summary. Altogether, we confirm that $R_{4,3}(\vec{v}_e, \vec{U}_a) \leq 0$ for any anisotropy of the diagonal and off-diagonal elements, at least when the weights are the same and $t_c \in [0, \frac{1}{2}]$. Then $c_{4,3}R_{4,3}(\vec{v}_e, \vec{U}_a) \leq 0$ when $\Lambda \geq \frac{1}{6}$. We suggest that this explains the advanced stability

of the scheme when $\Lambda = \Lambda^{(ext.)}(\Lambda_{bgk})$, and then $c_{4,4}R_{4,4} = 0$, providing that $\Lambda_{bgk} \geq \frac{1}{6}$ and then

$$\Lambda = \Lambda^{(ext.)}(\Lambda_{bgk}) \geq \frac{1}{6}.$$

C.3.2 Three dimensions

Again, in agreement with Eqs. (4.6) and (4.7) $R_{4,3}(\vec{v}_e, \vec{U}_a)$ vanishes when all weights are the same for isotropic tensors $\mathcal{D}_{\alpha\alpha}^+$, i.e., when $g^{(u)} = 0$. When $g^{(u)} = 1$ and the diffusion tensor is isotropic but the constructed tensor $\mathcal{D}_{\alpha\beta}^+ = (c_e + U_\alpha U_\beta)\delta_{\alpha\beta}$ has the anisotropic entries. However, the \vec{v}_e is parallel to the diagonal axis and then correction (C.4) vanishes. Then $U_a^2 = \frac{d}{d-1}c_e$, and $R_{4,3}(\vec{v}_e, \vec{U}_a) = 0$ for weight relationships (3.6). This explains the observed optimal stability of the d3Q15 model when $\Lambda = \Lambda^{(ext.)}(\Lambda_{bgk})$ for weights (3.6). Curiously, relationships (3.6) have been previously derived, and they are given by Eqs. (127) and (135) in [20], to guarantee sufficiency of the necessary advection line on the OTRT subclass when $g^{(u)} = 1$. This additionally confirms the existing relation between the sufficiency of necessary condition $\det[\mathcal{D}^{(eff)}] > 0$ and fourth-order truncation error.

C.4 The operator $R_{4,4} = S_1^4 - S_1 S_3$: Links to stability

The operator $R_{4,4}$ is independent of the symmetric weights $\{E_q^+\}$. In order to extend the boundary $\Lambda = \Lambda^{(ext.)}(\Lambda_{bgk})$ to the interval $\Lambda \in [\Lambda^{(ext.)}(\Lambda_{bgk}), \frac{1}{4}]$ (or, perhaps, $\Lambda \geq \Lambda^{(ext.)}(\Lambda_{bgk})$) we examine when $R_{4,4}(\vec{v}_e, \vec{U}_a)$ is non-positive, keeping in mind that then $c_{4,4}R_{4,4} \leq 0$ for $\Lambda \geq \Lambda^{(ext.)}(\Lambda_{bgk})$. Below we list the situations where we could verify this analytically. This covers the two cases: (a) $g^{(u)} = 0$, the anisotropic diagonal tensor in 2D and 3D, and (b) $g^{(u)} = 1$, the full anisotropic tensor in 2D or the isotropic tensor in 3D.

C.4.1 Diagonal lattice direction

We first consider $R_{4,4}(\vec{v}_e, \vec{U}_a)$ when the two vectors \vec{v}_e and \vec{U}_a are parallel to the diagonal axis ($\partial_\alpha = \partial$, hereafter). This is valid when: (a) $g^{(u)} = 1$ and \mathcal{D} is isotropic in 2D and 3D, and (b) $g^{(u)} = \{0,1\}$ and \mathcal{D} has the same diagonal elements in 2D. Then

$$\begin{aligned} R_{4,4} &= 4U^2(U^2 - a_c)\partial^4 & \text{with } a_c &= 2 - 3t_c^{(a)} & \text{for the d2Q9,} \\ R_{4,4} &= 9U^2(U^2 - a_c)\partial^4 & \text{with } a_c &= (7 - 12t_c^{(a)})/3 & \text{for the d3Q15,} \\ R_{4,4} &= 9U^2(U^2 - a_c)\partial^4 & \text{with } a_c &= 2(2 - 3t_c^{(a)})/3 & \text{for the d3Q19.} \end{aligned}$$

Then $R_{4,4}(\vec{v}_e, \vec{U}_a) \leq 0$ when $U^2 \leq a_c$. In general, this last constraint is sufficient to guarantee $R_{4,4}(\vec{v}_e, \vec{U}_a) \leq 0$ when $U^2 \leq U_a^2 \leq 1$. In particular, $a_c = 1/d$ for the minimal models, then $U_a^2 \leq a_c$ for $g^{(u)} = 0$ or $g^{(u)} = 1$.

C.4.2 Full anisotropic tensor in 2D when $g^{(u)} = 1$

This situation is discussed around relations (C.8). We then obtain that $R_{4,4}(\vec{v}_e, \vec{U}_a) \leq 0$ when $0 \leq c_e \leq c_{eR} = 1 - \frac{3}{2}t_c^{(a)}$ for any positive semi-definite tensor. Example: $c_{eR} = \frac{1}{4}$ for the d2Q5 model where $c_e = \frac{1}{4}$ is the bisection of the isotropic advection line ($U^2 = 2c_e$) and the diffusion line $U^2 = 1 - 2c_e$. Note, that $c_{eR} = 1$ when $t_c^{(a)} = 0$.

C.4.3 Isotropic tensor with $D = c_e \mathcal{I}$ when $g^{(u)} = 0$

In this case, the nullspace eigenvectors are parallel to velocity vector. Plugging them into $R_{4,4}$, we verify that $R_{4,4}(\vec{v}_e, \vec{U}_a) < 0$ when $U^2 \leq c_e^{(\max)}$, at least on the same weights (3.4).

C.4.4 Anisotropic diagonal tensor when $g^{(u)} = 0$

When the diffusion tensor is diagonal and anisotropic, then the velocity vector and the null space eigenvector are both parallel to the coordinate axis (with the minimal diffusion element), in 2D and 3D, and the problem reduces to 1d where $R_{4,4} = U^2(U^2 - 1)\partial^4$. Hence, $R_{4,4}(\vec{v}_e, \vec{U}_a) \leq 0$ when $U^2 \leq 1$.

D Equivalent, advection and anisotropic diffusion, finite-difference stencils

In this section, we write down the exact form of the finite-difference stencils for the advection and diffusion operators (2.5):

$$C(\vec{r}, t) = \sum_{q=1}^{Q_m} \bar{\Delta}_q e_q^-(\vec{r}, t) \quad \text{and} \quad D(\vec{r}, t) = \sum_{q=1}^{Q_m} \Delta_q^2 e_q^+(\vec{r}, t)$$

on the equilibrium (3.1), for the d2Q9, d3Q15 and d3Q19 schemes. We will use the following finite-difference operators on the regular grid with space step equal to 1:

$$\begin{aligned} \bar{\Delta}_\alpha s_0 &= \frac{s_\alpha - s_{-\alpha}}{2}, & \Delta_\alpha^2 s_0 &= s_\alpha - 2s_0 + s_{-\alpha}, \\ \bar{\Delta}_\alpha^{(\pm\beta)} s_0 &= \bar{\Delta}_\alpha s_{\pm\beta}, & \Delta_\alpha^{2(\pm\beta)} s_0 &= \Delta_\alpha^2 s_{\pm\beta}, \quad \beta \neq \alpha \\ \bar{\Delta}_\alpha^{(\pm\beta, \pm\gamma)} s_0 &= \bar{\Delta}_\alpha s_{\pm\beta, \pm\gamma}, & \Delta_\alpha^{2(\pm\beta, \pm\gamma)} s_0 &= \Delta_\alpha^2 s_{\pm\beta, \pm\gamma}, \quad \gamma \neq \beta \neq \alpha. \end{aligned} \tag{D.1}$$

Here, the operators $\bar{\Delta}_\alpha(\vec{r})$ and $\Delta_\alpha^2(\vec{r})$ are standard: the central difference and the Laplace operator with the central value $s(\vec{r}) = s_0$. Then the operators $\bar{\Delta}_\alpha^{(\pm\beta)}$ and $\Delta_\alpha^{2(\pm\beta)}$, and the operators $\bar{\Delta}_\alpha^{(\pm\beta, \pm\gamma)}$ and $\Delta_\alpha^{2(\pm\beta, \pm\gamma)}$, compute the convection and diffusion operators in the neighboring nodes, with $s_0 = s(\vec{r} + \vec{1}_{\pm\beta})$ and $s_0 = s(\vec{r} + \vec{1}_{\pm\beta, \pm\gamma})$, respectively.

Convection term. The finite-difference equivalents of the linear advection operator is read as:

$$\begin{aligned}
 \text{d2Q9, d3Q19: } \quad \mathcal{C}^{f.d.} &= 2 \sum_{\alpha} U_{\alpha} \left(t_c^{(a)} \bar{\Delta}_{\alpha} + t_d^{(a)} \sum_{\beta \neq \alpha} \bar{\Delta}_{\alpha}^{(\pm\beta)} \right), \\
 \text{d3Q15: } \quad \mathcal{C}^{f.d.} &= 2 \sum_{\alpha} U_{\alpha} \left(t_c^{(a)} \bar{\Delta}_{\alpha} + t_d^{(a)} \sum_{\beta \neq \gamma \neq \alpha} \bar{\Delta}_{\alpha}^{(\pm\beta, \pm\gamma)} \right), \tag{D.2}
 \end{aligned}$$

and $\mathcal{C}^{f.d.} s_0$ approximates $[\vec{U} \cdot \nabla] s_0$ at the leading order thanks to weight property (3.2).

Diagonal diffusion stencil. Without the cross-diffusion equilibrium components, the pure diffusion *diagonal* form D is read as:

$$\begin{aligned}
 \text{d2Q9: } \quad \mathcal{D}^{f.d.} &= 2c_e \sum_{\alpha} \left((t_c^{(m)} + t_d^{(m)}) \Delta_{\alpha}^2 + t_d^{(m)} \sum_{\beta \neq \alpha} \Delta_{\alpha}^{2(\pm\beta)} \right) + \sum_{\alpha} (\mathcal{D}_{\alpha\alpha} - c_e) \Delta_{\alpha}^2 \\
 &= 2 \sum_{\alpha} \mathcal{D}_{\alpha\alpha} \left((t_c^{(m)} + t_d^{(m)}) \Delta_{\alpha}^2 + t_d^{(m)} \sum_{\beta \neq \alpha} \Delta_{\alpha}^{2(\pm\beta)} \right), \tag{D.3}
 \end{aligned}$$

$$\begin{aligned}
 \text{d3Q15: } \quad \mathcal{D}^{f.d.} &= 2c_e \left(\sum_{\alpha} (t_c^{(m)} \Delta_{\alpha}^2 + t_d^{(m)} \Delta^{2(dig)}) + \sum_{\alpha} (\mathcal{D}_{\alpha\alpha} - c_e) \Delta_{\alpha}^2 \right) \\
 &= \sum_{\alpha} \mathcal{D}_{\alpha\alpha} \left((2t_c^{(m)} + \frac{8t_d^{(m)}}{3}) \Delta_{\alpha}^2 + \frac{2t_d^{(m)}}{3} \sum_{\beta \neq \alpha} \Delta_{\alpha}^{2(\pm\beta)} + \frac{2t_d^{(m)}}{3} \sum_{\beta \neq \gamma \neq \alpha} \Delta_{\alpha}^{2(\pm\beta, \pm\gamma)} \right) \\
 &\quad + \frac{2t_d^{(m)}}{3} \sum_{\alpha} \mathcal{D}_{\alpha\alpha} \delta_{\alpha}^{(4)}, \tag{D.4}
 \end{aligned}$$

$$\begin{aligned}
 \text{d3Q19: } \quad \mathcal{D}^{f.d.} &= c_e \sum_{\alpha} \left(2(t_c^{(m)} + 2t_d^{(m)}) \Delta_{\alpha}^2 + t_d^{(m)} \sum_{\beta \neq \alpha} \Delta_{\alpha}^{2(\pm\beta)} \right) \\
 &\quad + \sum_{\alpha} \frac{(\mathcal{D}_{\alpha\alpha} - c_e)}{6} \left(2\Delta_{\alpha}^2 + \sum_{\beta \neq \alpha} \Delta_{\alpha}^{2(\pm\beta)} \right) + \frac{w_c^{(m)}}{3} \sum_{\alpha} \mathcal{D}_{\alpha\alpha} \delta_{\alpha}^{(4)} \\
 &= \sum_{\alpha} \mathcal{D}_{\alpha\alpha} \left(2(t_c^{(m)} + 2t_d^{(m)}) \Delta_{\alpha}^2 + t_d^{(m)} \sum_{\beta \neq \alpha} \Delta_{\alpha}^{2(\pm\beta)} \right) \\
 &\quad - \frac{3 + 2t_c^{(m)} - 8w_c^{(m)}}{24} \sum_{\alpha} \mathcal{D}_{\alpha\alpha} \delta_{\alpha}^{(4)}. \tag{D.5}
 \end{aligned}$$

When $t_c^{(m)} = w_c^{(m)} = \frac{1}{2}$, all the models reduce to the minimal stencil,

$$\mathcal{D}^{f.d.} = \sum_{\alpha} \mathcal{D}_{\alpha\alpha} \Delta_{\alpha}^2.$$

We have accounted that

$$\begin{aligned}
 \text{d3Q15 : } \quad c_e \sum_{q_d} \Delta_q^2 t_d^{(m)} s &= 2c_e t_d^{(m)} \Delta^{2(\text{dig})} s, \\
 \text{where } \quad \Delta^{2(\text{dig})} s &= \sum_{\alpha \neq \beta \neq \gamma} s_{\pm\alpha, \pm\beta, \pm\gamma} - 8s_0 \\
 &= 2c_e t_d^{(m)} \sum_{\alpha} \left(\frac{4}{3} \Delta_{\alpha}^2 + \frac{1}{3} \sum_{\beta \neq \alpha} \Delta_{\alpha}^{2(\pm\beta)} + \frac{1}{3} \sum_{\beta \neq \gamma \neq \alpha} \Delta_{\alpha}^{2(\pm\beta, \pm\gamma)} \right) s. \quad (\text{D.6})
 \end{aligned}$$

The difference between the different-level Laplace operators is accounted for by the (fourth-order) operators:

$$\delta_{\alpha, \beta}^{(4)} = \Delta_{\alpha}^{2(\beta)} + \Delta_{\alpha}^{2(-\beta)} - 2\Delta_{\alpha}^2, \quad \beta \neq \alpha, \quad \delta_{\alpha}^{(4)} = \delta_{\beta, \gamma}^{(4)} + \delta_{\gamma, \beta}^{(4)} - (\delta_{\alpha, \beta}^{(4)} + \delta_{\alpha, \gamma}^{(4)}).$$

Consequently,

$$\delta_{\alpha}^{(4)} = \sum_{\alpha} \delta_{\alpha}^{(4)} = 0. \quad (\text{D.7})$$

Altogether, the d2Q9 model describes the isotropic and anisotropic diagonal elements on the same stencil, with $2(t_c^{(m)} + t_d^{(m)})$ for the central Δ_{α}^2 operator, and $2t_d^{(m)}$ for the two neighbor ones, $\Delta_{\alpha}^{2(\pm\beta)}$. This becomes also possible for the d3Q19 model when its last term vanishes, i.e. when $w_c^{(m)} = w_c^{(m)*}$ (cf. relations (3.5)).

The cross-diffusion. Equilibrium elements $\mathcal{D}_{\alpha\beta} c_{q\alpha} c_{q\beta} / \sum_{j=1}^{Q_m} c_{j\alpha}^2 c_{j\beta}^2$ give the cross-diffusion entries in the form:

$$\text{d2Q9, d3Q19 : } \quad \mathcal{D}_{\alpha\beta}^{f.d.} = \frac{s_{\alpha, \beta} + s_{-\alpha, -\beta} - s_{\alpha, -\beta} - s_{-\alpha, \beta}}{2}. \quad (\text{D.8})$$

They can be easily interpreted in the form of the mixed products $\bar{\Delta}_{\alpha} \bar{\Delta}_{\beta}$. The d3Q15 model replaces $s_{\alpha, \beta}$ with a half sum of its diagonal values $s_{\alpha, \beta, \pm\gamma}$, $\gamma \neq \beta \neq \alpha$.

Example D.1. The conventional nine-points FTCS scheme [24] is read as:

$$\begin{aligned}
 & \frac{s_0(t + \delta_t) - s_0(t)}{\delta_t} + \frac{1}{2 + \gamma^c} \frac{U_x}{2\delta_x} \left((s_{ne} - s_{nw}) + \gamma^c (s_e - s_w) + (s_{se} - s_{sw}) \right) \\
 & + \frac{1}{2 + \gamma^c} \frac{U_y}{2\delta_y} \left((s_{ne} - s_{se}) + \gamma^c (s_n - s_s) + (s_{ne} - s_{se}) \right) \\
 & = \frac{1}{2 + \gamma^d} \frac{H_{xx}}{\delta_x^2} \left((s_{se} - 2s_s + s_{sw}) + \gamma^d (s_e - 2s_0 + s_w) + (s_{ne} - 2s_n + s_{nw}) \right) \\
 & + \frac{1}{2 + \gamma^d} \frac{H_{yy}}{\delta_y^2} \left((s_{nw} - 2s_w + s_{sw}) + \gamma^d (s_n - 2s_0 + s_s) + (s_{ne} - 2s_e + s_{se}) \right) \\
 & + \frac{H_{xy}}{2\delta_x \delta_y} (s_{ne} - s_{nw} + s_{sw} - s_{se}). \quad (\text{D.9})
 \end{aligned}$$

This scheme can be regarded as the OTRT scheme (2.3) with

$$H_{\alpha\beta} = (\Lambda^- \mathcal{D}_{\alpha\beta} \delta_\alpha \delta_\beta) / \delta_t$$

when $\Lambda^- = \Lambda^+ = \frac{1}{2}$ (this is the BGK model with $\tau = 1$), and relating discretization factors γ^c and γ^d to weights as (cf. Eqs. (D.2) and (D.3)):

$$\gamma^c = -2 + \frac{1}{2t_d^{(a)}}, \quad \gamma^d = -2 + \frac{1}{t_d^{(m)}}, \quad \{t_d^{(m)}, t_d^{(a)}\} \leq \frac{1}{4}, \quad (\text{D.10})$$

or, equivalently,

$$t_c^{(a)} = \frac{\gamma^c}{2(2+\gamma^c)}, \quad t_d^{(a)} = \frac{1}{2(2+\gamma^c)}, \quad (\text{D.11})$$

$$t_c^{(m)} = \frac{\gamma^d - 2}{2(2+\gamma^d)}, \quad t_d^{(m)} = \frac{1}{(2+\gamma^d)}. \quad (\text{D.12})$$

The minimal stencils are included in the limit $\gamma^c \rightarrow \infty$ and $\gamma^d \rightarrow \infty$. The modified scheme (MFTCS in [24]) removes the numerical diffusion simply replacing $H_{\alpha\beta}$ by $H_{\alpha\beta} + u_\alpha u_\beta / 2$. This correction is a particular choice of the TRT scheme for same weights $t_q^{(u)} = t_q^{(m)}$, replacing $\mathcal{D}_{\alpha\beta}$ with $\mathcal{D}_{\alpha\beta} + U_\alpha U_\beta$ in Eqs. (D.3)-(D.5).

Acknowledgments

The author is thankful to D. d'Humières for his parallel work on the Fourier analysis of the TRT AADE model and to anonymous referee for constructive suggestions.

References

- [1] R. Adhikari and S. Succi, Duality in matrix lattice Boltzmann methods, *Phys. Rev. E*, 78:066701-1-9, 2008.
- [2] B. Ahrenholz, J. Tölke, and M. Krafczyk, Lattice-Boltzmann simulations in reconstructed parametrized porous media. *Int. J. Comput. Fluid Dyn.*, 20(6):369–377, 2006.
- [3] M. G. Ancona, Fully-Lagrangian and Lattice-Boltzmann Methods for solving systems of conservation equations. *J. Comput. Phys.*, 115:107–120, 1994.
- [4] R. Benzi, S. Succi, and M. Vergassola. The lattice Boltzmann equation: theory and applications. *Physics Reports*, 222:145–197, 1992.
- [5] B. Chun and A. J. C. Ladd, Interpolated boundary conditions for Lattice Boltzmann simulations of flows in narrow gaps. *Phys. Rev. E*, 75:066705-1-11, 2007.
- [6] Y. Dong, J. Zhang, and G. Yan, A higher-order moment method of the lattice Boltzmann model for the conservation law equation, *Appl. Math. Model.*, 34:481–494, 2010.
- [7] F. Dubois, Equivalent partial differential equations of a lattice Boltzmann scheme. *Comp. Math. Appl.*, 55:1441–1449, 2008.

- [8] F. Dubois and P. Lallemand, Towards higher order lattice Boltzmann schemes. *J. Stat. Mech.: Theory and Experiment*, PO6:P06006, 2009. doi: 10.1088/1742-5468/2009/06/006006.
- [9] F. Dubois, P. Lallemand, and M. Tekitek, On a superconvergent lattice Boltzmann boundary scheme. *Comp. Math. Appl.*, 59(7):2141–2149, 2010.
- [10] E. C. Du Fort and S. P. Frankel, Stability conditions in the numerical treatment of parabolic differential equations. *M.T.A.C.*, 7:135, 1953.
- [11] I. Ginzburg and D. d’Humières, Multi-reflection boundary conditions for lattice Boltzmann models. *Phys. Rev. E*, 68:066614-1-30, 2003.
- [12] I. Ginzburg, Equilibrium-type and Link-type Lattice Boltzmann models for generic advection and anisotropic-dispersion equation. *Adv. Wat. Res.*, 28:1171–1195, 2005.
- [13] I. Ginzburg, Generic boundary conditions for Lattice Boltzmann models and their application to advection and anisotropic-dispersion equations. *Adv. Wat. Res.*, 28:1196–1216, 2005.
- [14] I. Ginzburg, Variably saturated flow described with the anisotropic Lattice Boltzmann methods. *J. Comp. Fluids*, 25:831–848, 2006.
- [15] I. Ginzburg and D. d’Humières, Lattice Boltzmann and analytical modeling of flow processes in anisotropic and heterogeneous stratified aquifers. *Adv. Wat. Res.*, 30:2202–2234, 2007.
- [16] I. Ginzburg, Lattice Boltzmann modeling with discontinuous collision components. Hydrodynamic and advection-diffusion equations. *J. Stat. Phys.*, 126:157–203, 2007.
- [17] I. Ginzburg, Consistent Lattice Boltzmann schemes for the Brinkman model of porous flow and infinite Chapman-Enskog expansion. *Phys. Rev. E*, 77:0666704:1-12, 2008.
- [18] I. Ginzburg, F. Verhaeghe, and D. d’Humières, Two-relaxation-time Lattice Boltzmann scheme: about parametrization, velocity, pressure and mixed boundary conditions. *Commun. Comput. Phys*, 3:427–478, 2008.
- [19] I. Ginzburg, F. Verhaeghe, and D. d’Humières, Study of simple hydrodynamic solutions with the two-relaxation-times Lattice Boltzmann scheme. *Commun. Comput. Phys*, 3:519–581, 2008.
- [20] I. Ginzburg, D. d’Humières, and A. Kuzmin, Optimal stability of advection-diffusion Lattice Boltzmann models with two relaxation times for positive/negative equilibrium. *J. Stat. Phys.*, 139(6):1090-1143, 2010. DOI 10.1007/s10955-010-9969-9.
- [21] H. Hammou, I. Ginzburg, and M. Boulerhcha, Two-relaxation-times Lattice Boltzmann schemes for solute transport in unsaturated water flow, with a focus on stability. *Adv. Wat. Res.*, 34(6):779-793, 2011.
- [22] F. J. Higuera, S. Succi, and R. Benzi, Lattice gas dynamics with enhanced collisions. *Europhys. Lett.*, 9:345–349, 1989.
- [23] F. J. Higuera and J. Jiménez, Boltzmann approach to lattice gas simulations. *Europhys. Lett.*, 9:663–668, 1989.
- [24] A. C. Hindmarch, P. M. Gresho, and D. F. Griffiths, The stability of explicit time-integration for certain finite difference approximation of the multi-dimensional advection-diffusion equation. *Int. J. Num. Methods Fluids*, 4:853–897, 1984.
- [25] C. W. Hirt, Heuristic stability theory for finite-difference equations. *J. Comput. Phys.*, 2:339–355, 1968.
- [26] D. J. Holdych, D. R. Noble, J. G. Georgiadis, and R. O. Buckius, Truncation error analysis of Lattice Boltzmann methods. *J. Comput. Phys.*, 193(2):595–619, 2004.
- [27] D. d’Humières, Generalized Lattice-Boltzmann equations. *AIAA Rarefied Gas Dynamics: Theory and Simulations. Progress in Astronautics and Aeronautics*, 59:450–548, 1992.
- [28] D. d’Humières, M. Bouzidi, and P. Lallemand, Thirteen-velocity three-dimensional Lattice

- Boltzmann model. *Phys. Rev. E*, 63:066702-1-7, 2001.
- [29] D. d’Humières, I. Ginzburg, M. Krafczyk, P. Lallemand, and L.-S. Luo, Multiple-relaxation-time Lattice Boltzmann models in three dimensions. *Phil. Trans. R. Soc. Lond. A*, 360:437–451, 2002.
- [30] D. d’Humières and I. Ginzburg, Viscosity independent numerical errors for Lattice Boltzmann models: from recurrence equations to “magic” collision numbers. *Comp. Math. Appl.*, 58(5):823-840, 2009.
- [31] D. d’Humières, Some stability results, in preparation, 2010.
- [32] M. Junk and Z. Yang, Analysis and invariant properties of a Lattice Boltzmann method. *Adv. Appl. Math. Mech.*, 2/5:640–669, 2010.
- [33] V. Koivu, M. Decain, C. Geindreau, K. Mattila, J.-F. Bloch, and M. Kataja, Transport properties of heterogeneous materials. Combining computerised X-ray micro-tomography and direct numerical simulations. *Int. J. Comput. Fluid Dyn.*, 23(10):713–721, 2009.
- [34] A. Kuzmin, I. Ginzburg, and A. A. Mohamad, A role of the kinetic parameter on the stability of two-relaxation-times advection-diffusion Lattice Boltzmann scheme. *Comp. Math. Appl.*, 61:3417–3442, 2011.
- [35] Y.-K. Kwok and K.-K. Tam, Stability analysis of three-level difference schemes for initial boundary problems for multi-dimensional convective-diffusion equations. *Commun. Numer. Methods Engr.*, 9:595–605, 1993.
- [36] P. Lallemand and L.-S. Luo, Theory of the lattice Boltzmann method: dispersion, dissipation, isotropy, Galilean invariance, and stability. *Phys. Rev. E*, 61:6546–6562, 2000.
- [37] M. E. McCracken and J. Abraham, Multiple-relaxation-time lattice-Boltzmann model for multiphase flow. *Phys. Rev. E*, 71:036701-1-9, 2005.
- [38] Y. Li and P. Huang, A coupled lattice Boltzmann model for advection and anisotropic dispersion problem in shallow water. *Adv. Wat. Res.*, 31(12):1719–1730, 2008.
- [39] J. J. H. Miller, On the location of zeros of certain classes of polynomials with application to numerical analysis. *J. Inst. Math. Appl.*, 8:397–406, 1971.
- [40] C. Pan, L.-S. Luo, and C. T. Miller, An evaluation of lattice Boltzmann schemes for porous media simulation. *J. Comp. Fluids*, 35(4):898–909, 2006.
- [41] Y. Qian, D. d’Humières, and P. Lallemand, Lattice BGK models for Navier-Stokes equation. *Europhys. Lett.*, 17:479–484, 1992.
- [42] I. Rasin, S. Saucchi and W. Miller, A multi-relaxation lattice kinetic method for passive scalar diffusion, *J. Comput. Phys.*, 206:453–462, 2005.
- [43] M. Rheinländer, Stability and multiscale analysis of an advective Lattice Boltzmann scheme. *Progress Comp. Fluid Dynamics*, 8(1-4):56–68, 2008.
- [44] B. Servan-Camas and F. T. C. Tsai, Lattice Boltzmann method for two relaxation times for advection-diffusion equation: third order analysis and stability analysis. *Adv. Wat. Res.*, 31:1113-1126, 2008.
- [45] B. Servan-Camas and F. T. C. Tsai, Saltwater intrusion modeling in heterogeneous confined aquifers using two-relaxation-time Lattice Boltzmann method. *J. Comput. Phys.*, 228:236-256, 2009.
- [46] B. Servan-Camas and F. T. C. Tsai, Two-relaxation-time lattice Boltzmann method for the anisotropic dispersive Henry problem. *Water Resources Research*, 46:W02515-25, 2009.
- [47] R. G. M. van der Sman, MRT Lattice Boltzmann schemes for confined suspension flows. *Comp. Phys. Commun.*, 181:1562-1569, 2010.
- [48] S. Suga, Stability and accuracy of Lattice Boltzmann Schemes for anisotropic advection-diffusion equations. *Int. J. Mod. Phys. C*, 20(4):633–650, 2009.

- [49] S. Suga, An accurate multi-level finite difference scheme for 1D diffusion equations derived from the Lattice Boltzmann method. *J. Stat. Phys.*, 140:494–503.
- [50] S. Wolfram, software package “Mathematica 6”.
- [51] H. Yoshida and M. Nagaoka, Multiple-relaxation-time lattice Boltzmann model for the convection and anisotropic diffusion equation. *J. Comput. Phys.*, 229:7774–7795, 2010.
- [52] X. Zhang, A. G. Bengough, L. K. Deeks, J. W. Crawford, and I. M. Young. A lattice BGK model for advection and anisotropic dispersion equation. *Adv. Wat. Res.*, 25:1–8, 2002.